

## University of Groningen

### Dressing the nucleon causally

Kondratyuk, Sergey

**IMPORTANT NOTE: You are advised to consult the publisher's version (publisher's PDF) if you wish to cite from it. Please check the document version below.**

*Document Version*

Publisher's PDF, also known as Version of record

*Publication date:*

2000

[Link to publication in University of Groningen/UMCG research database](#)

*Citation for published version (APA):*

Kondratyuk, S. (2000). *Dressing the nucleon causally*. s.n.

**Copyright**

Other than for strictly personal use, it is not permitted to download or to forward/distribute the text or part of it without the consent of the author(s) and/or copyright holder(s), unless the work is under an open content license (like Creative Commons).

The publication may also be distributed here under the terms of Article 25fa of the Dutch Copyright Act, indicated by the "Taverne" license. More information can be found on the University of Groningen website: <https://www.rug.nl/library/open-access/self-archiving-pure/taverne-amendment>.

**Take-down policy**

If you believe that this document breaches copyright please contact us providing details, and we will remove access to the work immediately and investigate your claim.

*Downloaded from the University of Groningen/UMCG research database (Pure): <http://www.rug.nl/research/portal>. For technical reasons the number of authors shown on this cover page is limited to 10 maximum.*

# DRESSING THE NUCLEON CAUSALLY

Druk: Stichting drukkerij C. Regenboog, Groningen, augustus 2000.

RIJKSUNIVERSITEIT GRONINGEN

# Dressing the nucleon causally

**Proefschrift**

ter verkrijging van het doctoraat in de  
Wiskunde en Natuurwetenschappen  
aan de Rijksuniversiteit Groningen  
op gezag van de  
Rector Magnificus, dr. D.F.J. Bosscher,  
in het openbaar te verdedigen op  
maandag 18 september 2000  
om 14.15 uur

door

**Sergey Kondratyuk**

geboren op 21 november 1971  
te Kramatorsk, Oekraïne

**Promotor** : Prof. dr. R.A.R.L. Malfliet  
**Co-promotor** : Dr. O. Scholten  
**Beoordelingscommissie** : Prof. dr. J.H. Koch  
Prof. dr. A. Lande  
Prof. dr. J.A. Tjon

Part of the work described in this thesis is contained in the following publications.

1. S. Kondratyuk, G. Martinus, and O. Scholten,  
*Electromagnetic off-shell effects in proton-proton bremsstrahlung*,  
Phys. Lett. B **418**, 20 (1998).
2. S. Kondratyuk and O. Scholten,  
*Consistent off-shell  $\pi NN$  vertex and nucleon self-energy*,  
Phys. Rev. C **59**, 1070 (1999).
3. S. Kondratyuk and O. Scholten,  
*Model for the half-off-shell  $\pi NN$  vertex and the nucleon self-energy*,  
in Proceedings of the 8-th International Conference on the Structure of  
Baryons “Baryons’98”, Bonn, Germany, 22 – 26 September 1998, eds.  
D. W. Menze and B. Metsch (World Scientific, Singapore, 1999), p. 589.
4. S. Kondratyuk and O. Scholten,  
*Dressing the nucleon in a dispersion approach*,  
Phys. Rev. C **62**, 025203 (2000).
5. S. Kondratyuk and O. Scholten,  
*Nucleon dressing from dispersion relations*,  
to be published in Nucl. Phys. A (2000).
6. S. Kondratyuk and O. Scholten,  
*Compton scattering in a unitary approach with causality constraints*,  
Nucl. Phys. A **677**, 396 (2000).
7. S. Kondratyuk and O. Scholten,  
*Effects of nucleon dressing in pion photoproduction and Compton scattering*,  
in preparation.



# Contents

<b>1</b>	<b>Introduction</b>	<b>1</b>
<b>2</b>	<b>Dressing in a K-matrix approach</b>	<b>7</b>
2.1	Introduction . . . . .	7
2.2	K-matrix approach . . . . .	8
2.3	Structure of the $\pi NN$ vertex . . . . .	10
2.4	Dressing the $\pi NN$ vertex and nucleon propagator . . . . .	11
2.4.1	Preliminary considerations . . . . .	11
2.4.2	Dressing procedure . . . . .	14
2.4.3	Renormalization and regularization . . . . .	19
2.4.4	The hadronic dressing equations . . . . .	21
2.5	The T matrix up to one loop . . . . .	22
2.6	Numerical example (nucleons and pions only) . . . . .	25
2.6.1	$\pi NN$ form factors (nucleons and pions only) . . . . .	26
2.6.2	Nucleon self-energy (nucleons and pions only) . . . . .	29
2.7	Summary . . . . .	30
	Appendix A: The nucleon self-energy . . . . .	32
	Appendix B: The $\pi NN$ form factors . . . . .	34
<b>3</b>	<b>Pion-nucleon scattering</b>	<b>37</b>
3.1	Introduction . . . . .	37
3.2	K matrix for pion-nucleon scattering . . . . .	37
3.3	Vertices . . . . .	40
3.4	Dressed propagators . . . . .	43
3.5	Changing representation . . . . .	45
3.6	Effects of the dressing . . . . .	46
3.7	Summary . . . . .	52
	Appendix C: Checking the phase factors of loops integrals . . . . .	54



<b>4 Including the photon</b>	<b>57</b>
4.1 Introduction . . . . .	57
4.2 Coupled-channel K-matrix approach . . . . .	58
4.3 Structure of the $\gamma NN$ vertex . . . . .	61
4.4 Dressing the $\gamma NN$ vertex . . . . .	63
4.4.1 Dressing procedure . . . . .	63
4.4.2 The loop integrals . . . . .	64
4.4.3 The electromagnetic dressing equations . . . . .	69
4.5 Nucleon-photon form factors (nucleons, pions and photons only)	70
4.6 Application in Compton scattering . . . . .	74
4.7 Summary . . . . .	77
Appendix D: Projection method . . . . .	79
Appendix E.1: Minimal substitution in configuration space. $\gamma\pi NN$ vertex . . . . .	80
Appendix E.2: Minimal substitution in momentum space . . . . .	86
Appendix E.3: $\gamma\gamma NN$ vertex from minimal substitution . . . . .	88
Appendix F: Gauge invariance of the model . . . . .	90
Appendix G: Cusp from the dispersion integral . . . . .	92
<b>5 Pion photoproduction and Compton scattering</b>	<b>95</b>
5.1 Introduction . . . . .	95
5.2 Full K matrix and dressing procedure . . . . .	96
5.2.1 Vertices . . . . .	97
5.3 Discussion of the results . . . . .	99
5.3.1 Half-off-shell $\gamma NN$ form factors . . . . .	99
5.3.2 Pion photoproduction . . . . .	103
5.3.3 Compton scattering . . . . .	105
5.3.4 Nucleon polarizabilities . . . . .	107
5.4 Summary . . . . .	112
Appendix H: Feynman rules . . . . .	112
<b>Concluding remarks</b>	<b>117</b>
<b>Bibliography</b>	<b>119</b>
<b>Samenvatting</b>	<b>127</b>
<b>Acknowledgments</b>	<b>131</b>

# Chapter 1

## Introduction

All properties of hadrons, as well as their interactions, are believed to be expressible in terms of interactions of more “elementary” particles – quarks and gluons – and thus should be part of the solution of Quantum Chromodynamics. Due to the complexity of this theory, especially at energies of a few hundred MeV, such a solution has not been obtained up to now. However, the full knowledge of the underlying quark-gluon dynamics is not always necessary to describe many reactions involving hadrons. Rather than dealing with quarks and gluons, one often uses effective degrees of freedom which, though possibly having quite a complicated quark structure, are germane to the processes in the given energy range. Such effective approaches have been applied to study various properties of hadrons and their interactions. Thus, much interest has been drawn recently by the subject of nucleon polarizabilities. These fundamental constants characterize deformation of the nucleon in the external electromagnetic field and as such bear an imprint of the composite nature of the nucleon. The polarizabilities are extracted from the cross section of Compton scattering, one of the simplest processes involving the interaction between the nucleon ( $N$ ) and the photon ( $\gamma$ ). The theoretical framework of the present thesis, which falls into the category of dynamical approaches using hadronic degrees of freedom, can be conveniently introduced by considering Compton scattering.

To study Compton scattering  $\gamma N \rightarrow \gamma N$  at energies above the pion ( $\pi$ ) production threshold, one needs to take into account effects of the rescattering of a pion in the intermediate state,  $\gamma N \rightarrow \pi N \rightarrow \gamma N$ , which proceeds via the pion photoproduction reaction  $\gamma N \rightarrow \pi N$ . Pion photoproduction is in turn affected by pion-nucleon scattering through the rescattering  $\gamma N \rightarrow \pi N \rightarrow \pi N$ . Since the pion mass is small,  $m_\pi \approx 138$  MeV, the effects of pion rescattering are significant for understanding of Compton scattering even at

relatively low energies. A unified framework to describe these three reactions is thus necessary.

What constraints should be incorporated in such a coupled-channel approach? First of all, it should be two-body ( $\pi N$ ) unitary, i.e. it should yield a scattering matrix  $S$  which is unitary at energies below the three-body ( $\pi\pi N$ ) threshold. Unitarity takes care that the sum of probabilities of transitions from an initial state to all final states equals unity, even at energies where pion production is possible. Another crucial constraint is gauge invariance, which ensures conservation of electromagnetic current in the reactions involving photons. The next condition is related to the existence of identical particles in the incoming and outgoing states of the reactions  $\gamma N \rightarrow \gamma N$  and  $\pi N \rightarrow \pi N$ . This leads to certain restrictions on the scattering amplitude  $T$  (the T matrix) of these processes, known as the crossing symmetry relations and the invariance with respect to the charge conjugation, space inversion and time reversal (CPT) transformations. The gauge invariance, crossing and CPT symmetries constitute the basis of the low-energy theorem for Compton scattering [1], which gives the cross section up to first order in a small energy of the photon. An important constraint on pion-nucleon interaction at low energies stems from chiral symmetry [2, 3].

Motivated by the above considerations, the approach of this thesis is based on the K-matrix formalism. Such a framework provides an easy way to obtain a T matrix in which all rescattering contributions necessary for two-body unitarity are summed up, which is called unitarization. The kernel in this approach, the K matrix, determines the physical contents of the model. The K-matrix approach is very suitable for satisfying gauge invariance and crossing symmetry constraints for the T matrix: it suffices to construct a K matrix which satisfies these conditions. Another motivation for choosing the K-matrix formalism is that it presents an appropriate framework in which we embed a dynamical model for nucleon form factors relevant for Compton scattering, pion photoproduction and pion-nucleon scattering, so-called half-off-shell form factors.

In addition to the constraints mentioned above, the scattering amplitude should possess certain analyticity properties. It has been shown [4–9] that these properties are essential for reproducing the characteristic energy-dependence of the Compton scattering amplitude near the pion production threshold. From a theoretical point of view, analyticity is related to the condition of causality [10–13, 2]. It is an obvious requirement of causality that detection of a particle cannot precede its emission. Thus, the detectable – real – particles can transport only causal signals. The energy  $E$  and 3-momentum  $\vec{p}$  (together forming the 4-momentum  $p$ ) of a real particle are not independent

but rather confined to the so-called mass shell:

$$p^2 \equiv E^2 - \vec{p}^2 = m^2, \quad (1.1)$$

where  $m$  is the mass of the particle. Complementary to the notion of a real (on-shell) particle is the concept of a virtual (off-shell) particle, which is *defined* by requiring that its energy and 3-momentum do not obey Eq. (1.1). According to this definition, a particle cannot be detected if it is off the mass shell. In spite of being purely abstract objects, such particles do enter in the theoretical picture of scattering processes. In particular, intermediate states through which the scattering proceeds are described in terms of propagation of virtual particles. If a particle is off the mass shell, it may transport noncausal signals, which are unmeasurable (and, in this sense, unphysical). However, the presence of off-shell particles in the theoretical description of the intermediate states must not be in conflict with the observed fact that physical processes are causal and independent of the frame of reference (Lorentz invariant). This requirement is met if the functions characterizing propagation of and interactions among the intermediate off-shell particles have certain analyticity properties.

Every rescattering contribution is represented by a loop integral which can be written in terms of one or several spinor structures each of which is multiplied with a scalar function. In the loop integrals describing the rescattering  $\gamma N \rightarrow \pi N \rightarrow \gamma N$ , for example, the imaginary (pole) and real (principal-value) parts of the scalar functions are associated, respectively, with the propagation of on-shell and off-shell particles in the intermediate state. Due to analyticity properties, the real and imaginary parts of these functions are related through dispersion integrals [11, 14, 12, 15, 2]. Usually, in K-matrix models one does not include contributions from rescattering with off-shell particles in the intermediate state and thus constructs the K matrix as a sum of tree Feynman diagrams in which free propagators and bare vertices are used [16–20]. Such a form of the K matrix implies that, although the pole parts of the loop integrals are included in the T matrix due to unitarization, their principal-value parts are completely ignored. Consequently, the property of analyticity is strongly violated.

In contrast to the traditional approach, we construct the K matrix using vertices and propagators which contain the principal-value parts of a wide class of loop integrals whose pole parts are generated in the T matrix through unitarization. Since the T matrix now contains *both* pole and principal-value parts of these loop integrals, we incorporate some of the analyticity constraints in the K-matrix framework. The inclusion of the principal-value parts in an

iteration procedure constitutes a “dressing” of free propagators and bare vertices with an infinite number of meson loops corresponding to virtual rescattering contributions. The dressed nucleon propagator and the dressed vertices ( $\pi NN$  and  $\gamma NN$ ) are written in terms of scalar functions which are called self-energy functions and form factors, respectively. It is in the calculation of these functions that the analyticity properties are incorporated in the present model. Namely, we employ dispersion relations in the dressing procedure to obtain the real parts of the form factors and self-energy functions, in terms of which the K matrix is constructed.

The implementation of the analyticity properties of the self-energy functions and form factors is a necessary, albeit not sufficient, condition for the analyticity of the full T matrix. Violation of analyticity of the T matrix is mainly due to the fact that the K matrix does not contain the principal-value parts of *all* loop integrals whose pole parts are generated in  $T$ , which is most significant for Compton scattering. This deficiency is mitigated in the physically important region of energies near the pion threshold by adding an appropriate “contact”  $\gamma\gamma NN$  vertex to the K matrix.

Besides K-matrix models, other approaches have been utilized to calculate a two-body unitary S matrix for various reactions. For example, in the context of pion-nucleon scattering, a solution of the Bethe-Salpeter equation [21] has been presented recently [22]. Also, models based on other relativistic wave equations (such as three-dimensional reductions of the Bethe-Salpeter equation) have been developed [23–26]. While, compared to the present model, in these approaches one takes into account both pole and principal-value parts of all loop integrals which are included, the crossing symmetry constraint is usually not preserved. Another difference concerns the extension to channels including photons: unlike in the K-matrix approach, gauge invariance of the kernel of such a wave equation does not automatically lead to gauge invariance of the full amplitude [27–29]. In the present model, we obtain a crossing symmetric and gauge invariant amplitude by constructing a kernel, the K matrix, which possesses these properties.

To obey gauge invariance, we include appropriate  $\gamma\gamma NN$  and  $\gamma\pi NN$  contact terms both in the K matrix and in the dressing procedure for the  $\gamma NN$  vertex. These are constructed using the prescription of minimal substitution. An inherent limitation of minimal substitution is that it allows one to determine unambiguously only that part of a contact terms which is parallel to the photon 4-momentum. We exploit the ambiguity in the transverse part in order to reproduce the behaviour of the pion photoproduction and Compton amplitudes at the pion production threshold.

One of the main objectives of this work is to study effects of the dressing on

observables in Compton scattering, pion photoproduction and pion-nucleon scattering. In particular, we will show that the dressing has a considerable effect on nucleon polarizabilities, and the use of dispersion relations in the dressing procedure is essential for reproducing the observed cusp-like behaviour of the Compton amplitude in the vicinity of pion threshold. In the present work, the effects of nucleon dressing are expressed in terms of the constructed nucleon self-energy functions and  $\pi NN$  and  $\gamma NN$  form factors. One often considers only the dependence of form factors on the 4-momentum squared of the meson or photon. This dependence is important for the description of such reactions as electron-nucleon and nucleon-nucleon scattering. By contrast, both the dressing procedure and the calculation of the observables in our approach are arranged in a way that allows us to deal only with half-off-shell form factors. These form factors depend on the 4-momentum squared of the intermediate off-shell nucleon. Off-shell form factors are a ubiquitous ingredient of many models of hadronic reactions; they have been employed in calculations of proton-proton bremsstrahlung [30], pion photoproduction [27, 28, 31, 29, 33, 20], pion-nucleon scattering [23–25, 31, 18, 26], virtual Compton scattering [34], meson production in nucleon-nucleon collisions [35] and other reactions. Off-shell  $\pi NN$  and  $\gamma NN$  form factors have been studied in the past, using dispersion methods [14, 36, 37], field-theoretical models [38] and one-loop calculations [39]. The main distinguishing features of our dressing model for the half-off-shell form factors are the following. Firstly, we effectively include loop corrections up to infinite order. Secondly, in calculating the loop integrals, we implement analyticity properties of the form factors through the usage of dispersion relations. Thirdly, the form factors and the nucleon self-energy are calculated together, being obtained as a solution of a system of coupled integral equations in terms of which the dressing is formulated. Fourthly, our model for the form factors is developed as a built-in part of the K-matrix approach in which physical observables are calculated.

It is important that we use the same representation of the effective Lagrangian for both the dressing procedure and the calculation of the scattering amplitude. The off-shell 3-point functions (such as the dressed  $\pi NN$  and  $\gamma NN$  vertices considered in this work) and 2-point functions (propagators) as well as 4-point functions (for example, a  $\pi\pi NN$  contact term) may be entirely different in different representations, while the total scattering amplitude is the same [40–45, 13]. In other words, in transforming from one representation to another, all the n-point functions change consistently with each other in such a way that the scattering amplitude, which is built out of

these quantities, remains the same in all representations<sup>1</sup>. The representation-dependence of n-point functions implies, in particular, that the form factors and self-energy functions, which are central to the present approach, are not measurable quantities. Clearly, the scattering amplitude and all its off-shell building blocks should be calculated in the same representation. Each representation corresponds to a particular choice of interacting field coordinates and thus to a particular form of the effective Lagrangian. Using the fact that the full contents of a theory can be equivalently expressed either in terms of interacting fields or in terms of n-point functions [46, 42, 13], we define a representation by imposing constraints on n-point functions. In particular, in the representation used throughout this work 4-point  $\pi\pi NN$  (and higher-point) vertices are excluded.

In view of the special role that the dressed nucleon propagator and the dressed half-off-shell  $\pi NN$  and  $\gamma NN$  vertices play as principal building blocks of the K matrix, the dressing procedure for these 2- and 3-point functions will be described in detail, being in fact the central subject of this thesis. In Chapters 2 and 3 we shall discuss the purely hadronic sector of the model, including the K matrix for the pion-nucleon scattering, the dressed nucleon propagator and the dressed  $\pi NN$  vertex. To explain the dressing procedure retaining its most essential ingredients, in Chapter 2 we shall work in a simplified model including only the nucleon and pion degrees of freedom. This model will be augmented in Chapter 3 by incorporating the  $\Delta$  resonance and the  $\rho$  and  $\sigma$  mesons, providing a satisfactory quantitative description of pion-nucleon scattering up to pion laboratory energies of 400 MeV. The extension of the model to include the photon is described in Chapters 4 and 5, following the same line of presentation as laid out for the hadronic sector. In Chapter 4 the coupled-channel K-matrix approach is outlined and the dressing procedure for the half-off-shell  $\gamma NN$  vertex is explained employing only the nucleon, pion and photon degrees of freedom. Also, in Chapter 4 we describe the procedure of minimal substitution and prove gauge invariance of the model. The full development of the model is presented in Chapter 5, including calculations of observables in pion photoproduction and Compton scattering. A good agreement with experiment is achieved up to photon laboratory energies of 500 MeV. In particular, the calculated scalar and vector polarizabilities of the proton and neutron are shown to be consistent with the measured values. In presenting results of calculations, the main emphasis will be made on studying effects of the developed dressing procedure.

---

<sup>1</sup>For example, one can construct representations in which 3-point off-shell form factors are completely eliminated and their effect on the amplitude is encapsulated in an appropriate 4-point vertex.

## Chapter 2

# Dressing in a K-matrix approach

### 2.1 Introduction

Pion-nucleon scattering at very low energies can be described in the approximation in which the scattering amplitude is given by a sum of tree Feynman diagrams. To go beyond this approximation, one has to take into account pion rescattering contributions, i.e. one has to have a scheme for calculating pion-nucleon loop corrections. We use a two-stage approach to calculate these loop corrections. In the first stage, we solve a system of coupled integral equations for the  $\pi NN$  vertex and nucleon propagator. This solution amounts to a nonperturbative dressing of a bare  $\pi NN$  vertex and the free nucleon propagator with the principal-value parts of loop integrals. The K matrix is constructed as a sum of tree-like diagrams in which, however, the dressed vertices and propagators are used. In the second stage of the approach, the pole parts of the loop integrals are included in the T matrix through unitarization of the K matrix. In both stages of the calculation we adhere to the same model assumptions and use the same representation of the effective Lagrangian. In particular, 4-point  $\pi\pi NN$  vertices are excluded from this representation.

The essential ingredients of the approach are explained in this chapter, where, for clarity, we will work in a simplified model including only nucleons and pions. The most important feature of the dressing procedure for the  $\pi NN$  vertex and nucleon propagator is the use of dispersion relations. There are two main reasons for using such a technique. Firstly, this allows us to formulate the dressing procedure in terms of  $\pi NN$  vertices of the same type as required for the construction of the K matrix, namely, the half-off-shell



vertices. Secondly, through the use of dispersion relations we incorporate certain analyticity constraints in the K-matrix approach. These aspects will be addressed in the description of the dressing procedure in Section 2.4 and in a perturbative analysis of the T matrix in Section 2.5. A numerical example of the calculated half-off-shell  $\pi NN$  form factors and the nucleon self-energy is discussed in Section 2.6.

## 2.2 K-matrix approach

First we give essential formulae of the K-matrix approach [47, 16] in the context of pion-nucleon scattering. The S matrix is expressed in terms of the scattering amplitude  $\mathcal{T}$  (the T matrix) by

$$S = 1 + 2i\mathcal{T} . \quad (2.1)$$

A two-body ( $\pi N$ ) unitary<sup>1</sup> S matrix can be obtained if  $\mathcal{T}$  is a solution of the Bethe-Salpeter equation [21]

$$\mathcal{T} = V + V\mathcal{G}\mathcal{T} , \quad (2.2)$$

where  $V$  is the kernel (potential) and  $\mathcal{G}$  is a  $\pi N$  propagator. Usually,  $V$  is taken as a sum of tree diagrams in which free propagators and bare vertices are used. We also adhere to this assumption throughout.

Any integral over the 4-momenta in  $\mathcal{G}$  can be split into its pole and principal-value parts by writing  $\mathcal{G}$  as the sum

$$\mathcal{G} = i\delta + \mathcal{G}^R , \quad (2.3)$$

where the pole contribution, denoted by  $i\delta$ , describes the propagation of an on-shell nucleon and an on-shell pion, and the regular contribution, denoted by  $\mathcal{G}^R$ , corresponds to the situation when either one or both particles in the intermediate  $\pi N$  state are off the mass shell. The invariant functions in terms of which a  $\pi N$  loop integral is written (for example, self-energy functions or form factors) are purely imaginary or purely real if in this loop one uses  $i\delta$  or  $\mathcal{G}^R$ , respectively.

It is this separation of the pole and principal-value parts that is exploited in the K-matrix formalism. Namely, on defining the K matrix by the equation

$$K = V + V\mathcal{G}^R K , \quad (2.4)$$

---

<sup>1</sup>Unless specified otherwise, the discussion in this thesis will be limited to *two-body* unitarity only.

Eq. (2.2) can be written in the form

$$\mathcal{T} = K + K i\delta \mathcal{T}, \quad (2.5)$$

which can be solved, yielding the central equation of the K-matrix approach,

$$\mathcal{T} = (1 - K i\delta)^{-1} K. \quad (2.6)$$

The S matrix can be obtained in a two step approach: 1) given a potential  $V$ , construct  $K$  according to Eq. (2.4), and 2) solve Eq. (2.5) for the amplitude  $\mathcal{T}$  and use Eq. (2.1) to calculate the S matrix.

Given a hermitian K matrix, Eq. (2.5) can be solved relatively easily – for instance, by expanding  $K$  in partial wave amplitudes and using Eq. (2.6). The simplicity of Eq. (2.5) is due to the fact that it contains  $i\delta$ , thus involving integrals only over the mass shells of intermediate particles. By iterating a hermitian K matrix according to Eq. (2.5), the pole parts of the loop integrals are included which are necessary for the unitarity of the S matrix. To solve Eq. (2.4) is harder since one has to integrate over off-shell 4-momenta of  $\mathcal{G}^R$ . For this reason one usually avoids solving Eq. (2.4) in K-matrix models [16–19] by approximating  $K$  by a sum of tree level diagrams in which free propagators and bare vertices are used, i.e.  $K = V$ , which is equivalent to setting  $\mathcal{G}^R = 0$  (see Eq. (2.4)). Thus, in this approximation only the pole parts of the loop integrals are retained in the T matrix and the principal-value parts are neglected and therefore the loop integrals are written in terms of purely imaginary invariant functions. Having identically zero real parts, such invariant functions do not obey the necessary analyticity constraints which require the real parts to be related to the imaginary parts through a dispersion integral. Consequently, if one sets  $K = V$ , analyticity of the scattering amplitude cannot be fulfilled, which is the main drawback of this common approximation.

In the present approach the K matrix is constructed as the sum of diagrams shown in Fig. 2.1 (throughout this chapter, only the pion and nucleon degrees of freedom are included). The K matrix is explicitly crossing symmetric, being the sum of an uncrossed and crossed diagrams. These diagrams contain *dressed*  $\pi NN$  vertices and nucleon propagators and thus are *not* the usual s- and u-type tree diagrams<sup>2</sup>. In the dressed vertices and propagators, only the real parts of the form factors and self-energy functions enter since Eq. (2.4) requires that only the principal-value parts of loop integrals must be included

---

<sup>2</sup>The tree diagrams with dressed vertices and propagators are sometimes called “skeleton diagrams” [48], to emphasize their difference from the ordinary tree diagrams composed of free propagators and bare vertices.

in  $K$ . The corresponding pole parts are generated in the T matrix through Eq. (2.5). We exclude 4-point  $\pi\pi NN$  (and higher-point) vertices at all stages



Figure 2.1: *The sum of diagrams included in the calculation of the K matrix in the model with nucleons and pions only. The solid lines are nucleons, the dashed lines pions. The nucleon propagators are dressed, as indicated by the thicker lines. The circle represents the dressed  $\pi NN$  vertex.*

of the calculations, and the discussion is carried out solely in terms of the nucleon self-energy and form factors in the  $\pi NN$  vertex. In other words, the effective pion-nucleon interaction Lagrangian is assumed to contain only 3-point  $\pi NN$  vertices. The  $\pi NN$  vertices needed for the construction of the K matrix are so-called half-off-shell vertices, which contain one off-shell nucleon, while the other nucleon and the pion are on-shell.

Once the K matrix is constructed, the T matrix is calculated from Eq. (2.6) using a partial wave decomposition as in Refs. [17, 19], and the S matrix obtained from Eq. (2.1) obeys two-body unitarity exactly.

### 2.3 Structure of the $\pi NN$ vertex

The irreducible (or proper)  $\pi NN$  vertex operator can be defined as the sum of all connected Feynman diagrams with one incoming nucleon (carrying the momentum<sup>3</sup>  $p$ ), one outgoing nucleon ( $p'$ ) and one pion ( $q = p - p'$ ), with the propagators for the external legs stripped away. The most general form compatible with Lorentz covariance and isospin invariance reads<sup>4</sup> [50]

$$\begin{aligned} \Gamma_\alpha(p', p, q) = & \tau_\alpha \left( \gamma^5 G_1(p'^2, p^2, q^2) + \gamma^5 \frac{\not{p}' - m}{m} G_2(p'^2, p^2, q^2) \right. \\ & + \frac{\not{p}' - m}{m} \gamma^5 G_3(p'^2, p^2, q^2) \\ & \left. + \frac{\not{p}' - m}{m} \gamma^5 \frac{\not{p}' - m}{m} G_4(p'^2, p^2, q^2) \right), \end{aligned} \quad (2.7)$$

where  $m$  denotes the nucleon mass and  $\tau_\alpha, \alpha = 1, 2, 3$ , are the isospin Pauli matrices. The full-off-shell form factors  $G_i$  depend on the three Lorentz scalars,

<sup>3</sup>Unless specified otherwise, when saying “momentum”, we shall imply “4-momentum”.

<sup>4</sup>The notation and conventions of Refs. [49] are used throughout this thesis.

$p'^2, p^2$  and  $q^2$ . Usually the situation is considered in which both nucleons are on the mass shell, i.e.  $p'^2 = p^2 = m^2$ , and only the on-shell form factor  $G_1(m^2, m^2, q^2)$  enters in Eq. (2.7). By contrast, to calculate the diagrams for the K matrix in Fig. 2.1 we need half-off-shell  $\pi NN$  vertices, in which the pion and only one of the nucleons are on-shell,  $p'^2 = m^2$  (or  $p^2 = m^2$ ) and  $q^2 = m_\pi^2$ , where  $m_\pi$  denotes the pion mass.

If the operator of Eq. (2.7) acts on the positive energy spinor  $\bar{u}(p')$  to the left, the last two terms in Eq. (2.7) vanish due to the Dirac equation,  $\bar{u}(p') \not{p}' = \bar{u}(p') m$ , and the vertex contains only the half-off-shell form factors  $G_1(m^2, p^2, m_\pi^2)$  and  $G_2(m^2, p^2, m_\pi^2)$ . Similarly, if the initial nucleon is on the mass shell, only  $G_1(p'^2, m^2, m_\pi^2)$  and  $G_3(p'^2, m^2, m_\pi^2)$  are left. Charge conjugation, space inversion and time reversal symmetries allow us to relate these form factors,

$$G_1(p^2, m^2, m_\pi^2) = G_1(m^2, p^2, m_\pi^2), \quad G_3(p^2, m^2, m_\pi^2) = G_2(m^2, p^2, m_\pi^2). \quad (2.8)$$

Hence, we can consider only the vertex with the outgoing on-shell nucleon. Omitting the trivial arguments in  $G_i$ , this vertex can be written

$$\Gamma_\alpha(m, p, m_\pi) = \tau_\alpha \Gamma(m, p, m_\pi) = \tau_\alpha \gamma^5 \left( G_1(p^2) + \frac{\not{p} - m}{m} G_2(p^2) \right), \quad (2.9)$$

where the notation  $\Gamma_\alpha(m, p, m_\pi)$  implies that  $q^2 = m_\pi^2$  and  $\bar{u}(p') \not{p}' = \bar{u}(p') m$  in all expressions for the vertex. Along with Eq. (2.9), we shall use another form for the half-off-shell  $\pi NN$  vertex,

$$\Gamma_\alpha(m, p, m_\pi) = \tau_\alpha \gamma^5 \left( G_S(p^2) + \frac{\not{p} + m}{2m} G_V(p^2) \right), \quad (2.10)$$

where

$$G_S(p^2) = G_1(p^2) - 2G_2(p^2), \quad G_V(p^2) = 2G_2(p^2), \quad (2.11)$$

denote the form factors corresponding to the usual pseudoscalar and pseudovector couplings.

## 2.4 Dressing the $\pi NN$ vertex and nucleon propagator

### 2.4.1 Preliminary considerations

The dressing of the nucleon propagator and  $\pi NN$  vertex with pion-nucleon loops, developed in our approach, is in many respects similar to solving the

Dyson equation [48] coupled with an equation for the vertex. Therefore, a discussion of these equations, presented in this subsection, helps expound the actual dressing procedure, to be described in Subsections 2.4.2–2.4.4.

Solving the Dyson equation is, in principle, equivalent to summing up all pion-nucleon loop corrections to the free nucleon propagator. Part of these can be regarded as loop corrections to a  $\pi NN$  vertex. Thus, such a dressing with the pion-nucleon loops can be conveniently formulated as a system of coupled integral equations for the propagator and the vertex. Unfortunately, to solve these equations in their full complexity is impossible as the general equation for the vertex cannot be written in a closed form: the unknown vertex enters in an infinite number of terms on the right-hand side (r.h.s.) of the equation [11, 51]. Therefore, in formulating a dressing procedure based on the Dyson equation, one has to truncate the r.h.s. of the general equation for the  $\pi NN$  vertex. This results in a closed system of integral equations for the propagator and vertex. As a prelude to our dressing procedure, let us consider such a truncated system of equations for  $\pi NN$  vertex  $\Gamma_\alpha(m, p, m_\pi)$  and nucleon propagator  $S(p)$ :

$$\left\{ \begin{array}{l} \Gamma_\alpha(m, p, m_\pi) = \Gamma_\alpha^0(m, p, m_\pi) - i \int \frac{d^4 k}{(2\pi)^4} \left( \Gamma_\beta(m, p' + k, k) S(p' + k) \right. \\ \quad \left. \times \Gamma_\alpha(p' + k, p + k, m_\pi) S(p + k) \Gamma_\beta(p + k, p, -k) D(k^2) \right), \\ S(p) = S^0(p) + S(p) \Sigma(p) S^0(p), \\ \Sigma(p) = -i \int \frac{d^4 k}{(2\pi)^4} \left( \Gamma_\alpha(p, p + k, k) S(p + k) \Gamma_\alpha^0(p + k, p, -k) \right. \\ \quad \left. \times D(k^2) \right) - (Z_2 - 1)(\not{p} - m) - Z_2 \delta m. \end{array} \right. \quad (2.12)$$

Here  $D(k^2) = (k^2 - m_\pi^2 + i0)^{-1}$  is the pion propagator (which we assume to be free),  $S^0(p) = (\not{p} - m + i0)^{-1}$  the free nucleon propagator,  $\Gamma_\alpha^0(m, p, m_\pi)$  a bare  $\pi NN$  vertex and  $\Sigma(p)$  the nucleon self-energy<sup>5</sup>. The last two terms in the equation for the self-energy are part of the renormalization procedure and will be discussed in Section 2.4.3. The graphical representation of Eqs. (2.12) is shown in Fig. 2.2. These equations describe a nonperturbative dressing of the propagator and vertex with an infinite number of pion-nucleon loops. The second of Eqs. (2.12) is the Dyson equation, and the first is a truncated version of the general integral equation for the vertex function. The equation for the vertex is nonlinear, there being three vertices on the r.h.s.<sup>6</sup> The trun-

<sup>5</sup>For brevity throughout this thesis we use the term “self-energy” for the one-particle irreducible part of the self-energy, which is sometimes also called “the mass operator”.

<sup>6</sup>General properties of such equations have been discussed in Ref. [52].

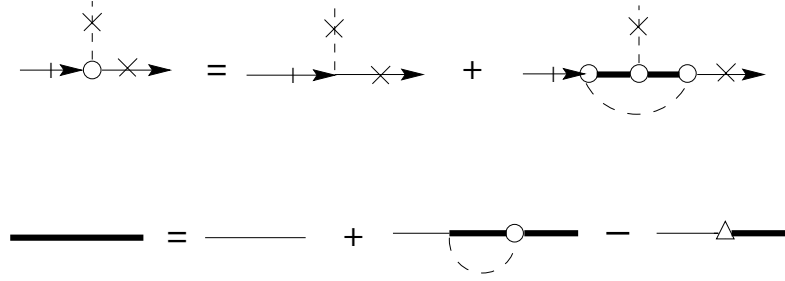


Figure 2.2: *The graphical representation of Eqs. (2.12). The notation is the same as in Fig. 2.1. In addition, the triangle stands for the counterterm contribution to the nucleon self-energy. In the equation for the irreducible vertex the propagator of the incoming off-shell nucleon is stripped away, as indicated by the dash. The lines with crosses are on-shell.*

cation resulting in Eqs. (2.12) can be illustrated at the two-loop level. While all seven terms in Fig. 2.3 should be present on the r.h.s. of the most general equation for the vertex, the lower terms, including the crossed loop and the loop with a dressed pion propagator, are not generated by Eqs. (2.12). There

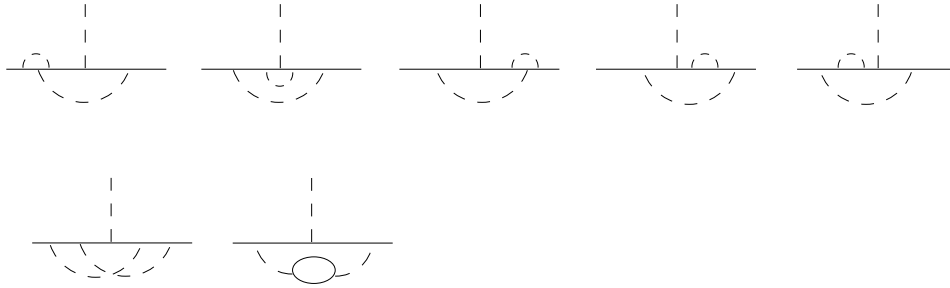


Figure 2.3: *The five upper loops are included in the dressing described by Eqs.(2.12); the lower loops are truncated.*

are two main reasons for the truncation of the crossed loop diagrams in our model. One of the reasons is that, due to the essential two-loop topology of the crossed loop diagrams, their calculation is considerably (if not prohibitively) more involved as compared to the loop diagrams of the kind shown in the upper part of Fig. 2.3. The latter have a one-loop topology, the higher loops being corrections to the vertices and propagators included in the leading loop, and therefore a solution of Eqs. (2.12) can be set up which involves recursive calculations of a one-loop diagram in which at each iteration step vertices and

propagators from the previous iteration step are substituted. The actual iteration procedure applied in this model should, in addition, yield a vertex which is suitable for the application in the K-matrix approach. This requirement is related to the other reason for excluding the crossed loop vertex corrections. Since this reason can be made clear only after the dressing procedure has been explained, we postpone its discussion until Section 2.5. The second diagram in the lower part of Fig. 2.3 is truncated since we do not consider dressing of the pion propagator. This point will be addressed further in Section 2.4.3.

As mentioned earlier, our dressing procedure does not amount to solving Eqs. (2.12) as they stand. Rather, we will show in the following three subsections that the actual equations solved in our approach are given by Eqs. (2.30) which, although having many similarities with, are nevertheless different from Eqs. (2.12). The most important difference stems from the observation that the loop integrals arising from Eqs. (2.12) contain both pole and regular parts, whereas Eq. (2.4) requires that the dressed vertices and propagators used in the K matrix must contain only the regular parts.

### 2.4.2 Dressing procedure

We shall denote the half-off-shell vertices as  $\Gamma_\alpha(p)$  wherever possible, dropping the trivial parameters for brevity. In the dressing procedure we take advantage of the analyticity properties of the form factors and the self-energy functions [11, 14]: at each iteration step, the imaginary parts of these Lorentz invariant functions are obtained by applying cutting rules to the integrals in Eqs. (2.12), and the real parts are calculated through the application of dispersion relations.

Since we do not consider asymptotic states with a nucleon and more than one pion, in applying Cutkosky rules [53, 54] only the one-pion threshold discontinuity of the loop integrals is taken into account and hence the cut nucleon and pion propagators depending on momentum  $p$  are taken as

$$-2\pi i (\not{p} + m) \delta(p^2 - m^2) \theta(p_0) \quad \text{and} \quad -2\pi i \delta(p^2 - m_\pi^2) \theta(p_0), \quad (2.13)$$

respectively, which amounts to putting  $p$  on the mass shell.

The dressing procedure can be explained best by going in some detail through one complete step of the iteration procedure. From the  $n$ th iteration step we have obtained the form factors  $G_{1,2}^n(p^2)$  which define the vertex through Eq. (2.9), and the self-energy functions  $A^n(p^2)$  and  $B^n(p^2)$  which define the dressed propagator, written as

$$S^n(p) = \left( Z_2 (\not{p} - m_B) - \left[ A^n(p^2) \not{p} + B^n(p^2) m \right] + i0 \right)^{-1}, \quad (2.14)$$

where the term in square brackets is the loop contribution  $\Sigma_L^n(p)$  to the self-energy. The parameters  $Z_2$  and  $m_B = m - \delta m$  are renormalization constants as defined in Section 2.4.3.

At the next,  $(n + 1)$ st, iteration step, the imaginary parts of the form factors and the self-energy functions arise from the pole parts of the loop integrals shown in Fig. 2.4. These contributions occur when the momenta in the loops are such that the contour of integration is “pinched” between the poles of the pion and nucleon propagators, hence the cut through these propagators. It should be noted that, as dictated by Eq. (2.4), only the real

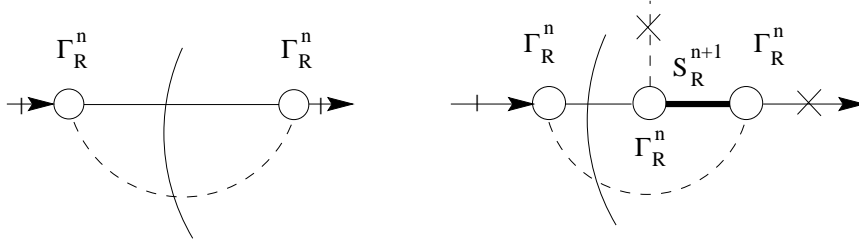


Figure 2.4: The pole contributions of iteration step  $n + 1$  to the self-energy (the left picture) and the vertex (the right picture), as expressed by Eqs. (2.15-2.19). The notation is as in Fig. 2.2, with the subscript  $R$  indicating that the vertex and propagator are calculated using only the real parts of the form factors and self-energy functions. The cuts through pion-nucleon loops are shown explicitly, where the energy flows through the cut from the left to the right.

parts of the form factors and self-energy functions from the previous step  $n$  are retained in calculating the pole contributions at step  $n + 1$ . We will further elaborate on this point later in this subsection and in Section 2.5.

The pole contributions in Fig. 2.4, which will be labelled by the subscript  $I$ , are evaluated using the cutting rules Eq. (2.13). For the self-energy one has

$$\Sigma_I^{n+1}(p) = -\bar{\Gamma}_{\alpha,R}^n(p) I_{pole}(p) \Gamma_{\alpha,R}^n(p), \quad (2.15)$$

where the subscript  $R$  denotes the vertex in which only the real parts of the form factors  $G_{1,2}^n$  are retained, the Dirac conjugated vertex is denoted as  $\bar{\Gamma} \equiv \gamma^0 \Gamma^\dagger \gamma^0$ , and

$$I_{pole}(p) = \frac{1}{8\pi^2} \int d^4k (\not{p} + \not{k} + m) \delta((p+k)^2 - m^2) \theta(p_0 + k_0) \delta(k^2 - m_\pi^2) \theta(-k_0). \quad (2.16)$$

The explicit form for  $I_{pole}(p)$  is given in Appendix A. The imaginary parts of  $A^{n+1}(p^2)$ ,  $B^{n+1}(p^2)$  can now readily be written using Eq. (2.14).



The real parts of the self-energy functions are calculated via the dispersion relations [11],

$$\text{Re } A^{n+1}(p^2) = \frac{\mathcal{P}}{\pi} \int_{W_{th}^2}^{\infty} dp'^2 \frac{\text{Im } A^{n+1}(p'^2)}{p'^2 - p^2}, \quad (2.17)$$

and similar for  $\text{Re } B(p^2)$ . Here  $W_{th} \equiv (m + m_\pi)$  is the one-pion threshold, and  $\mathcal{P}$  denotes the principal-value integral.

The pole term in the loop integral for the vertex reads

$$\Gamma_{\alpha,I}^{n+1}(p) = J_{pole}(p) \Gamma_{\alpha,R}^n(p), \quad (2.18)$$

with

$$\begin{aligned} J_{pole}(p) &= -\frac{(-1)}{8\pi^2} \int d^4k \Gamma_R^n(p' + k) S_R^{n+1}(p' + k) \bar{\Gamma}_R^n(p' + k) (\not{p} + \not{k} + m) \\ &\quad \times \delta((p + k)^2 - m^2) \theta(p_0 + k_0) \delta(k^2 - m_\pi^2) \theta(-k_0), \end{aligned} \quad (2.19)$$

where the last integral is independent of  $p'$ , the momentum of the outgoing on-shell nucleon, as shown in Appendix B. The factor  $(-1)$  in Eq. (2.19) stems from commuting the isospin matrices. The kinematics of the cut vertex loop is such that  $(p' + k)^2 \leq (m - m_\pi)^2$  and therefore the index  $R$  of  $S_R^{n+1}(p' + k)$  in Eq. (2.19) is actually superfluous: the general propagator  $S^{n+1}(p' + k)$  anyway contains only the real parts of  $A^{n+1}((p' + k)^2)$  and  $B^{n+1}((p' + k)^2)$  which have been calculated from Eqs. (2.15–2.17). Casting  $\Gamma_{\alpha,I}^{n+1}(p)$  in the form of Eq. (2.9), the imaginary parts of the form factors  $G_{1,2}^{n+1}(p^2)$  are found (see Appendix B for details).

To construct the real parts of the form factors we take advantage of their analyticity properties [14] and apply the dispersion relations

$$\text{Re } G_i^{n+1}(p^2) = G_i^0(p^2) + \frac{\mathcal{P}}{\pi} \int_{W_{th}^2}^{\infty} dp'^2 \frac{\text{Im } G_i^{n+1}(p'^2)}{p'^2 - p^2}, \quad (2.20)$$

where the first term on the r.h.s. derives from the bare vertex in Eqs. (2.12), which is used at the zeroth iteration step. In the simplified model of this chapter, including pions and nucleons only, the bare vertex is chosen to be purely pseudovector,  $G^0(p^2) \equiv G_V^0(p^2)$ ,

$$\Gamma_\alpha^0(p) = \tau_\alpha \gamma^5 \frac{\not{p} + m}{2m} G^0(p^2), \quad (2.21)$$

in terms of Eq. (2.10). When presenting the full model in the next chapter, it will be shown that an agreement with experiment can be achieved for pion-nucleon scattering only provided the amount of pseudoscalar admixture in

the  $\pi NN$  vertex is small, which is supported by chiral symmetry. We use unsubtracted dispersion relations Eqs. (2.17,2.20) since convergence of the integrals can be guaranteed by the bare form factor (also called the cut-off function)  $G_0(p^2)$ . The function  $G_0(p^2)$  will be further discussed later in this subsection as well as in Subsection 2.4.3 and Section 2.6.

There are a few points that need special stressing here.

- In calculating the imaginary parts for the  $(n + 1)$ st iteration step, we retain only the real parts of the form factors from the  $n$ th step (as pointed out above, the self-energy functions entering in the cut vertex loop are real automatically due to the kinematics). This is required by Eqs. (2.4,2.5). To be specific, if both real and imaginary parts of the form factors  $G_{1,2}^n$  were kept in Eqs. (2.15,2.18,2.19), the on-shell contribution  $i\delta$  would be counted twice for every  $\pi N$  propagator  $\mathcal{G}$  appearing in the one-particle reducible graphs contributing to the T matrix. An illustration of this statement will be given in Section 2.5.

- Except the cuts depicted in Fig. 2.4, any other cuts of the loop diagrams result in vanishing contributions. Firstly, cuts through the circles in Fig. 2.4 would give non-zero contributions only if the vertices  $\Gamma_R^n$  had discontinuities, i.e. if the imaginary parts of the form factors from the iteration step  $n$  were retained. Secondly, since the outgoing nucleon and the pion are on-shell, cuts through any other pair of propagators in the vertex loop give rise to products of  $\delta$ - and  $\theta$ -functions which are zero identically.

- In cutting the self-energy loop diagram in Fig. 2.4, dressed vertices  $\Gamma_R^n$  on both sides of the cut are taken into account. Seemingly, this is in conflict with the Dyson equation in Fig. 2.2, where the second circle (dressed vertex) would lead to a double counting of pion-nucleon loops. However, the presence of the two circles in the *cut* diagram is necessary to sum up *all* contributions from one-pion-nucleon cuts. Perturbatively, this is illustrated in Fig. 2.5: while the diagram with three overlapping loops must be included in the self-energy only once, its pole part should contain all three cut diagrams in Fig. 2.5 (plus terms contributing above the  $\pi\pi N$  threshold and therefore excluded in our approach), which is ensured by the presence of two dressed vertices  $\Gamma_R^n$  in Fig. 2.4.

- Our dressing procedure avoids dealing with the *full*-off-shell vertices present in Eqs. (2.12). Indeed, as can be seen from Fig. 2.4, we need only half-off-shell  $\pi NN$  vertices throughout the iteration process. To calculate the K matrix shown in Fig. 2.1, we also need only this type of vertices.

Through the use of the cutting rules and dispersion relations, properties of unitarity and analyticity are exploited in the dressing procedure. In this connection, the following remarks are in order.

$$\text{Im} \text{---} \text{---} \text{---} = \text{---} \text{---} \text{---} \text{---} \text{---} + \text{---} \text{---} \text{---} \text{---} \text{---} + \text{---} \text{---} \text{---} \text{---} \text{---} + \dots$$

Figure 2.5: A contribution to the pole part of the self-energy diagram depicted in Fig. 2.4. According to the dressing procedure, only the real parts of the form factors describing the uncut part of the diagrams are taken into account, which is indicated by the labels *Re*.

### *Unitarity*

The application of cutting rules Eq. (2.13) for the calculation of  $\text{Im } G_{1,2}(p^2)$ ,  $\text{Im } A(p^2)$  and  $\text{Im } B(p^2)$  at each iteration step implies that we take into account only those contributions to the imaginary parts that come from one-pion-nucleon intermediate states. Although this one-pion threshold contribution is sufficient to ensure the exact two-body unitarity in the K-matrix approach, the dressing procedure for the vertices and propagators can be extended to take into account effects of higher thresholds. This can be done either explicitly, by computing diagrams with two or more loops<sup>7</sup> or effectively, by including heavier baryon and meson degrees of freedom, such as the  $\Delta$  resonance, the  $\rho$  and  $\sigma$  mesons. The latter approach is pursued in the extension of the model, which is the subject of the next chapter.

### *Analyticity.*

In principle, the use of the dispersion relations should guarantee that the form factors and the self-energy functions be analytic in the complex  $p^2$ -plane cut from  $W_{th}^2$  to  $\infty$  along the real axis. However, the actual invariant functions calculated in the model contain also additional singularities of the bare form factor  $G^0(p^2)$  regularizing the dispersion integrals. We neglect the residue contributions from these singularities, which is justified if the bare form factor has a large enough width, so that its singularities are removed from the region of physical interest. This is supported by the tenet that the width of the form factor should be larger than the masses of the mesons included explicitly.

<sup>7</sup>Analyses of two-loop Feynman diagrams in which all particles have non-zero masses have appeared in the literature recently, see [55] and references therein.

### 2.4.3 Renormalization and regularization

The renormalized dressed nucleon propagator can be written as (this form follows from the Dyson equation, see Eqs. (2.12)),

$$S(p) = (\not{p} - m - \Sigma(p) + i0)^{-1}, \quad (2.22)$$

where the nucleon self-energy reads

$$\Sigma(p) = \Sigma_L(p) - (Z_2 - 1)(\not{p} - m) - Z_2 \delta m. \quad (2.23)$$

The first term in Eq. (2.23) is the contribution of pion loops,

$$\Sigma_L(p) = A(p^2)\not{p} + B(p^2)m, \quad (2.24)$$

while the last two terms in Eq. (2.23) come from the counterterms in the Lagrangian.

The construction of the counterterms is based on the usual renormalization procedure [2] as explained by the following example. Let the Lagrangian, written in terms of the “bare” fields, masses and coupling constant (bearing the subscript  $B$ ), be

$$\mathcal{L} = \frac{1}{2}(\partial_\nu \phi_B \partial^\nu \phi_B - m_{\pi,B}^2 \phi_B^2) + \bar{\psi}_B(i\not{\partial} - m_B)\psi_B - \frac{g_B}{2m_B} \bar{\psi}_B \gamma^5 (\not{\partial} \phi_B) \psi_B. \quad (2.25)$$

Defining the renormalized nucleon field  $\psi = Z_2^{-1/2} \psi_B$ , the renormalized nucleon mass  $m = m_B + \delta m$  and the constant  $f/(2m) = g_B Z_2/(2m_B)$ , Eq. (2.25) can be rewritten as

$$\begin{aligned} \mathcal{L} = & \frac{1}{2}(\partial_\nu \phi \partial^\nu \phi - m_\pi^2 \phi^2) + \bar{\psi}(i\not{\partial} - m)\psi \\ & - \left( \frac{f}{2m} \bar{\psi} \gamma^5 (\not{\partial} \phi) \psi - Z_2 \delta m \bar{\psi} \psi - (Z_2 - 1) \bar{\psi}(i\not{\partial} - m)\psi \right). \end{aligned} \quad (2.26)$$

Because we encounter only cut pion lines during the iteration procedure (see Fig. 2.4), we need only the pole contribution of the pion propagator. Those contributions to the dressed  $\pi NN$  vertex and nucleon propagator which contain loop corrections to the pion propagator (such as the second diagram in the lower part of Fig. 2.3) vanish below the three-nucleon threshold and are therefore neglected. Hence, in our approach, the dressing of the pion propagator does not have to be considered and the pion field and mass need not be renormalized,  $\phi = \phi_B$ ,  $m_\pi^2 = m_{\pi,B}^2$ .

The renormalization constants  $Z_2$ ,  $\delta m$  and  $f$  are determined by fixing  $\Gamma_\alpha(m, m, m_\pi)$  and the pole structure of the propagator  $S(p)$ ,

$$\begin{cases} S^{-1}(m) = 0, \\ \text{Res}[S(p), \not{p} = m] = 1, \\ \bar{u}(p') \Gamma_\alpha(m, m, m_\pi) u(p) = \bar{u}(p') \tau_\alpha \gamma^5 g u(p), \end{cases} \quad (2.27)$$

where the last equation can be reduced to  $G_1(m^2) = g$ , the physical pion-nucleon coupling constant (we take  $g = 13.02$  [19]). The left-hand side of this condition is calculated at the kinematically forbidden point, where all the external legs of the vertex are on the mass shell. However, this is of no harm for the renormalization prescription. We could choose any convenient renormalization point as long as the form factors calculated at that point are real (see, e.g., [2], where the freedom of the choice of a renormalization procedure is discussed in general).

In the context of the iteration procedure described in the previous section, the constants  $Z_2$  and  $\delta m$  are chosen to provide the correct pole properties of the *converged* propagator. This implies that the pole location and residue of the propagator are off in the course of the first few iterations. To check that this feature is immaterial for the final result, we applied also another solution procedure. Its main difference from the one described above is that the renormalization of the propagator is done at each iteration step by calculating the renormalization constants  $Z_2$  and  $\delta m$  from the equations

$$Z_2 = 1 + \text{Re} A(m^2) + 2m^2 \frac{d}{d(p^2)} [\text{Re} A(p^2) + \text{Re} B(p^2)] \Big|_{p^2=m^2}, \quad (2.28)$$

$$\delta m = \frac{m}{Z_2} [\text{Re} A(m^2) + \text{Re} B(m^2)] , \quad (2.29)$$

which are the formal solution of the two first equations in Eqs. (2.27), thereby ensuring the correct pole properties at any iteration. We found that both methods lead to identical results for the converged vertex and propagator. The reason is that when convergence has been reached, a nonperturbative solution for the dressed  $\pi NN$  vertices and nucleon propagator has been obtained. From this point of view, the intermediate steps in the iteration procedure are an irrelevant technical detail.

The loop integrals, or rather the dispersion integrals Eqs. (2.17,2.20), will diverge unless a regularization is applied. The cut-off function  $G^0(p^2)$  in the bare  $\pi NN$  vertex, Eq. (2.21), is introduced to regularize the dispersion integrals.  $G^0(p^2)$  is normalized to the constant  $f$  at  $p^2 = m^2$  and must fall off sufficiently fast at infinity. In the numerical example discussed later we use two different functions  $G^0(p^2)$ , see Eqs. (2.31,2.32).

The cut-off function, associated with the bare vertex, is an input of our model. A self-consistent procedure was presented in Ref. [56] to construct meson-nucleon form factors where both nucleons in the vertex are on-shell and the meson is off-shell. There, no phenomenological form factor was needed. The approach of Ref. [56] amounts to solving a vertex equation which is similar to that given in Eqs. (2.12), but without the bare vertex on the r.h.s. It was shown in Ref. [52] that such an equation may have non-zero solutions *only* provided the external nucleons are on the mass shell. By contrast, for the construction of the K matrix in our approach, we need *half-off-shell* form factors in which  $p^2 \neq m^2$ . Therefore, the presence of a bare vertex is necessary in the present dressing procedure in order to obtain a nontrivial solution.

#### 2.4.4 The hadronic dressing equations

When the above dressing procedure has converged, a solution of a system of coupled integral equations has been found. Similar to Eqs. (2.12), these equations describe the summation of an infinite number of pion-nucleon loop corrections to the free nucleon propagator and the bare  $\pi NN$  vertex. In this summation, the provisions necessary for the application of the dressed vertex and propagator in the K-matrix approach are incorporated, as described in the previous two subsections. The system of dressing equations reads

$$\left\{ \begin{array}{l} \Gamma_{\alpha,I}(p) = \frac{-1}{8\pi^2} \int d^4k \left( \Gamma_{\beta,R}(p'+k) S(p'+k) \bar{\Gamma}_{\alpha,R}(p'+k) \right. \\ \quad \times (\not{p} + \not{k} + m) \Gamma_{\beta,R}(p+k) \\ \quad \left. \times \delta((p+k)^2 - m^2) \theta(p_0+k_0) \delta(k^2 - m_\pi^2) \theta(-k_0) \right), \\ \\ \Sigma_I(p) = \frac{-1}{8\pi^2} \bar{\Gamma}_{\alpha,R}(p) \int d^4k \left( (\not{p} + \not{k} + m) \delta((p+k)^2 - m^2) \right. \\ \quad \left. \times \theta(p_0+k_0) \delta(k^2 - m_\pi^2) \theta(-k_0) \right) \Gamma_{\alpha,R}(p), \\ \\ \text{Re } G_i(p^2) = G_i^0(p^2) + \frac{\mathcal{P}}{\pi} \int_{(m+m_\pi)^2}^{\infty} dp'^2 \frac{\text{Im } G_i(p'^2)}{p'^2 - p^2}, \quad i = 1, 2, \\ \\ \text{Re } \left\{ \frac{A}{B} \right\} (p^2) = \frac{\mathcal{P}}{\pi} \int_{(m+m_\pi)^2}^{\infty} dp'^2 \frac{\text{Im } \left\{ \frac{A}{B} \right\} (p'^2)}{p'^2 - p^2}, \end{array} \right. \quad (2.30)$$

where the following notation has been used. The regular and pole parts of the dressed half-off-shell  $\pi NN$  vertex are denoted as  $\Gamma_{\alpha,R}$  and  $\Gamma_{\alpha,I}$ , respectively.

The expression for  $\Gamma_{\alpha,R}(p)$  ( $\Gamma_{\alpha,I}(p)$ ) is given by the r.h.s. of Eq. (2.9) where only the real (imaginary) parts of the form factors  $G_{1,2}(p^2)$  are substituted. The regular part of the nucleon self-energy, denoted as  $\Sigma_R(p)$ , is given by the r.h.s. of Eq. (2.23) with only the real parts of the self-energy functions  $A(p^2)$  and  $B(p^2)$  used in Eq. (2.24). Since the renormalization constants  $Z_2$  and  $\delta m$  are real, the counterterm contribution does not enter in the pole part  $\Sigma_I(p)$  of the self-energy, and thus the expression for  $\Sigma_I(p)$  is read off the r.h.s. of Eq. (2.24) where only the imaginary parts of  $A(p^2)$  and  $B(p^2)$  are retained. The expression for the dressed nucleon propagator is given by the formal solution of the Dyson equation,  $S(p) = [1 - \Sigma(p)S^0(p)]^{-1} S^0(p)$ . The renormalization constants are obtained by solving Eqs. (2.27).

Taking into account that each of the first two (explicitly written) equations in Eqs. (2.30) contains two independent spinor structures, it is seen that the system of dressing equations is neither under- nor over-determined, meaning that Eqs. (2.30) are 8 coupled scalar equations for 8 scalar functions:  $\text{Im}G_1(p^2)$ ,  $\text{Im}G_2(p^2)$ ,  $\text{Im}A(p^2)$ ,  $\text{Im}B(p^2)$ ,  $\text{Re}G_1(p^2)$ ,  $\text{Re}G_2(p^2)$ ,  $\text{Re}A(p^2)$  and  $\text{Re}B(p^2)$ .

## 2.5 The T matrix up to one loop

Although in the T matrix an infinite series of meson loops are included, many features of the model can be illustrated at the one-loop level, see Fig. 2.6. The T matrix can in general be written as a sum of a term which has a nucleon pole, denoted by  $T_P$ , and a regular term,  $T_{NP}$  [57]. Iterating Eq. (2.5) up to second order in  $K$ , we obtain  $T_P$  and  $T_{NP}$  as shown in the top part of Fig. 2.6. The cut pion-nucleon loops imply including only the pole parts of these loop integrals, whose contribution to the T matrix is written in terms of purely imaginary invariant functions. The vertices and propagators that have to be used in the diagrams for  $T_P$  and  $T_{NP}$  are given in the middle part of Fig. 2.6 (up to one loop), where the counterterm contribution, explicitly shown in Fig. 2.2, is assumed to be absorbed in the renormalized propagator. As explained above, only the principal-value parts of the pion-nucleon loops are included in the dressing through the application of the dispersion integrals to the corresponding pole parts. These contributions contain only the real parts of the invariant functions, as indicated explicitly in the figure. On substituting the dressed propagator and vertices in the upper part of Fig. 2.6 and retaining at most one loop corrections, one obtains the lower part of Fig. 2.6.

It is seen that  $T_P^{(1)}$  contains loop corrections to the tree s-type diagram. The pole (imaginary) parts of these loops are due to the iteration of the K

$$\begin{aligned}
\mathbf{K} &= \text{---} \circ \text{---} + \text{---} \circ \text{---} \\
\mathbf{T}_P &= \text{---} \circ \text{---} + \text{---} \circ \text{---} \text{---} \circ \text{---} + \text{---} \circ \text{---} \text{---} \circ \text{---} + \text{---} \circ \text{---} \text{---} \circ \text{---} + 2, 3, \dots \text{ Im loops} \\
\mathbf{T}_{NP} &= \text{---} \circ \text{---} + \text{---} \circ \text{---} \text{---} \circ \text{---} + 2, 3, \dots \text{ Im loops} \\
\text{---} \circ \text{---} &= \text{---} \text{---} + \text{---} \text{---} \text{---} \text{---} \text{---} + 2, 3, \dots \text{ Re loops} \\
\text{---} &= \text{---} + \text{---} \text{---} \text{---} + 2, 3, \dots \text{ Re loops} \\
\mathbf{T}_P^{(1)} &= \text{---} \text{---} + \left[ \text{---} \text{---} \text{---} \text{---} + \text{---} \text{---} \text{---} \text{---} \right] \\
&+ \left[ \text{---} \text{---} \text{---} \text{---} + \text{---} \text{---} \text{---} \text{---} \right] + \left[ \text{---} \text{---} \text{---} \text{---} + \text{---} \text{---} \text{---} \text{---} \right] \\
\mathbf{T}_{NP}^{(1)} &= \text{---} \text{---} + \text{---} \text{---} \text{---} \text{---} + \text{---} \text{---} \text{---} \text{---} + \text{---} \text{---} \text{---} \text{---} + \text{---} \text{---} \text{---} \text{---}
\end{aligned}$$

Figure 2.6: *The diagrams contributing to the T matrix,  $T = T_P + T_{NP}$ , up to one loop, in the model with nucleons and pions only. The notation is the same as in Fig. 2.4. The imaginary parts of the loops (cut loop corrections) are due to iterating the K matrix; the real parts are included through the use of dressed vertices and propagators in the K matrix.*

matrix, while the real parts come from the dressed propagator and vertices used in the K matrix. Note that if the K matrix were constructed with the free propagator and bare vertices (as is done in traditional K-matrix models), the real parts of the loops would not be included in  $T_P^{(1)}$ . It is also clear that if the dressed propagator and vertices contained the pole parts of the loops (or, equivalently, if the imaginary parts of the form factors and self-energy



functions were retained in calculating the K matrix and also in subsequent iteration steps of the dressing procedure), these pole parts would be double-counted in the T matrix.

By contrast with  $T_P^{(1)}$ , in the expansion for  $T_{NP}^{(1)}$  some contributions are not present which one would have expected from a solution of the Bethe-Salpeter equation. In particular only the imaginary part of the first loop correction on the r.h.s. is generated and the corresponding real part is not. The absence of this particular  $\pi\pi NN$  loop correction is one of the approximations intrinsic to our procedure. In principle, it could be included as a contact term (in which case the K matrix should also receive a contribution from the corresponding crossed diagram to keep crossing symmetry) which, for simplicity, has been omitted in the present calculation. The three real contributions to  $T_{NP}^{(1)}$  restore crossing symmetry of the full amplitude. Due to kinematics, the pole terms corresponding to these three loop corrections vanish.

The above analysis becomes quite lengthy at the two-loop level, resulting however in similar conclusions about the structure of the amplitude: both pole and principal-value parts of loop diagrams are included in  $T_P^{(2)}$ , while a limited set of diagrams is included in  $T_{NP}^{(2)}$ . Nevertheless, no double counting is done and crossing symmetry is maintained.

Now we can present the second reason for the truncation of the crossed-loop diagrams of the type shown in the lower part of Fig. 2.3 from the dressing procedure (the first reason – that of calculational tractability – was mentioned in Subsection 2.4.1). Such terms do not have to be included in the dressing procedure because their pole parts are not generated by iterating the K matrix. The diagrams retained in the dressing equations Eqs. (2.30) are sufficient to yield the principal-value parts of exactly the same loop corrections as those whose pole parts are generated in the one-particle reducible diagrams contributing to the T matrix.

The omission of certain one-particle irreducible diagrams in  $T_{NP}$ , such as the principal-value part corresponding to the cut “handbag” diagram in  $T_{NP}^{(1)}$ , precludes the exact analyticity of the T matrix<sup>8</sup>. When considering Compton scattering in Chapter 4, we will show that this violation of analyticity can be mitigated in the important region near the pion production threshold by introducing a  $\gamma\gamma NN$  contact term which accounts for the non-pole contribution of the handbag two-photon diagram.

---

<sup>8</sup>In fact, difficulties in constructing a T matrix possessing all three properties of unitarity, analyticity and crossing symmetry are of a rather general origin, as has been pointed out in Refs. [58].

## 2.6 Numerical example (nucleons and pions only)

To show effects of the dressing, we discuss numerical results for the  $\pi NN$  vertex and nucleon self-energy calculated in the dressing procedure including only nucleons and pions. Two sets of calculations were done, corresponding to the two following cut-off functions  $G^0(p^2)$  in Eq. (2.21):

$$G_I^0(p^2) = f \left[ \frac{(\lambda^2 - m^2)^2}{(\lambda^2 - m^2)^2 + (p^2 - m^2)^2} \right]^2 \quad (2.31)$$

and

$$G_{II}^0(p^2) = f \exp \left[ -\frac{(p^2 - m^2)^2}{2dm^4} \right]. \quad (2.32)$$

The functional dependence of  $G_I^0(p^2)$  is taken from Ref. [24], where it was used as an off-shell form factor in a model for pion-nucleon scattering. We define a half-width  $\Lambda_N^2 = p_{1/2}^2 - m^2$ , where  $p_{1/2}^2$  is the point at which  $G^0(p^2)$  reduces by factor two comparing to its maximum value  $f$ . A typical energy scale introduced by a bare form factor is  $\sqrt{p_{1/2}^2} - m$ . For the calculations with the functions Eq. (2.31) and Eq. (2.32),  $\Lambda_N^2$  equals

$$\Lambda_{N,I}^2(\lambda) = (\lambda^2 - m^2) \sqrt{\sqrt{2} - 1} \quad (2.33)$$

and

$$\Lambda_{N,II}^2(d) = m^2 \sqrt{2d \ln 2}, \quad (2.34)$$

respectively.

The convergence of the iteration procedure was considered achieved at step  $m$  if all the results of steps  $m + 1, \dots, m + 20$  were identical to those of the step  $m$  up to six significant digits. With this strong criterion, convergence was reached after about 100 iterations. We mention that, for example, the self-energy after 10 iterations differs still quite noticeably from the converged result.

We find that the iteration procedure satisfies the above convergence criterion only if  $\lambda \leq \lambda_c \approx 1.7$  GeV for  $G_I^0(p^2)$ , and if  $d \leq d_c \approx 1.65$  for  $G_{II}^0(p^2)$ . The corresponding ‘‘critical’’ values for the half-widths can be inferred from Eq. (2.33) and Eq. (2.34):  $\Lambda_{N,I}^2(\lambda_c) = 1.28$  GeV<sup>2</sup> and  $\Lambda_{N,II}^2(d_c) = 1.33$  GeV<sup>2</sup>. Note that the typical energy scales associated with these bare form factors, 0.53 GeV and 0.55 GeV, respectively, are larger than the mass of the pion,  $m_\pi = 0.138$  GeV. This fact is important as it warrants the omission of the residues of the singularities of the bare form factor from the dispersion relations (see remark *Analyticity* in Section 2.4.2). Even if we imposed a milder

convergence criterion, a convergent solution could be obtained only for half-widths  $\Lambda_N^2$  bounded from above (see the next chapter).

Results of calculations are presented below for the following two cases:

**Case (I)** Using the cut-off function Eq. (2.31), where  $\lambda = \lambda_c = 1.7$  GeV;

**Case (II)** Using the cut-off function Eq. (2.32), where  $d = d_c = 1.65$ .

As stated above, the constants  $f$ ,  $Z_2$  and  $\delta m$  are chosen to satisfy Eqs. (2.27). The values of these constants for cases (I) and (II) are given in Table 2.1. A

Table 2.1: *Values of the renormalization constants  $f$ ,  $Z_2$  and  $\delta m$  for the two choices for the function  $G^0(p^2)$ , Eq. (2.31) and Eq. (2.32).*

Case	$f$	$Z_2$	$\delta m$ (MeV)
(I)	12.70	0.842	-61.4
(II)	12.71	0.842	-58.9

comparison of results obtained with the two different cut-off functions show how these reflect in the final results. The nonperturbative aspect is stressed by comparing the results of the first iteration (basically a one-loop calculation) with those of the converged calculation. It should be borne in mind that the results presented in this chapter are obtained in the simplified version of the model in which only the nucleon and pion degrees of freedom are included. For this reason, we postpone a comparison of pion-nucleon phase shifts with experiment until the next chapter where the results of the full model, including the  $\rho$  and  $\sigma$  mesons and the  $\Delta$  resonance, will be given.

### 2.6.1 $\pi NN$ form factors (nucleons and pions only)

The imaginary parts of the form factors  $G_V(p^2)$  and  $G_S(p^2)$  are shown in Fig. 2.7. The results of calculations for the two cut-off functions in Eq. (2.31) and Eq. (2.32) are shown next to each other. For case (II) the tails of the form factors at large off-shellness are suppressed due to the exponential in the cut-off function. Independent of the choice of the cut-off function, there is a marked difference in the results of the first iteration and the converged results for the pseudovector form factor. The reason for this difference is the small pseudoscalar component of the final form factor. The converged and first iteration results for the pseudoscalar form factor differ much less, as can be seen from the bottom panels of Fig. 2.7.

The real parts of the form factors are shown in Fig. 2.8. The top panels show the pseudovector form factor  $G_V(p^2)$  (the solid line) together with

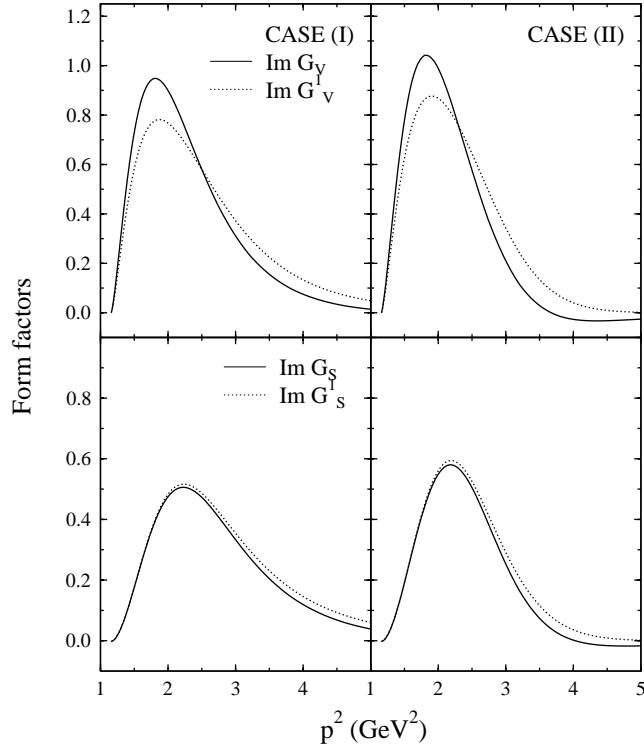


Figure 2.7: *The imaginary parts of the pseudovector and pseudoscalar  $\pi NN$  form factors as functions of the momentum squared of the off-shell nucleon, defined in Eq. (2.10), in the calculation with pion and nucleon degrees of freedom only. The calculations are done using the two cut-off functions Eq. (2.31) (the left panels) and Eq. (2.32) (the right panels). The drawn (dotted) curves show the converged (first iteration) results.*

the zeroth iteration form factor  $G_V^0(p^2)$  (the dotted line) which equals the bare form factors Eq. (2.31) (left) and Eq. (2.32) (right). It is seen that the bulk of  $G_V(p^2)$  is contained already in  $G_V^0(p^2)$ , and only a small part comes from the loop corrections. This manifests itself also in the small difference between the constant  $f$  and the physical coupling constant  $g$ , as can be read from Table 2.1. We conclude that, in the present model, the shape of the converged form factor  $G_V$  depends strongly on the introduced cut-off function. The middle panels of Fig. 2.8 give more insight in the role of the pion dressing. There, the real part of the pseudoscalar form factor  $G_S(p^2)$  of the first iteration (the dashed line) is shown together with the converged result (the solid line). Since the zeroth iteration vertex is chosen purely pseudovector, Eq. (2.21),  $G_S(p^2)$  appears solely due to the dressing. Also shown is the difference  $\text{Re}(G_V(p^2) - G_V^0(p^2))$  which is the dressing contribution to the real

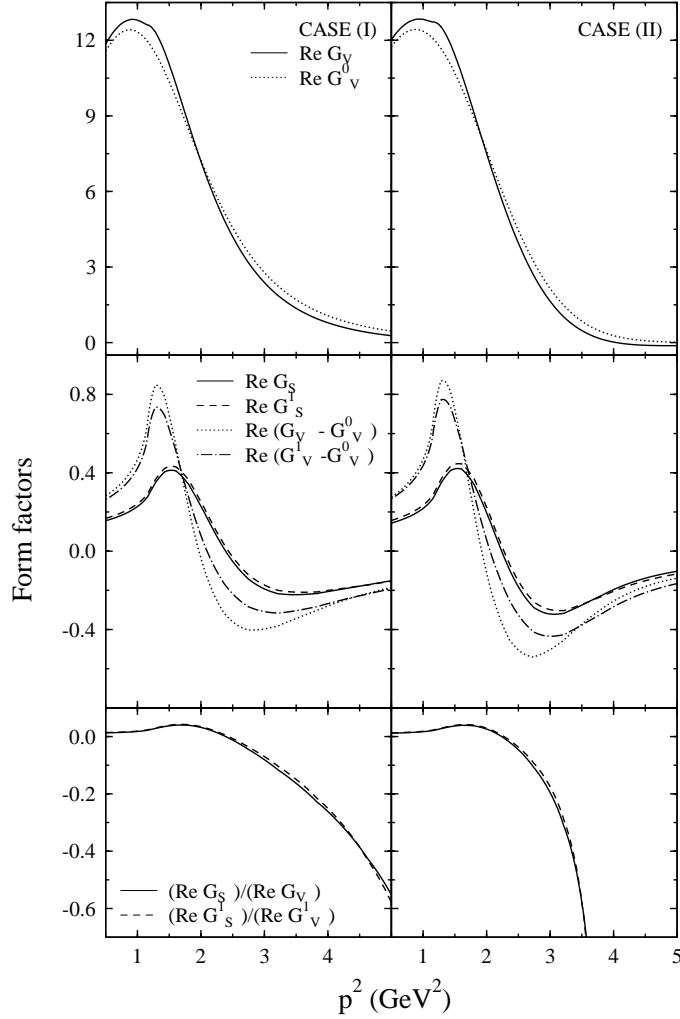


Figure 2.8: *The real parts of the pseudovector and pseudoscalar  $\pi NN$  form factors as functions of the momentum squared of the off-shell nucleon, in the calculation with pion and nucleon degrees of freedom only. In the top panels the zeroth iteration and the converged form factors are given (the left and right panels and the curves are explained in Fig. 2.7 and in the text). In the middle panels the converged results and those of the first iteration are shown for the pseudoscalar form factor and the loop contribution to the pseudovector form factor. The bottom panels show the ratio of the pseudoscalar and pseudovector form factors.*

part of the pseudovector form factor (the dash-dotted and dotted lines for the first iteration and the converged result, respectively). Note that the deviation

of the nonperturbative result from that of the first iteration is considerable for this quantity. The ratio of the real parts of the  $G_S(p^2)$  and  $G_V(p^2)$  form factors is given in the bottom panel of Fig. 2.8. It is small at moderate values of  $p^2$  (e.g.,  $G_S(W_{th}^2)/g$  is about 2 % for both cases (I) and (II)), but becomes larger at higher  $p^2$ . Note that  $G_V(p^2)$  decreases for case (II) faster than for case (I), whereas the behaviour of  $G_S(p^2)$  for the two cases is comparable. This explains why the absolute value of  $(\text{Re}G_S(p^2))/(\text{Re}G_V(p^2))$  grows faster for case (II) than for case (I).

We remark that admixtures of the pseudovector and pseudoscalar pion-nucleon couplings have been studied in the past in connection with the  $NN$ ,  $\pi N$  scattering processes and pion photoproduction, where the vertex has been determined by adjusting phenomenological parameters to fit data (see Refs. [32, 24, 16, 28]). In those calculations the admixture is assumed to be constant. Instead, the present results indicate that the ratio is strongly dependent on the momentum of the off-shell nucleon. Evidence for considerable pseudoscalar admixtures for far off-shell momenta has also been observed in calculations of pion photoproduction [33].

### 2.6.2 Nucleon self-energy (nucleons and pions only)

The imaginary and real parts of the self-energy functions  $A(p^2)$  and  $B(p^2)$  are shown in Figs. 2.9 and 2.10, respectively. The solid (dotted) lines are the converged (first iteration) results. One can see that these functions approach zero faster for case (II) than for case (I). This is entailed by the softer behaviour of  $G_V^0(p^2)$  for case (II) as opposed to case (I) (see Fig. 2.8). The difference between the converged results and those of the first iteration is substantial, especially for the function  $B(p^2)$ . The on-shell value  $\Sigma_L(m) = m(A(m^2) + B(m^2)) = Z_2\delta m$  is negative and equals  $-61.4$  MeV for case (I) and  $-58.9$  MeV for case (II), see Table 2.1. Please note that had we chosen smaller values for the cut-off width, these self-energy corrections would have been less. For comparison, we mention that the contribution to the nucleon mass shift from one-pion loop calculated in the baryon chiral perturbation theory yields a nucleon mass shift of about  $-15$  MeV [59].

Having obtained  $A(p^2)$  and  $B(p^2)$ , one can calculate the spectral function of the self-energy  $T(W)$  from Eq. (A.9). Fig. 2.11 shows this spectral function for the two cases considered (the upper and lower panels). The dotted and dash-dotted lines are, respectively, the first iteration and the converged results. In spite of the fact that  $\text{Im}B^1(p^2)$  differs considerably from  $\text{Im}B(p^2)$ , having the opposite sign at some momenta squared (see Fig. 2.9), the spectral function remains positive for all iterations (as it should). The

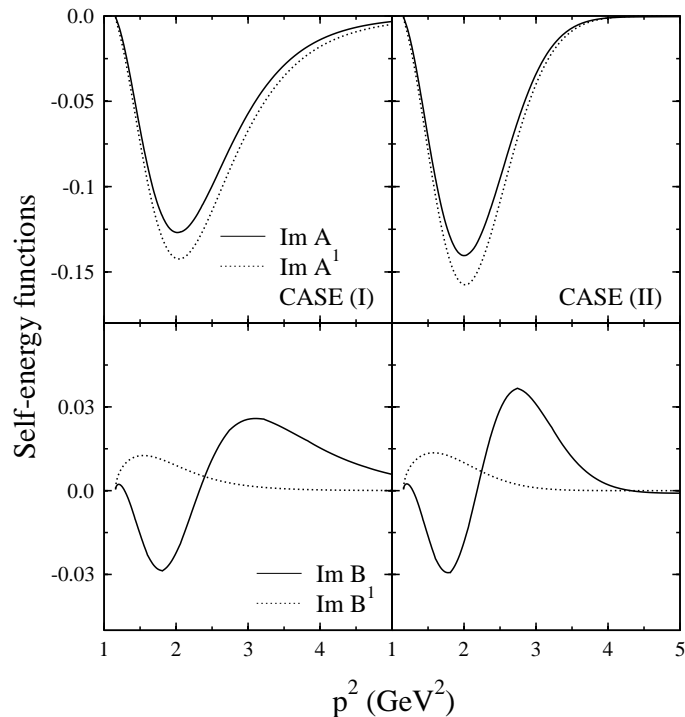


Figure 2.9: *The imaginary parts of the self-energy functions  $A(p^2)$  and  $B(p^2)$ , as defined in Eq. (2.24), calculated in the model with nucleon and pions only. The explanation of the panels and curves is the same as in Fig. 2.7.*

spectral function of the nucleon propagator (which is simply related to the self-energy spectral function  $T$ ) was considered in Refs. [60] whose approach is, however, different from the present work. In particular, there the vertex was parametrized rather than dressed simultaneously with the nucleon propagator.

## 2.7 Summary

We have presented the dressing procedure for the nucleon self-energy and the half-off-shell  $\pi NN$  vertex, which are the principal building blocks of the K matrix for pion-nucleon scattering. We have utilized a simplified model comprising the degrees of freedom which are most essential to explain the procedure, the nucleon and the pion. The dressing is a converging iteration scheme based on a recursive application of cutting rules and dispersion rela-

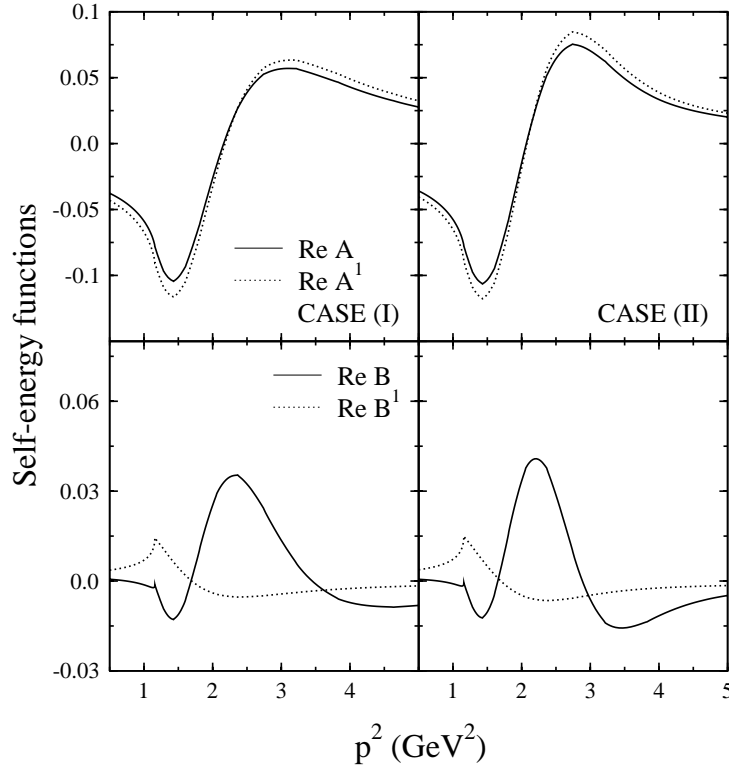


Figure 2.10: *The same as in Fig. 5, but for the real parts of  $A(p^2)$  and  $B(p^2)$ .*

tions to calculate the principal-value parts of pion loop corrections to a bare form factor. The latter has to be introduced as part of the regularization procedure.

We observe a large difference between one-loop and the converged results. We found that in our model there exists a critical half-width below which a nonperturbative solution for the  $\pi NN$  form factors and nucleon self-energy functions can be obtained. Even though the dressed vertex near threshold is largely pseudovector in nature, we find a pseudoscalar admixture which depends on the momentum squared of the off-shell nucleon.

As a result of constructing the K matrix out of the *dressed*  $\pi NN$  vertices and nucleon propagators, the s-type diagram for the T matrix contains *both* pole and principal-value parts of pion-nucleon corrections. Since these principal-value parts are calculated from dispersion integrals in the dressing procedure, we incorporate constraints due to the analyticity properties of the form factors and self-energy functions. Lest analyticity of the solution of the



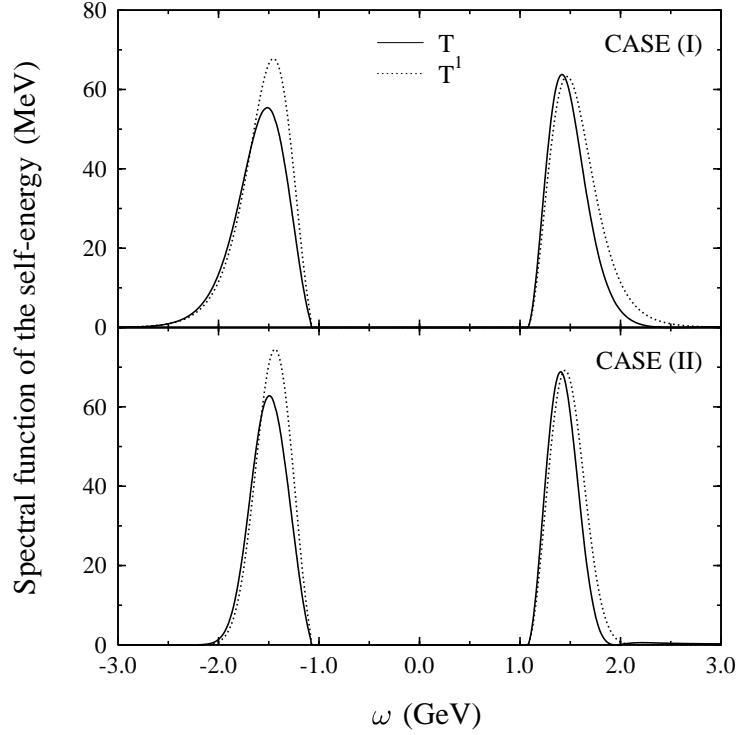


Figure 2.11: *The self-energy spectral function  $T(W)$  as function of invariant mass of the nucleon, obtained in the model with nucleons and pions only. The curves are explained in the text.*

dressed equations be broken, we choose the width of the bare form factor larger than the scale due to the explicitly included mesons (which is the pion, in the model of this chapter).

## Appendix A: The nucleon self-energy

To calculate the imaginary parts of the self-energy functions, we need to evaluate the pole contribution  $I_{pole}(p)$  as given in Eq. (2.16). In general the integral can be expressed as  $I_{pole}(p) = \gamma_\mu \tilde{I}_1^\mu(p) + \tilde{I}_2(p)$ , where  $\tilde{I}_1^\mu$  and  $\tilde{I}_2$  are scalars in spinor space. Since the only Lorentz vector in the problem is  $p^\mu$ ,  $\tilde{I}_1^\mu$  must be proportional to it,  $\tilde{I}_1^\mu(p) = ((\tilde{I}_1 \cdot p)/p^2) p^\mu$ . Hence, one may write  $I_{pole}(p) = \not{p} I_1(p^2) + I_2(p^2)$ , where  $I_1(p^2) = (\tilde{I}_1 \cdot p)/p^2$  and  $I_2(p^2) = \tilde{I}_2(p^2)$  are

Lorentz scalars. They equal

$$I_1(p^2) = \frac{p^2 + m^2 - m_\pi^2}{32\pi p^4} r(p^2) \theta(p^2 - (m + m_\pi)^2), \quad (\text{A.1})$$

$$I_2(p^2) = \frac{m}{16\pi p^2} r(p^2) \theta(p^2 - (m + m_\pi)^2). \quad (\text{A.2})$$

where  $r(p^2) = \sqrt{\lambda(p^2, m^2, m_\pi^2)}$ , with the Källén function defined as  $\lambda(x, y, z) \equiv (x - y - z)^2 - 4yz$ . Using these expressions and introducing the shorthand notation,  $g_{1,2} \equiv \text{Re}G_{1,2}^n(p^2)$ , the imaginary parts of the self-energy functions can be determined from Eqs. (2.14,2.15,2.9),

$$\begin{aligned} \text{Im}A^{n+1}(p^2) &= 3 \left( - (g_1 - g_2)^2 I_1(p^2) + 2(g_1 - g_2)g_2 \frac{I_2(p^2)}{m} - g_2^2 \frac{p^2 I_1(p^2)}{m^2} \right) \\ &= -\frac{3}{32\pi p^2} r(p^2) \theta(p^2 - (m + m_\pi)^2) \left\{ \frac{p^2 + m^2 - m_\pi^2}{p^2} g_1^2 \right. \\ &\quad \left. + \left( \frac{5p^2 + m^2 - m_\pi^2}{p^2} + \frac{p^2 + m^2 - m_\pi^2}{m^2} \right) g_2^2 \right. \\ &\quad \left. - 2 \frac{3p^2 + m^2 - m_\pi^2}{p^2} g_1 g_2 \right\}, \quad (\text{A.3}) \end{aligned}$$

$$\begin{aligned} \text{Im}B^{n+1}(p^2) &= 3 \left( (g_1 - g_2)^2 \frac{I_2(p^2)}{m} - 2(g_1 - g_2)g_2 \frac{p^2 I_1(p^2)}{m^2} + g_2^2 \frac{p^2 I_2(p^2)}{m^3} \right) \\ &= \frac{3}{16\pi p^2} r(p^2) \theta(p^2 - (m + m_\pi)^2) \\ &\quad \times \left\{ g_1^2 + \frac{2p^2 + 2m^2 - m_\pi^2}{m^2} g_2^2 - \frac{p^2 + 3m^2 - m_\pi^2}{m^2} g_1 g_2 \right\}. \quad (\text{A.4}) \end{aligned}$$

The factor 3 in the above equations results from the multiplication of the isospin matrices,  $\tau_\alpha \tau_\alpha = 3$ , and the minus sign in front of  $I_1(p^2)$  arises from commuting the  $\gamma^5$  matrices. The real parts of  $A^{n+1}(p^2)$  and  $B^{n+1}(p^2)$  are found by applying dispersion relations Eq. (2.17), where all integrals are done numerically.

The inverse of the dressed nucleon propagator is written as (retaining only the real parts of the self-energy functions)

$$S_R^{-1}(p) = Z_2(\not{p} - m_B) - \left( \text{Re}A(p^2)\not{p} + \text{Re}B(p^2)m \right) = \alpha(p^2) \left( \not{p} - \xi(p^2) \right), \quad (\text{A.5})$$

where

$$\alpha(p^2) = Z_2 - \text{Re}A(p^2), \quad \xi(p^2) = \frac{Z_2(m - \delta m) + \text{Re}B(p^2)m}{\alpha(p^2)}. \quad (\text{A.6})$$

To introduce the spectral function of the self-energy, we first write the loop contribution to the self-energy in the form

$$\Sigma_L(p) = \zeta(W)P^+(p) + \zeta(-W)P^-(p), \quad (\text{A.7})$$

where  $P^\pm(p) = (\pm\not{p} + W)/(2W)$  are the projectors on positive- and negative-energy states of the nucleon with the invariant mass  $W = \sqrt{p^2} > 0$ . The self-energy spectral function can now be defined as [11]

$$T(\pm W) = \mp \frac{1}{\pi} \text{Im} \zeta(\pm W). \quad (\text{A.8})$$

Equating the r.h.s. of Eq. (A.7) and the form of  $\Sigma_L(p)$  from Eq. (2.24) yields for the spectral function

$$T(\pm W) = -\frac{1}{\pi} (W \text{Im} A(p^2) \pm m \text{Im} B(p^2)). \quad (\text{A.9})$$

## Appendix B: The $\pi NN$ form factors

The calculation of the imaginary parts of the form factors can be reduced to computing one-dimensional integrals which are done numerically. First consider the integral on the r.h.s. of Eq. (2.19).  $J_{pole}$  can be split as  $J_{pole} = \gamma_\mu \tilde{J}_1^\mu + \tilde{J}_2$ , where  $\tilde{J}_1^\mu$  and  $\tilde{J}_2$  are scalars in spinor space, and a possible rank-2 tensor structure vanishes since  $\bar{u}(p')\not{p}' = \bar{u}(p')m$ . For the same reason  $\tilde{J}_1^\mu$  is proportional to only the vector  $p^\mu$ . Following the same argumentation as used in Appendix A, we can write

$$J_{pole} = \not{p} J_1 + J_2, \quad (\text{B.1})$$

where we have introduced the Lorentz scalars  $J_1$  and  $J_2$ . To write down expressions for  $J_1$  and  $J_2$ , we define the following functionals:

$$K_1[f] \equiv \int_{-1}^1 dx \frac{f(W'^2)}{\alpha(W'^2)}, \quad (\text{B.2})$$

$$K_2[f] \equiv \int_{-1}^1 dx x \frac{f(W'^2)}{\alpha(W'^2)}, \quad (\text{B.3})$$

$$K_3[f] \equiv \int_{-1}^1 dx \frac{f(W'^2)}{\alpha(W'^2)(W'^2 - \xi^2(W'^2))}, \quad (\text{B.4})$$

$$K_4[f] \equiv \int_{-1}^1 dx x \frac{f(W'^2)}{\alpha(W'^2)(W'^2 - \xi^2(W'^2))}, \quad (\text{B.5})$$

where  $f$  is any function for which the integrals exist,  $\alpha$  and  $\xi$  are given by Eq. (A.6) for the  $(n+1)$ st iteration, and

$$W'^2 = (p' + k)^2 = m^2 + m_\pi^2 - \frac{p^4 - (m^2 - m_\pi^2)^2}{2p^2} - \frac{r(p^2)^2}{2p^2} x, \quad (\text{B.6})$$

with  $x$  being the cosine of the polar angle between the three vectors  $\vec{p}'$  and  $\vec{k}'$ . Now  $J_1$  and  $J_2$  can be written as

$$\begin{aligned} J_1 \equiv J_1(p^2) = & - \left\{ (K_1 - K_2) \left[ \frac{p^2 + m^2 - m_\pi^2}{2p^2} (g_1 g_2 + \frac{\xi - 4m}{2m} g_2^2) + \frac{g_2^2}{2} \right] \right. \\ & \left. + (K_3 - K_4) \left[ \left( \frac{p^2 + m^2 - m_\pi^2}{p^2} \frac{\xi}{4m} - \frac{m^2 - m_\pi^2}{2p^2} \right) (m g_1 + (\xi - m) g_2)^2 \right] \right\} \\ & \times \frac{r(p^2)}{16\pi p^2} \theta(p^2 - (m + m_\pi)^2) \end{aligned} \quad (\text{B.7})$$

and

$$\begin{aligned} J_2 \equiv J_2(p^2) = & - \left\{ (K_1 + K_2) \left[ \left( \frac{\xi - 4m}{2m} + \frac{p^2 + m^2 - m_\pi^2}{4m^2} \right) g_2^2 + g_1 g_2 \right] \right. \\ & \left. + (K_3 + K_4) \left[ \left( \frac{\xi - 2m}{2m} + \frac{p^2 + m^2 - m_\pi^2}{4m^2} \right) (m g_1 + (\xi - m) g_2)^2 \right] \right\} \\ & \times \frac{r(p^2)}{16\pi p^2} \theta(p^2 - (m + m_\pi)^2). \end{aligned} \quad (\text{B.8})$$

Since for a given  $f$  in Eqs. (B.2-B.5) the  $K_i$  are functions of  $p^2$  only, Eqs. (B.7, B.8, B.1) show that  $J_{pole}$  depends only on the Lorentz vector  $p$  and does not depend on  $p'$  as it might appear from the r.h.s. of Eq. (2.19).

Using Eqs. (B.1, 2.18, 2.9), one obtains for the imaginary parts of the form factors:

$$\text{Im} G_1^{n+1}(p^2) = g_1 J_2(p^2) + \left( \frac{m^2 - p^2}{m^2} g_2 - g_1 \right) J_1(p^2) \quad (\text{B.9})$$

and

$$\text{Im} G_2^{n+1}(p^2) = g_2 J_2(p^2) + (g_2 - g_1) J_1(p^2), \quad (\text{B.10})$$

where  $J_1$  and  $J_2$  are given by Eqs. (B.7) and (B.8). Finally, Eq. (2.20) is applied to obtain the real parts of the the form factors at the  $(n+1)$ st iteration step.



# Chapter 3

## Pion-nucleon scattering

### 3.1 Introduction

In this chapter the full development of the K-matrix approach to pion-nucleon scattering is presented, including the dressing procedure for the  $\pi NN$  vertex and nucleon propagator. In addition to the nucleon and pion, we include other low-lying meson and baryon degrees of freedom, in particular, the  $\rho$  and  $\sigma$  mesons and the  $\Delta$  resonance, which are important for a realistic description of  $\pi N$  scattering at intermediate energies [23–26, 16–19, 31]. The associated coupling parameters are fixed by considering phase shifts for pion-nucleon scattering. The requirement that the dressing procedure converges for a given bare  $\pi NN$  form factor puts additional constraints on the allowed range of these parameters. In discussing the calculated phase shifts, we focus primarily on effects of the dressing.

As already stated, in this work all calculations are performed in a particular representation in which only 2- and 3-point functions are nontrivial and 4-point  $\pi\pi NN$  functions are absent. In Section 3.5 we construct a different representation in which the nucleon self-energy vanishes and no 4- or higher-point vertices are introduced. While leading to the same observables in virtue of the equivalence theorem, this representation is convenient for interpreting the effects of nucleon dressing in terms of calculated effective  $\pi NN$  vertices. In particular, we will show that the dressing leads to rather soft form factors.

### 3.2 K matrix for pion-nucleon scattering

The full K matrix for pion-nucleon scattering has the form shown in Fig. 3.1. The K matrix is composed of dressed half-off-shell  $\pi NN$  vertices

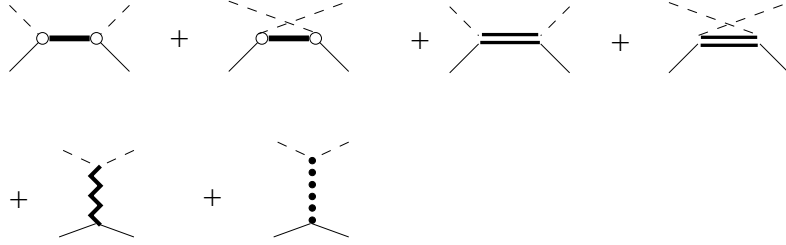


Figure 3.1: *The sum of diagrams included in the calculation of the K matrix for pion-nucleon scattering. The solid lines are nucleons, the dashed lines pions, the solid double-lines  $\Delta$ s; the zigzag and dotted lines represent  $\rho$  and  $\sigma$  mesons, respectively. The intermediate propagators are dressed, as indicated by the thicker lines. The circle represents the dressed  $\pi NN$  vertex.*

and dressed nucleon propagators as well as dressed propagators of the  $\Delta$ ,  $\rho$  and  $\sigma$ . In these vertices and propagators, only the real parts of the form factors and self-energy functions are kept, as dictated by Eq. (2.4). The corresponding imaginary parts are generated in the T matrix by iterating the K matrix in Eq. (2.5).

Since, besides the nucleon and pion, other particles have been included in the K matrix, the dressing of the nucleon self-energy and  $\pi NN$  vertices must also include contributions from these additional degrees of freedom. The resulting system of coupled integral equations, shown diagrammatically in Fig. 3.2, is a generalization of Eqs. (2.30) discussed in the previous chapter. At every iteration step of the dressing procedure, the imaginary parts of the  $\pi NN$  form factors and nucleon self-energy functions are obtained by applying cutting rules [53, 54] to the loop integrals: for a cut particle propagator which depends on momentum  $p$ , we substitute

$$-2\pi i \rho(p) \theta(p_0), \quad (3.1)$$

where  $\rho(p)$  denotes the spectral function of the propagator. For the stable particles (nucleon and pion), the latter is taken as a  $\delta$ -function, see Eq. (2.13). The spectral functions of the  $\Delta$  resonance and  $\rho$  and  $\sigma$  mesons are proportional, with a coefficient  $-1/\pi$ , to the imaginary parts of the corresponding dressed propagators. These imaginary parts are calculated from cut one-loop diagrams, as explained below and in Section 3.4. In calculating the pole contributions to the loops at the  $(n+1)$ st iteration step, we retain only real parts of the form factors and self-energies from the previous step  $n$ , as required by Eq. (2.4). The real parts of the  $\pi NN$  form factors and nucleon self-energy

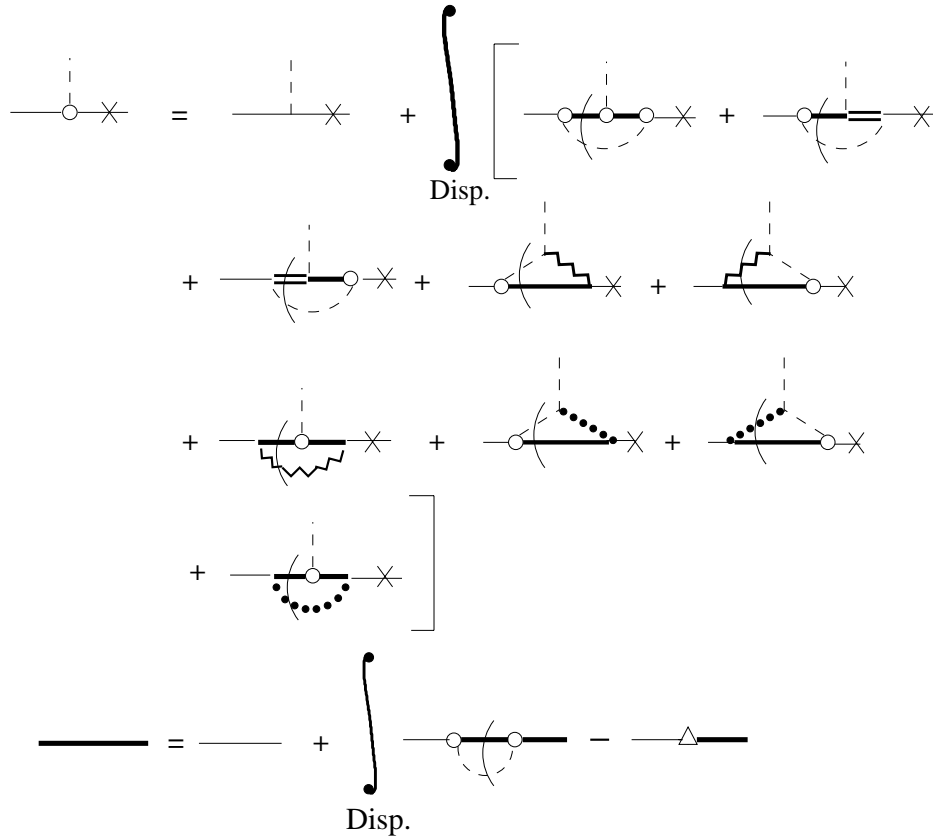


Figure 3.2: *Diagrammatic representation of the dressing procedure for the irreducible half-off-shell  $\pi NN$  vertex and nucleon propagator. The notation is the same as in Fig. 3.1. The crossed lines correspond to the outgoing on-shell nucleon (the pion is on the mass shell throughout). The cuts applied at each iteration step to calculate the pole contributions of the diagrams are shown explicitly. The triangle in the second equation is the counterterm contribution to the nucleon self-energy. The symbols of integral indicate that dispersion relations are applied at each iteration step.*

functions are calculated at every iteration step by applying dispersion relations Eqs. (2.17) and (2.20) to the imaginary parts. This procedure is repeated until a converged solution is reached. We use a normalized root-mean-square difference  $d_n$  between two subsequent iteration steps  $n$  and  $n + 1$  for the form factors and self-energy functions; the convergence criterion is that  $d_n < 10^{-4}$  for at least a hundred iteration steps. As zeroth iteration step the free nucleon propagator and a  $\pi NN$  vertex with the bare form factors in Eq. (3.2)



are taken. It is worth pointing out that the  $K$  matrix contains only  $\pi N$  asymptotic states, which is sufficient for the exact two-body unitarity. By iterating this  $K$  matrix in the unitarization procedure, Eq. (2.5), the pole contributions of the 3rd, 5th, 6th, 8th and 9th cut loop diagrams in Fig. 3.2 are not generated in the  $T$  matrix, although the corresponding principal-value parts are included through the dressed  $\pi NN$  vertex.

The dressing procedure amounts to an inclusion of regular parts of meson loop corrections to the bare vertices and free propagators. Since the nucleon propagator and the  $\pi NN$  vertex are dressed simultaneously in the converging iteration procedure, the nucleon self-energy<sup>1</sup> comprises an infinite number of loops, as does the  $\pi NN$  vertex. Unlike the  $\pi NN$  vertex, the vertices including the  $\Delta$ ,  $\rho$  and  $\sigma$  are not dressed, and the self-energies of the  $\Delta$ ,  $\rho$  and  $\sigma$  are obtained through an inclusion of a one-loop correction (a  $\pi N$  loop in the case of the  $\Delta$  and a  $\pi\pi$  loop in the case of the  $\rho$  and  $\sigma$ ). The dressing of the  $\Delta$ ,  $\rho$  and  $\sigma$  is explained in more detail in Section 3.4. The structure of the vertices used is described in the next section.

### 3.3 Vertices

#### $\pi NN$ vertex

The bare  $\pi NN$  vertex in the dressing procedure is chosen in the general form given by Eq. (2.10), i.e. containing both pseudovector and pseudoscalar form factors,

$$G_V^0(p^2) = f(1 - \chi)G^0(p^2), \quad G_S^0(p^2) = f\chi G^0(p^2) \quad (3.2)$$

with

$$G^0(p^2) = \exp\left[-\ln 2 \frac{(p^2 - m^2)^2}{\Lambda_N^4}\right]. \quad (3.3)$$

The functional form of the bare form factor  $G^0(p^2)$  is the same as in Eq. (2.32).  $\Lambda_N^2$  is the half-width of the bare form factor, the parameter  $\chi$  is the amount of pseudoscalar admixture in the bare vertex, and  $f$  is a bare coupling constant. The latter is fixed from the renormalization condition imposed on the dressed vertex at the on-shell point, see Eqs. (2.27), where it should be noted that, because of the coupled structure of the dressing equations in Fig. 3.2, the renormalization of the vertex and that of the propagator are done simultaneously.

---

<sup>1</sup>We remind the reader that throughout this thesis the term “self-energy” is used for the one-particle irreducible part of the full self-energy.

The role of the bare  $\pi NN$  vertex is two-fold. On the one hand, it serves as the driving vertex at the zeroth iteration step. On the other hand, it is used for regularization of the dispersion integrals. The bare vertex is supposed to encapsulate the physics due to degrees of freedom not included explicitly in the dressing.

### Vertices with $\Delta$ , $\rho$ and $\sigma$

In principle, the dressing procedure should also apply to vertices with the  $\Delta$  resonance as well as with the  $\rho$  and  $\sigma$  mesons. In such an approach one would have to solve a system of 10 coupled equations, instead of the system of two equations shown in Fig. 3.2. In addition, most of these 10 operator equations would contain several scalar equations, depending on the structure of the corresponding vertices and propagators (similar to the equations in Fig. 3.2 containing implicitly 8 scalar equations, see Section 2.4.4). Such a calculation is beyond the present scope.

For this reason, for all other vertices except  $\pi NN$  we ignore the dressing and restrict ourselves to one particular Lorentz covariant form. With each vertex a form factor is associated which is required for regularization of the loop integrals.

The  $\sigma\pi\pi$  and  $\rho\pi\pi$  vertices for a  $\sigma$  or  $\rho$  meson with momentum  $p = q + q'$  are taken as<sup>2</sup>

$$(\Gamma_{\rho\pi\pi})_{\alpha\beta\gamma}^{\nu} = (\hat{e}_{\alpha\beta\gamma}) i g_{\rho\pi\pi} F_{\rho}(p^2) \left[ k^{\nu} - \frac{(p \cdot k)}{p^2} p^{\nu} \right], \quad (3.4)$$

$$(\Gamma_{\sigma\pi\pi})_{\alpha\beta} = -i \frac{g_{\sigma\pi\pi}}{m_{\pi}} F_{\sigma}(p^2) \delta_{\alpha\beta} (q \cdot q'), \quad (3.5)$$

where  $q$  and  $q'$  are the momenta of the outgoing pions with isospin indices  $\alpha$  and  $\beta$ , respectively,  $k = q - q'$  and  $(\hat{e}_{\alpha\beta\gamma}) = -i\epsilon_{\alpha\beta\gamma}$ . The  $\rho$  meson carries the isospin index  $\gamma$  and the Lorentz vector index  $\nu$ .  $g_{\rho\pi\pi}$  and  $g_{\sigma\pi\pi}$  are coupling constants (the values of all coupling constants are given in Table 3.3 and will be discussed later).

For the vertices with the  $\Delta$ ,  $\rho$  and  $\sigma$  a generic form factor  $F_r$  is introduced as part of the regularization procedure. Its functional form is similar to that of the bare  $\pi NN$  form factor in Eq. (3.3),

$$F_r(p_r^2) = \exp \left[ - \ln 2 \frac{(p_r^2 - \tilde{m}_r^2)^2 - (m_r^2 - \tilde{m}_r^2)^2}{\Lambda^4} \right], \quad (3.6)$$

normalized to unity at the on-shell point  $p_r^2 = m_r^2$  with the half-width  $\Lambda^2$ , the latter taken the same for all vertices considered in this subsection. For

<sup>2</sup>A complete list of all vertices and propagators used is given in Appendix H.

the  $\rho\pi\pi$  and the  $\sigma\pi\pi$  vertices,  $\tilde{m}_r$ , the position of the maximum of the form factor, is set equal to the mass of the meson,  $\tilde{m}_r = m_r$ .

The  $\rho\pi\pi$  vertex, Eq. (3.4), is chosen so that it vanishes when contracted with the momentum  $p$  of the  $\rho$  meson. As a consequence, the spin-0 part of the  $\rho$  propagator does not contribute to any matrix element, because the projection operator on the spin-0 component is  $\mathcal{P}_{\mu\nu}^0(p) = p_\mu p_\nu / p^2$ . The apparent singularity at  $p^2 = 0$  of the vertex Eq. (3.4) lies outside the kinematical range covered in the calculations. In any case, the  $1/p^2$ -pole behaviour could be compensated by choosing in Eq. (3.4) a form factor with a zero at  $p^2 = 0$ .

The  $\rho NN$  and  $\sigma NN$  vertices are taken as

$$(\Gamma_{\rho NN})_\gamma^\nu = -i g_{\rho NN} F_N(p_N^2) \frac{\tau_\gamma}{2} \left[ \gamma^\nu + i \kappa_\rho \frac{\sigma^{\nu\lambda} q_\lambda}{2m} \right], \quad (3.7)$$

$$\Gamma_{\sigma NN} = -i g_{\sigma NN} F_N(p_N^2), \quad (3.8)$$

where  $q$  is the incoming momentum of the  $\rho$ -meson, and  $g_{\rho NN}$ ,  $\kappa_\rho$  and  $g_{\sigma NN}$  are coupling constants. The form factor  $F_N(p_N^2)$ , where  $p_N$  is the momentum of the off-shell nucleon, is given by Eq. (3.6) with  $\tilde{m}_N = m$ , the nucleon mass.

The  $\pi N \Delta$  vertex used in this calculation reads

$$(\Gamma_{\pi N \Delta})_\alpha^\nu = i \frac{g_{\pi N \Delta}}{m_\pi^2} T_\alpha F_\Delta(p^2) F_N(p_N^2) [\not{p} q^\nu - (p \cdot q) \gamma^\nu], \quad (3.9)$$

where  $p$  is the momentum of the  $\Delta$  and  $p_N = p - q$  is the outgoing momentum of the nucleon,  $g_{\pi N \Delta}$  is a coupling constant and  $T_\alpha$ ,  $\alpha = 1, 2, 3$ , are isospin 3/2 to 1/2 transition operators defined by the equations

$$\sum_{\alpha=1}^3 T_\alpha^\dagger T_\alpha = 1, \quad T_\alpha T_\beta^\dagger = \delta_{\alpha\beta} - \frac{\tau_\alpha \tau_\beta}{3}. \quad (3.10)$$

The form factors  $F_\Delta$  and  $F_N$  are taken as in Eq. (3.6) with  $\tilde{m}_N = m$ ; the parameter  $\tilde{m}_\Delta^2$  has to be smaller than  $m_\Delta^2$ , the mass squared of the  $\Delta$ , to obtain a good description of the  $P33$  phase shift in pion-nucleon scattering (see the discussion of results in Section 3.6). Indications in favour of a  $\pi N \Delta$  form factor slightly asymmetric with respect to the  $\Delta$  mass have been also found in other works [24, 18], even though  $\pi N \Delta$  vertices different from Eq. (3.9) have been used there. The dependence of the form factor in Eq. (3.9) on  $p_N^2$  turns out to be necessary to regularize the contribution of the 3rd loop diagram on the r.h.s. of the equation in Fig. 3.2.

The reason for the particular structure Eq. (3.9) of the  $\pi N \Delta$  vertex is that it has the property  $p \cdot (\Gamma_{\pi N \Delta})_\alpha = 0$ . As a consequence, the ‘‘sandwich’’

of the spin-1/2 part of the Rarita-Schwinger  $\Delta$  propagator between two  $\pi N\Delta$  vertices vanishes since every term in the spin-1/2 part of the  $\Delta$  propagator is proportional to either  $p_\mu$  or  $p_\nu$ . Thus only the spin-3/2 part of the  $\Delta$  propagator gives rise to non-vanishing matrix elements [61], and it suffices to calculate only the spin-3/2 part of the  $\Delta$  self-energy.

### 3.4 Dressed propagators

The dressed nucleon propagator is written as in Eq. (2.22), where the nucleon field and mass renormalization constants  $Z_2$  and  $\delta m$  are fixed by Eqs. (2.27) requiring that the propagator have a simple pole with a unit residue at  $\not{p} = m$ . The solution of the renormalization equations is given by Eqs. (2.28) and (2.29).

For dressing the  $\Delta$  propagator, we use only a one  $\pi N$ -loop approximation. This means that, in contrast to the nucleon self-energy and the  $\pi NN$  vertex, the  $\Delta$  self-energy is not calculated together with the  $\pi N\Delta$  vertex in an iteration scheme. Rather, the  $\Delta$  self-energy is calculated from a  $\pi N$ -loop diagram where the vertex Eq. (3.9) is used with a fixed form factor. The imaginary parts of the resonance self-energy functions are calculated by cutting through the  $\pi N$  loop, i.e. using the cutting equations Eqs. (2.13), and the real parts are obtained from dispersion integrals similar to Eq. (2.17).

As explained in the previous section, the structure of the  $\pi N\Delta$  vertex Eq. (3.9) allows us to retain only the spin-3/2 part of the  $\Delta$  propagator,

$$S_{\mu\nu}(p) = \frac{1}{\not{p} - m_\Delta - \Sigma_\Delta(p)} \mathcal{P}_{\mu\nu}^{3/2}(p), \quad (3.11)$$

where the spin-3/2 projection operator

$$\mathcal{P}_{\mu\nu}^{3/2}(p) = g_{\mu\nu} - \frac{1}{3}\gamma_\mu\gamma_\nu - \frac{1}{3p^2}(\not{p}\gamma_\mu p_\nu + p_\mu\gamma_\nu\not{p}). \quad (3.12)$$

Due to the elimination of the spin-1/2 components, the  $\Delta$  self-energy can be written in terms of only two Lorentz invariant functions,  $A_\Delta(p^2)$  and  $B_\Delta(p^2)$ , instead of 10 functions which would be needed in the general case with the spin-1/2 part present. The structure of the self-energy is thus the same as for the nucleon, Eqs. (2.23,2.24). The counterterm contribution to the  $\Delta$  self-energy contains real constants  $Z_2^\Delta$  and  $\delta m_\Delta$  which are fixed by the renormalization condition [54] that the  $\Delta$  resonance propagator in which *only the real parts* of the self-energy functions  $A_\Delta(p^2)$  and  $B_\Delta(p^2)$  are retained has a simple pole with a unit residue at the physical mass of the  $\Delta$ . The resulting

expressions for  $Z_2^\Delta$  and  $\delta m_\Delta$  in terms of  $\text{Re}A_\Delta(p^2)$  and  $\text{Re}B_\Delta(p^2)$  are given by equations completely analogous to Eqs. (2.28,2.29). The term  $\sim 1/p^2$  in Eq. (3.12) does not lead to a singularity if the  $\pi N\Delta$  vertices from Eq. (3.9) are used.

The meson propagators are dressed through the insertion of a  $\pi\pi$  loop, analogously to the dressing of the  $\Delta$  through the insertion of a  $\pi N$  loop. The pion propagator thus remains undressed. The dressed propagator of the  $\sigma$  meson has the form

$$D_\sigma(p^2) = \frac{1}{p^2 - m_\sigma^2 - \Pi_\sigma(p^2)}, \quad (3.13)$$

where  $m_\sigma$  is the physical mass of  $\sigma$  and  $\Pi_\sigma(p^2)$  is its self-energy. The latter can be written as a sum of the loop and counterterm contributions,

$$\Pi_\sigma(p^2) = \Pi_{\sigma,L}(p^2) - (Z_\sigma - 1)(p^2 - m_\sigma^2) - Z_\sigma \delta m_\sigma^2, \quad (3.14)$$

where  $Z_\sigma$  and  $\delta m_\sigma^2$  play the role of the field and mass renormalization constants. These constants are fixed by requiring that the expansion of  $\text{Re}\Pi_\sigma(p^2)$  contain only second and higher powers of  $(p^2 - m_\sigma^2)$  [54]. In other words, similar to the renormalization of the  $\Delta$  resonance propagator, the quantity

$$(p^2 - m_\sigma^2 - \text{Re}\Pi_\sigma(p^2))^{-1} \quad (3.15)$$

is required to have a simple pole with a unit residue at  $p^2 = m_\sigma^2$ . This yields  $Z_\sigma$  and  $\delta m_\sigma^2$  in terms of  $\text{Re}\Pi_{\sigma,L}(p^2)$ ,

$$Z_\sigma = 1 + \left. \frac{d}{d(p^2)} \text{Re}\Pi_{\sigma,L}(p^2) \right|_{p^2=m_\sigma^2}, \quad (3.16)$$

$$\delta m_\sigma^2 = \frac{\text{Re}\Pi_{\sigma,L}(m_\sigma^2)}{Z_\sigma}. \quad (3.17)$$

Following similar arguments as for the  $\Delta$ , the structure of the  $\rho\pi\pi$  vertex Eq. (3.4) has been chosen such that only the spin-1 part of the dressed  $\rho$  propagator can be retained,

$$(D_\rho)_{\mu\nu}(p) = \frac{\mathcal{P}_{\mu\nu}^1(p)}{p^2 - m_\rho^2 - \Pi_\rho(p^2)}, \quad (3.18)$$

where

$$\mathcal{P}_{\mu\nu}^1(p) = g_{\mu\nu} - \frac{p_\mu p_\nu}{p^2}, \quad (3.19)$$

is the spin-1 projection operator and  $\Pi_\rho(p^2)$  is the self-energy which has the same structure as for a scalar particle.

### 3.5 Changing representation

It is known that interacting  $n$ -point Green's functions depend on the representation of interacting fields in the Lagrangian: there exist a wide class of field transformations which do not affect the asymptotic behaviour of the fields, leaving the  $S$  matrix (and thus all observables) invariant [40–45, 13].

In this section we will take advantage of the irrelevance of representation and transform the effect of the dressing of the nucleon propagator into new  $\pi NN$  vertices, which is convenient for interpreting results of the dressing. The representation constructed in this section is an example of the “physical representation” discussed in Ref. [62].

We introduce the notation where the subscript  $\Sigma$  labels the representation in which the nucleon propagator  $S(p)$  contains a nontrivial self-energy (note that all calculations in Chapter 2 were done in this representation, but the subscript  $\Sigma$  was not used there). The new representation is defined by the two requirements: 1) the nucleon propagator must be equal to the free propagator  $S^0(p)$ , 2) it must be possible to construct the  $K$  matrix as in Fig. 3.1, i. e. solely in terms of 2- and 3-point Green's functions. The new  $\pi NN$  vertex  $\Gamma$  must thus be a solution of the equation

$$\Gamma(p) S^0(p) \bar{\Gamma}(p) = \Gamma_\Sigma(p) S(p) \bar{\Gamma}_\Sigma(p) , \quad (3.20)$$

where only the dependence on the off-shell nucleon momentum,  $p$ , is indicated. All effects of the dressing are now contained in the difference between the new dressed and the bare vertex,  $\Gamma(p) - \Gamma^0(p)$ .

The solution of Eq. (3.20) can be written as

$$\left[ \text{Re}G(p^2) \pm \frac{W}{2m} \text{Re}G_V(p^2) \right] = \left[ \text{Re}G_\Sigma(p^2) \pm \frac{W}{2m} \text{Re}G_{\Sigma,V}(p^2) \right] \sqrt{\frac{S(\pm W)}{S^0(\pm W)}} \quad (3.21)$$

where  $G = G_S + G_V/2$  and  $W = \sqrt{p^2} \geq 0$  is the invariant mass of the virtual nucleon. Also,  $S^0(\pm W) = -(m \mp W)^{-1}$  and

$$S(\pm W) = - \left[ Z_2(m \mp W) - Z_2\delta m \pm \text{Re}A(p^2)W + \text{Re}B(p^2)m \right]^{-1} \quad (3.22)$$

are positive- and negative-energy parts of the free and dressed nucleon propagators, respectively.

In the present work we consider only those solutions for the dressed propagator  $S$  that do not have real poles in addition to the nucleon pole  $W = m$ . With this qualification, the solution Eq. (3.21) for the  $\pi NN$  form factors

in the new representation is well defined, since, due to the renormalization procedure, the ratios  $S(\pm W)/S^0(\pm W)$  are positive.

An extra pole at positive  $W$  would correspond to an additional asymptotic state, different from the free nucleon<sup>3</sup>. To take it into account properly, certain modifications would be necessary of the standard renormalization of the nucleon field, Eq. (2.28): an additional field renormalization constant would be required to account for the fact that a new particle species occurred as a result of the dressing [2]. Such a study lies outside the scope of the present work.

### 3.6 Effects of the dressing

The masses of the particles included in the model, see Table 3.1, where taken from Ref. [19] and kept fixed in the calculation of pion-nucleon phase shifts.

Table 3.1: *Physical masses of particles included in the model. All the masses were fixed in the calculations of the  $\pi N$  scattering phase shifts.*

Particle	$N$	$\pi$	$\Delta$	$\rho$	$\sigma$
Mass (GeV)	0.938	0.138	1.232	0.770	0.760

An important characteristic of the bare vertex is its half-width  $\Lambda_N^2$ , see Eq. (3.3). To investigate the dependence of the dressing on  $\Lambda_N^2$ , calculations have been done for two values:  $\Lambda_N^2 = 2 \text{ GeV}^2$ , referred to as calculation N (“narrow” bare form factor), and  $\Lambda_N^2 = 3 \text{ GeV}^2$ , calculation W (“wide” bare form factor). The requirement that a converged solution of the dressing procedure can be obtained, without developing additional poles of the propagator (see Section 3.5), puts an upper bound on  $\Lambda_N^2$ . Although the precise value of this limit may vary depending on other parameters of the model, it is certain that the bare form factor cannot be arbitrarily hard. Note however that the energy scale introduced by the bare form factor, which is of the order of  $\sqrt{m^2 + \Lambda_N^2} - m$ , is larger than the scale due to the degrees of freedom explicitly included in the dressing. (For each diagram in Fig. 3.2, the typical scale is the sum of the masses of the particles propagating through the cut minus the nucleon mass.) The values of the bare coupling constant  $f$ , introduced in

<sup>3</sup>An extensive study of the pole structure of the nucleon propagator, including complex “ghost” poles, has been done in Ref. [60].

Eq. (3.2), are given in Table 3.2, where also the values of the field and mass renormalization constants are listed.

Table 3.2: *Bare  $\pi NN$  coupling constant and field and mass renormalization constants obtained in calculations N and W. The mass shifts are given in GeV (or  $\text{GeV}^2$  for the  $\rho$  and  $\sigma$  mesons).*

Calc.	$f$	$Z_2$	$Z_2^\Delta$	$Z_\rho$	$Z_\sigma$	$\delta m$	$\delta m_\Delta$	$\delta m_\rho^2$	$\delta m_\sigma^2$
N	11.04	0.77	1.10	1.17	1.05	-0.11	-0.07	-0.09	-0.65
W	10.80	0.60	1.09	1.17	1.05	-0.28	-0.08	-0.09	-0.65

We find that a sizable pseudoscalar admixture in the bare vertex (with  $|\chi| > 0.1$  in Eq. (3.2)) leads to a poor description of low energy phase shifts. This is intimately related to the smallness of explicit chiral symmetry breaking. Besides, even without resorting to phenomenology, the range of variation of  $\chi$  is severely constrained by the requirement of convergence. Both calculations presented were done with  $\chi = 0.055$ .

The values of the parameters in the vertices for the  $\Delta$ ,  $\rho$  and  $\sigma$ , Eqs. (3.4–3.9), are summarized in Table 3.3. The constants  $g_{\pi N \Delta}$ ,  $g_{\rho \pi \pi}$  and  $g_{\sigma \pi \pi}$  were

Table 3.3: *Parameters of the model used in calculations N and W. Parameters in the last five columns only were varied in the calculations of the  $\pi N$  scattering phase shifts. The parameters  $\Lambda_N^2$ ,  $\Lambda^2$  and  $\tilde{m}_\Delta^2$  are given in  $\text{GeV}^2$ .*

Calc.	$\Lambda_N^2$	$\Lambda^2$	$g_{\pi N \Delta}$	$g_{\rho \pi \pi}$	$g_{\sigma \pi \pi}$	$\chi$	$g_{\rho NN}$	$\kappa_\rho$	$g_{\sigma NN}$	$\tilde{m}_\Delta^2$
N	2	1	0.248	6.07	1.88	0.055	7.83	0.54	19.0	1.04
W	3	1	0.248	6.07	1.88	0.055	8.03	-1.43	18.5	1.06

fixed from the decay widths [63] of the  $\Delta$ ,  $\rho$  and  $\sigma$ , respectively. The value of half-width  $\Lambda^2$ , see Eq. (3.6), was kept fixed and had to be sufficiently soft to provide convergence of the dressing procedure. The coupling constants  $g_{\rho NN}$ ,  $\kappa_\rho$ ,  $g_{\sigma NN}$ , the parameter  $\tilde{m}_\Delta^2$  and  $\chi$ , discussed above, were chosen from a comparison of the calculated  $\pi N$  phase shifts with the data, taken from [64]. Only these five parameters, given in the last five columns of Table 3.3, were adjusted in the calculations. It should be stressed that a convergent solution



of the dressing procedure could be found only for a rather restricted range of these constants.

The phase shifts in pion-nucleon scattering are shown in Figs. 3.3 and 3.4 as functions of the pion kinetic energy in the laboratory system, corresponding to calculations N and W, respectively. The solid lines are the phase shifts

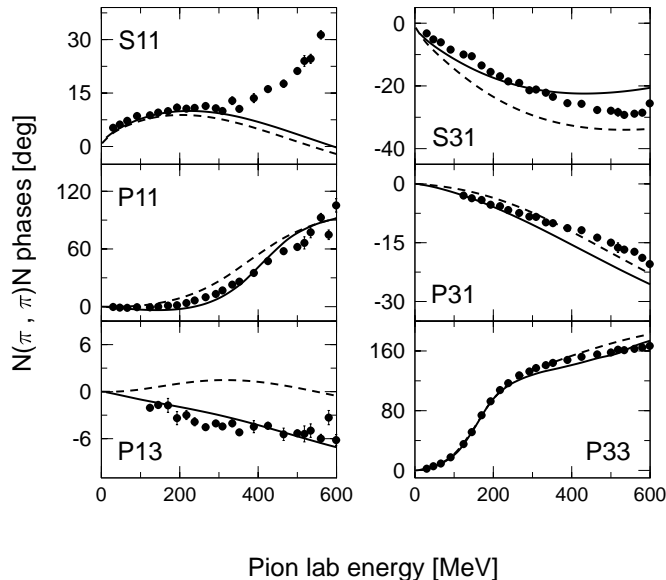


Figure 3.3: *Pion-nucleon phase shifts from calculation N. The drawn curves are obtained in the full calculation. The dashed curves represent the calculation with the bare form factors and free propagators. The data are from [64].*

calculated with the  $K$  matrix shown in Fig. 3.1, in which the dressed vertices and propagators are used. The dashed lines are obtained in the approximation where  $K$  is constructed as in traditional  $K$ -matrix models [16–19], i.e. using the bare vertices and free propagators, hence without taking the dressing into account. As explained in the previous chapter, the effects of the dressing can be regarded as effects of the inclusion of the principal-value parts of loop integrals (which are omitted in the usual approximation for the  $K$  matrix). Effects of principal-value parts were also considered in Ref. [23] in a calculation based on three-dimensional reductions of the Bethe-Salpeter equation. In our approach we keep the most general Lorentz structure for the  $\pi NN$  vertex, Eq. (2.10). Another difference with [23] is that we obtain the principal-value parts through the use of dispersion integrals.

The effect of the dressing on the  $\pi NN$  vertex can be seen more clearly from Figs. 3.5 (calculation N) and 3.6 (calculation W), where the form fac-

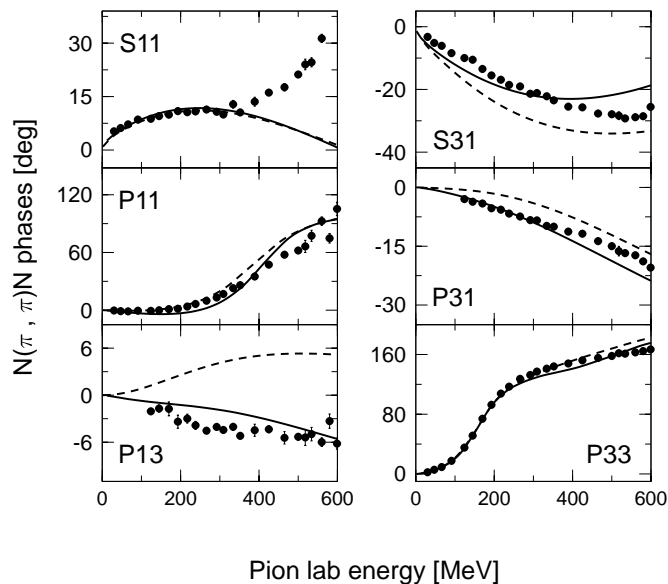


Figure 3.4: Same as in Fig. 3.3, but for calculation  $W$ .

tors are shown as functions of  $p^2$ , the invariant mass squared of the virtual nucleon. The representation constructed in Section 3.5 is particularly useful because it uses the free nucleon propagator, and the effects of nucleon dressing are encapsulated solely in the difference  $G_{V,S}(p^2) - G_{V,S}^0(p^2)$  between the dressed and bare  $\pi NN$  form factors. It should be stressed that, in virtue of the equivalence theorem [40, 43], either of the two representations described in Section 3.5 lead to identical results for the phase shifts. The upper and lower panels contain pseudovector and pseudoscalar form factors, respectively (please note that Fig. 3.5 and Fig. 3.6 have different vertical scales). The dotted lines are the bare form factors, see Eq. (3.2), with the constants  $f$  and  $\chi$  given in Tables 3.2 and 3.3. The dashed lines are the form factors obtained after the first iteration step (essentially, a one-loop correction to the bare vertex) and the solid lines are the fully dressed form factors. A comparison of the solid and dashed lines exhibits a nonperturbative aspect of the dressing in the sense that it goes beyond an inclusion of few loop corrections. It can be seen that the ratio of pseudoscalar and pseudovector form factors remains small if the nucleon is not far off the mass shell. The dash-dotted curves correspond to the form factors of the vertex  $\Gamma_\Sigma$  calculated in the representation where the nucleon self-energy has not been eliminated. We see that the dressed  $\pi NN$  vertex may depend significantly on the representation chosen.

While the nucleon self-energy has been transformed to zero in the repre-

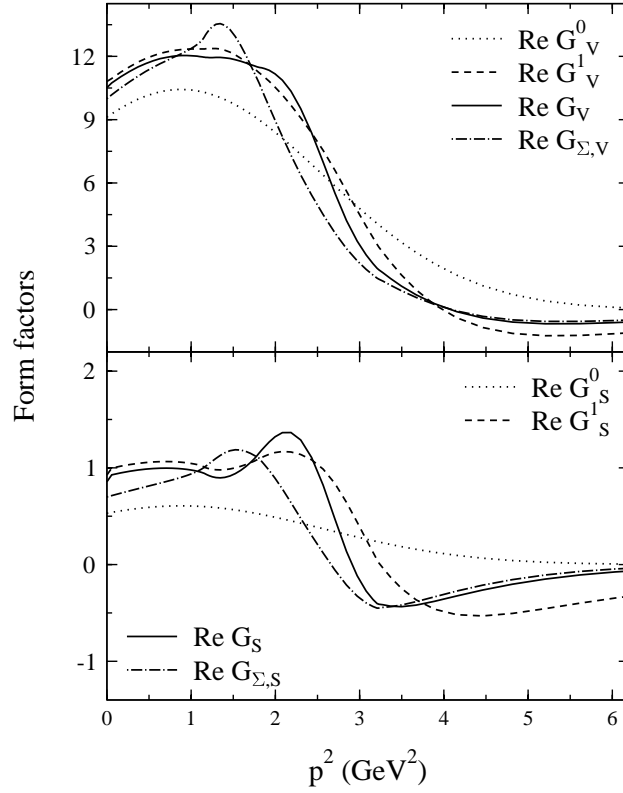


Figure 3.5: *Pion-nucleon form factors from calculation N. The different curves are explained in the text.*

sensation in which the  $\pi NN$  vertex is  $\Gamma$ , this self-energy is nontrivial in the representation with the vertex  $\Gamma_\Sigma$ . The corresponding self-energy functions are shown in Figs. 3.7 (calculation N) and 3.8 (calculation W). Note that there is a large difference between the converged nonperturbative results and the results including a one-loop correction only. A comparison of the one-loop self-energy function  $\text{Re}B^1$  with that obtained in the simplified calculation in the preceding chapter, shown in Fig. 2.10, reveals a role of the small pseudoscalar admixture in the bare vertex. Indeed, now we obtain  $\text{Re}B^1$  whose behaviour is *qualitatively* different from that seen in Fig. 2.10. The reason is that in the present calculation we take  $\chi = 0.055 \neq 0$ , while in the calculation of the previous chapter the bare vertex was purely pseudovector, i.e.  $\chi = 0$  (another difference is the width of the bare form factor, but it turns out to be immaterial for the observed difference in the tendency of  $\text{Re}B^1$ ). It is

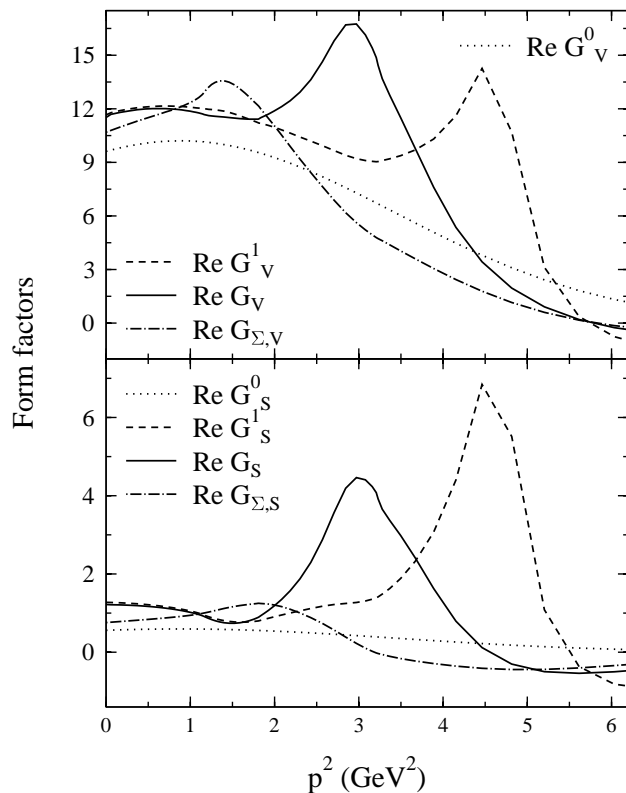


Figure 3.6: Same as in Fig. 3.5, but for calculation  $W$ .

noteworthy that the qualitative behaviour of the *converged* solution for  $\text{Re}B$ , unlike that of the one-loop result, is not affected by the small pseudoscalar admixture in the bare vertex.

Comparing the form factors in Fig. 3.5 with those in Fig. 3.6, we conclude that the converged solution depends strongly on the width of the bare form factor. However, independent of this width, the dressing causes considerable softening of the form factors at higher invariant masses. The calculations in Figs. 3.3 and 3.4 demonstrate that it is possible to obtain a reasonable description of pion-nucleon phase shifts up to pion laboratory energies of about 400 MeV starting from bare form factors with rather different widths.

In the present model, only the lowest lying resonance of the  $\pi N$  scattering, the  $\Delta$ , was included. The lack of other resonances becomes especially conspicuous at higher energies. In fact, in the calculations of phase shifts we also included the Roper resonance, though it is not taken into account in the

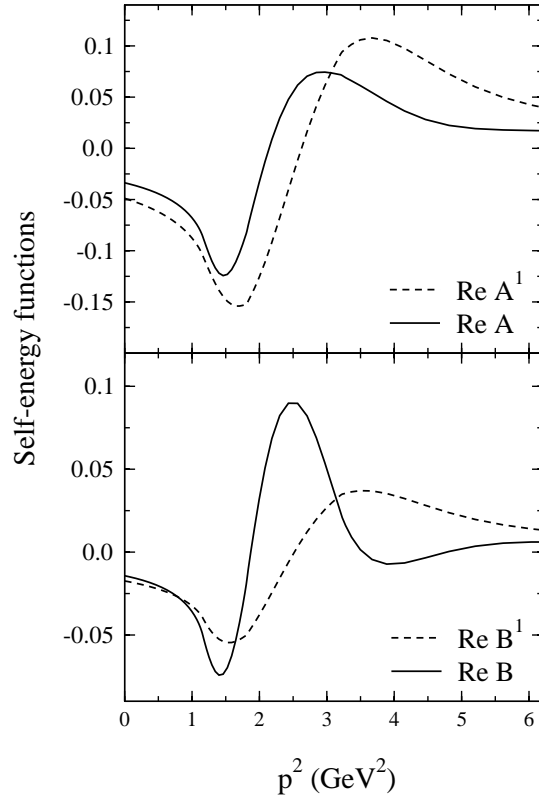


Figure 3.7: *Nucleon self-energy functions from calculation N. The solid (dashed) curves are the converged (first iteration) results.*

dressing. This improved the calculated P11 phase shift at energies of about 300 MeV and higher, with a negligible effect on the other phase shifts. In principle, the dressing procedure can be extended to include the Roper resonance as well as other important degrees of freedom, such as the S11 resonance.

### 3.7 Summary

In this chapter the K-matrix approach to pion-nucleon scattering has been augmented by including the  $\Delta$  resonance and the  $\rho$  and  $\sigma$  mesons. Correspondingly, the dressing procedure for the  $\pi NN$  vertex and nucleon propagator has also been extended to include these degrees of freedom.

By transforming away the nucleon self-energy, we have been able to interpret effects of the dressing in terms of the  $\pi NN$  form factors. At large

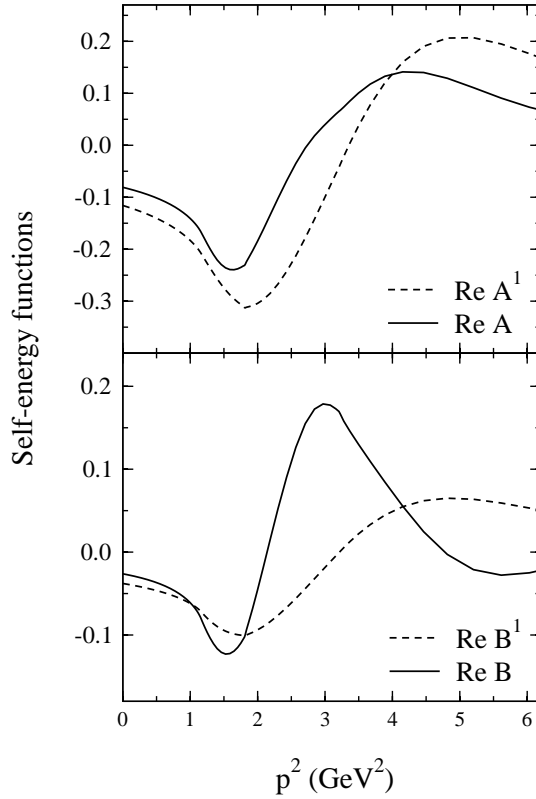


Figure 3.8: Same as in Fig. 3.7 but for calculation  $W$ .

momenta squared of the off-shell nucleon, the dressed form factors decrease faster than the bare form factors.

The five parameters of the model are constrained considerably by the requirement of convergence of the dressing procedure. By the same token, there is an implicit interdependence of the parameters. We showed that a satisfactory quantitative description of phase shifts for  $\pi N$  scattering can be achieved in our model at the energies exceeding the scale due to the degrees of freedom explicit in the model. This indicates that the developed dressing procedure provides a physically reasonable method for studying higher-order correction to the Born approximation traditionally adopted for the K matrix.

## Appendix C: Checking the phase factors of loops integrals

To check that the relative phase factors arising in calculating the loop integrals are consistent with those used for computing the diagrams for the K matrix, we use the following method. The use of cutting rules in the dressing procedure allows us to relate cut loop diagrams for the  $\pi NN$  vertex to diagrams contributing to the K matrix for the pion-nucleon scattering. Let us denote the 1st cut loop diagram in Fig. 3.2 as  $(\pi N)_{cut}N$  and the 2nd cut loop diagram as  $(\pi N)_{cut}\Delta$ . These loops contain the same  $\pi NN$  vertex on the left from the cut, while the diagrams on the right are exactly the crossed (u-channel) nucleon and  $\Delta$  exchange diagrams in Fig. 3.1, which will be denoted as  $N_u$  and  $\Delta_u$ . Therefore, the ratio of the imaginary parts of the form factors calculated from the loop  $(\pi N)_{cut}N$  to those from the loop  $(\pi N)_{cut}\Delta$  must be equal to the ratio of the amplitudes calculated from the tree diagram  $N_u$  to those from the tree diagram  $\Delta_u$ .

Such a relation can be written in terms of the positive- and negative-energy form factors  $F(\pm W)$ , which are related to the pseudovector and pseudoscalar ones by

$$F(\pm W) = G_S(p^2) + (m \pm W) \frac{G_V(p^2)}{2m}, \quad (\text{C.1})$$

where  $W = \sqrt{p^2} \geq 0$  is the invariant mass of the off-shell nucleon.

A correspondence can be established between  $\text{Im}F(\pm W)$  and partial scattering amplitudes. The standard notation for partial waves with the orbital momenta  $L = 0, 1, 2, \dots$  is S  $2I 2J$ , P  $2I 2J$ , D  $2I 2J, \dots$ , respectively, where  $I$  and  $J = L \pm 1/2$  are the total isospin and angular momentum of the  $\pi N$  pair. Next we determine the quantum numbers  $I, J, L$  which correspond to  $\text{Im}F(\pm W)$ . These quantum numbers are associated with the  $\pi N$  pair through which the cut is drawn, and, due to conservation laws, must be determined by the state of the incoming virtual nucleon. Thus, it is clear that  $I = J = 1/2$ . Given  $J = 1/2$ , the orbital momentum  $L$  of the  $\pi N$  pair can be either 0 or 1, corresponding to the partial waves S11 and P11, respectively. If  $L = 0$ , the  $\pi N$  system has negative parity, and if  $L = 1$ , the parity is positive (the parity is related to  $L$  through  $\pi = (-1)^{L+1}$ ). Since the virtual nucleon with positive or negative parity propagates through positive- or negative-energy states, respectively, we have thus established that the positive-energy form factor  $\text{Im}F(+W)$  is associated with the partial amplitude P11, while the negative-energy form factor  $\text{Im}F(-W)$  with S11.

Since the relative factors of the loops  $(\pi N)_{cut}N$  and  $(\pi N)_{cut}\Delta$  must be

the same as those of the diagrams  $N_u$  and  $\Delta_u$ , the following equations must hold:

$$\frac{\text{Im}F(-W) [(\pi N)_{cut}N]}{\text{Im}F(-W) [(\pi N)_{cut}\Delta]} = \frac{\text{S11} [N_u]}{\text{S11} [\Delta_u]}, \quad (\text{C.2})$$

$$\frac{\text{Im}F(+W) [(\pi N)_{cut}N]}{\text{Im}F(+W) [(\pi N)_{cut}\Delta]} = \frac{\text{P11} [N_u]}{\text{P11} [\Delta_u]}, \quad (\text{C.3})$$

where the form factors and partial amplitudes are calculated from the diagrams indicated in the square brackets. Clearly, similar relations must also hold pairwise for the 1st, 2nd, 4th and 7th cut loops in Fig. 3.2 in relation to the 2nd, 4th, 5th and 6th tree diagrams in Fig. 3.1, respectively. We checked numerically that these relations are indeed satisfied in the present calculations, proving consistency of the factors of different loops in Fig. 3.2 with those of the corresponding graphs in Fig. 3.1.





# Chapter 4

## Including the photon

### 4.1 Introduction

In this chapter the formalism is extended to include processes involving photons, resulting in a coupled-channel K-matrix approach for pion-nucleon scattering, pion photoproduction and Compton scattering. The key element of the approach is a system of integral equations which describes a dressing of a half-off-shell  $\gamma NN$  vertex with principal-value parts of pion-nucleon loops. As in Chapter 2, the dressing procedure will be explained in detail using a simplified model including only the nucleon, pion and photon degrees of freedom.

It is known [4–9, 65, 66] that in photon induced processes important constraints are imposed by the condition that the amplitude for the process has to be analytic, especially at energies near the pion production threshold. The usage of dispersion relations for the construction of propagators and vertices allows us to implement some of these analyticity constraints in the unitary K-matrix approach.

As with any process involving photons, one should take care to obey gauge invariance of the amplitude since otherwise low-energy theorems may be violated. Gauge invariance imposes an important relation between the  $\gamma NN$  vertex and the nucleon propagator, known as the Ward-Takahashi identity [67]. This constraint is obeyed in our model due to the inclusion of a contact 4-point  $\gamma\pi NN$  vertex, which is constructed based on the dressed  $\pi NN$  vertex using the prescription of minimal substitution. We discuss this method in some detail and present general formulae in both configuration and momentum spaces (Appendices E.1–E.3). Minimal substitution yields a unique result only for the longitudinal (with respect to the photon momentum) part

of the contact vertex. To investigate the role of the transverse terms, we compare the electromagnetic form factors calculated using two different  $\gamma\pi NN$  vertices. Due to the inclusion of the  $\gamma\pi NN$  term in the K matrix, we obtain a gauge invariant amplitude for pion photoproduction. To provide current conservation in the description of Compton scattering, we build a contact  $\gamma\gamma NN$  term, also employing the method of minimal substitution.

Although the use of dispersion relations in the dressing procedure invokes analyticity properties of the 3-point vertices and nucleon propagator, it does not suffice to obtain an analytic T matrix. To correct this in the important region near the pion production threshold, we construct an additional gauge invariant and crossing symmetric contact term (Section 4.6).

We will discuss effects of the dressing on the  $f_{EE}^{1-}$  partial amplitude for Compton scattering on the proton, emphasizing the importance of the analyticity and unitarity constraints to understand the specific behaviour of this amplitude at the pion threshold.

## 4.2 Coupled-channel K-matrix approach

The K-matrix formalism of Chapter 2 can be extended to describe simultaneously pion-nucleon scattering, pion photoproduction and Compton scattering, yielding a unitary coupled-channel S matrix. As before, we restrict ourselves to two-body unitarity, explicitly taking into account only one-pion threshold discontinuities of the loop integrals.

The coupled-channel scattering amplitude  $\mathcal{T}_{c'c}$  has two indices corresponding to the channel in the initial ( $c$ ) and final ( $c'$ ) state, where the indices can be  $\pi$  or  $\gamma$  for the channels  $\pi N$  or  $\gamma N$ , respectively. The Bethe-Salpeter equation for the scattering matrix can be written as

$$\mathcal{T}_{c'c} = V_{c'c} + \sum_{c''} V_{c'c''} \mathcal{G}_{c''} \mathcal{T}_{c''c}, \quad (4.1)$$

where the potential  $V_{c'c}$  describing the process  $c \rightarrow c'$  is usually taken as a sum of tree diagrams with free propagators and bare vertices, and  $\mathcal{G}_{c''}$  is the two-body propagator pertinent to the channel  $c''$ . As in the single-channel case,  $\mathcal{G}_{c''}$  can be split into its pole and principal-value parts,

$$\mathcal{G}_{c''} = i\delta_{c''} + \mathcal{G}_{c''}^R. \quad (4.2)$$

The coupled-channel K matrix is introduced as the solution of the equation

$$K_{c'c} = V_{c'c} + \sum_{c''} V_{c'c''} \mathcal{G}_{c''}^R K_{c''c}. \quad (4.3)$$

According to this formula, only the principal-value parts of the loop diagrams contribute to the K matrix. The remaining pole parts are generated in the T matrix by iterating the K matrix in the unitarization procedure,

$$\mathcal{T}_{c'c} = K_{c'c} + \sum_{c''} K_{c'c''} i\delta_{c''} \mathcal{T}_{c''c}, \quad (4.4)$$

which can be derived from Eqs. (4.1–4.3). The solution of Eq. (4.4) can be expressed as in Eq. (2.6), from which it follows that the S matrix,  $S = 1 + 2i\mathcal{T}$ , is unitary provided  $K$  is hermitian. Comparing Eqs. (4.1–4.4) with their single-channel counterparts, Eqs. (2.2–2.5), we see that the only difference of the coupled-channel K-matrix formalism from the single-channel one is that now all operators become  $2 \times 2$  matrices in the channel space, e.g.,

$$K = \begin{bmatrix} K_{\gamma\gamma} & K_{\gamma\pi} \\ K_{\pi\gamma} & K_{\pi\pi} \end{bmatrix}. \quad (4.5)$$

Eq. (4.3) suggests an interpretation of the K matrix in terms of a dressing of a potential  $V_{c'c}$  with principal-value parts of loop integrals. To illustrate this for the case of Compton scattering, in the present simplified model including only nucleons, pions and photons, we choose  $V_{\gamma\gamma}$  and  $V_{\gamma\pi}$  as follows.  $V_{\gamma\gamma}$  is taken as a sum of s- and u-channel nucleon exchange tree diagrams. For  $V_{\gamma\pi}$  we take a sum of s- and u-channel nucleon exchange and t-channel pion exchange tree diagrams plus a contact 4-point vertex (such as the Kroll-Ruderman term [68], which is necessary in order that  $V_{\gamma\pi}$  should conserve current, if the pseudovector pion-nucleon vertex is used in  $V_{\gamma\pi}$ ). In these tree diagrams, the free nucleon propagator and bare nucleon-photon vertices are used. Up to second order in  $V_{c'c}$  and leading order in the electromagnetic coupling constant, i.e. up to one-loop corrections,  $K_{\gamma\gamma}$  can be written as

$$K_{\gamma\gamma}^{(1)} = V_{\gamma\gamma} + V_{\gamma\pi} \mathcal{G}_{\pi}^R V_{\pi\gamma}. \quad (4.6)$$

The set of diagrams corresponding to the r.h.s. of this equation is depicted in Fig. 4.1. The notation  $ss$ ,  $su$  etc. for the loop diagrams refers to their structure in terms of the s-, u-, t-channel and contact (c) tree diagrams contributing to  $V_{\gamma\pi}$ . The index  $Re$  at the loops indicates that only the principal-value integrals are taken into account, in accordance with Eq. (4.6). Consequently, only the real parts of the self-energy functions and form factors enter in these loops. From the one-particle reducible diagrams in Fig. 4.1 (diagrams  $ss$ ,  $su$ ,  $st$ ,  $sc$ ,  $us$ ,  $ts$  and  $cs$ ) one can see that these real parts are obtained as a result of a dressing of the free nucleon propagator and half-off-shell bare  $\gamma NN$  vertices with the principal-value loop integrals. The other diagrams in Fig. 4.1,

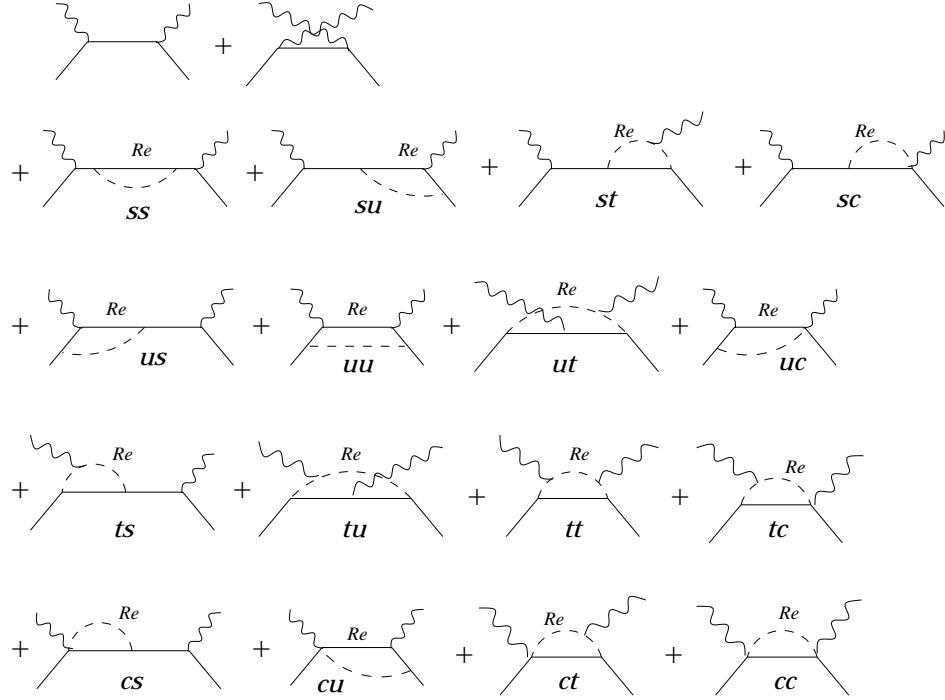


Figure 4.1: The Feynman diagrams forming the  $K$  matrix for Compton scattering up one-loop corrections, according to Eq. (4.6). The solid, dashed and wavy lines are nucleons, pions and photons, respectively. The label  $Re$  shows that only the principal-value parts of the loop integrals are included. The structure of the loop diagrams is labeled in terms of the tree diagrams for pion photoproduction:  $ss$ ,  $su$ ,  $st$ ,  $sc$  etc.

which are one-particle irreducible, are necessary, in particular, to ensure the gauge invariance of  $K_{\gamma\gamma}^{(1)}$ .

The above analysis of  $K_{\gamma\gamma}^{(1)}$  serves as an introduction to the description of the  $K$  matrix in which loop corrections are summed up to infinite order. In the simplified model of this chapter, including only nucleons, pions and photons, we construct the  $K$  matrix which enters in Eq. (4.4) as the sum of diagrams depicted in Fig. 4.2 for  $K_{\gamma\gamma}$  and  $K_{\gamma\pi}$  and in Fig. 2.1 for  $K_{\pi\pi}$ . Unlike the usual tree diagrams, these diagrams are composed of *dressed* nucleon propagators and *dressed* irreducible half-off-shell  $\pi NN$  and  $\gamma NN$  vertices, plus contact terms needed for gauge invariance of the  $K$  matrix (and thus, of the full scattering amplitude  $\mathcal{T}$ ). The use of dressed quantities is dictated

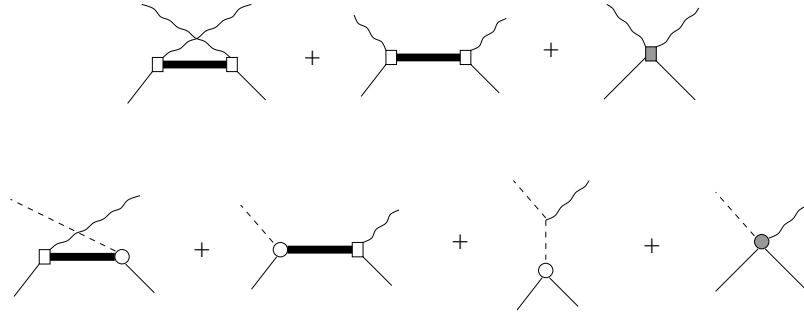


Figure 4.2: *The diagrams, including the contact terms, contributing to the  $K$  matrix for Compton scattering (top) and pion photoproduction (bottom). The notation is the same as in Fig. 4.1. In addition, the thick line is the dressed nucleon propagator. The empty circle (square) is the dressed  $\pi NN$  ( $\gamma NN$ ) vertex, and the shaded circle and square stand for the contact vertices.*

by Eq. (4.3), where, due to taking the principal-value integrals, effects of the dressing are expressed in terms of the real parts of form factors and self-energy functions. The dressing procedure amounts to summing up an infinite series of pion-nucleon loop integrals, which is expressed in terms of a system of integral equations and solved by iteration. At each iteration step, we calculate the real parts of the form factors and self-energy functions by applying dispersion relations to their imaginary parts which enter in the one-particle reducible diagrams from Eq. (4.4). The dressing of the nucleon propagator and  $\pi NN$  vertex was explained in Chapter 2. In Section 4.4 we shall give a detailed description of the dressing procedure for the  $\gamma NN$  vertex.

### 4.3 Structure of the $\gamma NN$ vertex

The irreducible (or proper)  $\gamma NN$  vertex operator can, in principle, be defined as the sum of all connected Feynman diagrams with one incoming nucleon (carrying the momentum  $p$ ), one outgoing nucleon ( $p'$ ) and one photon ( $q = p' - p$ ), with the propagators for the external legs stripped away. The most general Lorentz covariant form of the  $\gamma NN$  vertex can be written as [14]

$$e \Gamma_\mu(p', p) = e \sum_{k,l=\pm} \Lambda_k(p') \left\{ \gamma_\mu F_1^{kl} + i \frac{\sigma_{\mu\nu} q^\nu}{2m} F_2^{kl} + \frac{q_\mu}{m} F_3^{kl} \right\} \Lambda_l(p), \quad (4.7)$$

where, in addition to the previously introduced notations,  $e$  is the elementary electric charge,

$$\Lambda_{\pm}(p) \equiv \frac{\pm \not{p} + m}{2m}, \quad (4.8)$$

and the 12 form factors  $F_i^{kl}$  depend on the momenta squared of the three particles in the vertex,  $F_i^{kl} = F_i^{kl}(p'^2, p^2, q^2)$ . Throughout this thesis we deal only with real photons, for which  $q^2 = 0$  and  $q \cdot \epsilon = 0$ , where  $\epsilon^\mu$  is the photon polarization vector. Since in the description of physical processes with real photons, the vertex Eq. (4.7) always enters in the scalar product  $\Gamma(p', p) \cdot \epsilon$ , the form factors  $F_3^{kl}$  do not have to be considered further. The isospin structure of the form factors is  $F = F^s + \tau_3 F^v$  (the eigenvalue of  $\tau_3$  is +1 for the proton and -1 for the neutron).

Invariance of the theory with respect to charge conjugation and space-time inversion allows one to write the following relations for the vertex [1]:

$$C^{-1} \Gamma_\mu(p', p) C = -\Gamma_\mu^T(-p, -p'), \quad \gamma_5 \Gamma_\mu(p', p) \gamma_5 = -\Gamma_\mu(-p', -p), \quad (4.9)$$

where  $C = i\gamma_2\gamma_0$  is the charge conjugation matrix. Successive application of these two transformations gives

$$\gamma_1 \gamma_3 \Gamma_\mu(p', p) \gamma_3 \gamma_1 = \Gamma_\mu^T(p, p'), \quad (4.10)$$

leading, on substituting Eq. (4.7), to the following relations among the form factors:

$$F_{1,2}^{kl}(p'^2, p^2) = F_{1,2}^{lk}(p^2, p'^2). \quad (4.11)$$

For the construction of the K matrix we need only half-off-shell  $\gamma NN$  vertices. On account of Eqs. (4.11), it suffices to consider only the half-off-shell vertex with the outgoing on-shell nucleon,

$$e \Gamma_\mu(p) = e \sum_{l=\pm} \left\{ \gamma_\mu F_1^l(p^2) + i \frac{\sigma_{\mu\nu} q^\nu}{2m} F_2^l(p^2) \right\} \Lambda_l(p), \quad (4.12)$$

where  $F_i^+(p^2) \equiv F_i^{++}(m^2, p^2)$  and  $F_i^-(p^2) \equiv F_i^{+-}(m^2, p^2)$ .

## 4.4 Dressing the $\gamma NN$ vertex

### 4.4.1 Dressing procedure

The dressing procedure for the  $\gamma NN$  vertex Eq. (4.12) is expressed in terms of a system of integral equations<sup>1</sup>, shown diagrammatically in Fig. 4.3,

$$\Gamma_{\mu,R}(p) = \Gamma_{\mu}^0(p) + \text{D.I.} \left\{ \Gamma_{\mu,I}[1] + \Gamma_{\mu,I}[2] + \Gamma_{\mu,I}[3] \right\}, \quad (4.13)$$

where ‘‘D.I.’’ implies taking a dispersion integral,  $\Gamma_{\mu,R}$  ( $\Gamma_{\mu,I}$ ) contains only the real (imaginary) parts of the form factors and each term is discussed in detail in the following. These equations express the dressing of a bare vertex

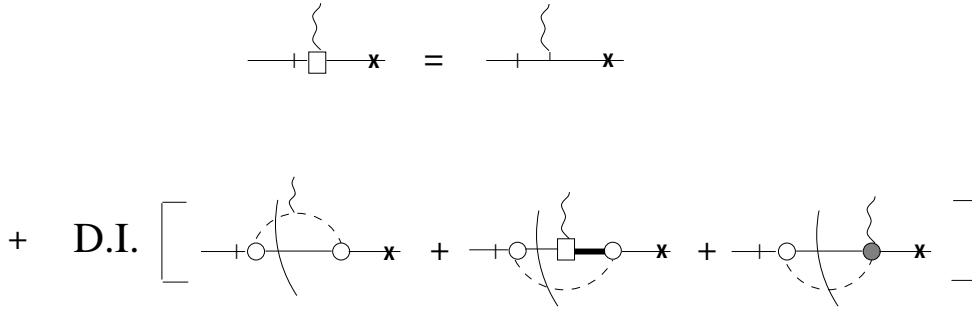


Figure 4.3: *The graphical representation of Eqs. (4.13). The notation of Fig. 4.2 is used. The cuts applied at each iteration step are shown by the slashes through the loops. Crosses denote the outgoing on-shell nucleon (the photon is real throughout). The vertex is irreducible, hence the propagator of the off-shell nucleon is stripped away, as indicated by the dash on the incoming line.*

$\Gamma_{\mu}^0(p)$  with an infinite series of pion loops. The bare vertex is taken as

$$\Gamma_{\mu}^0(p) = (\gamma_{\mu} \hat{e}_N + i \hat{\kappa}_B \frac{\sigma_{\mu\nu} q^{\nu}}{2m}), \quad (4.14)$$

where  $\hat{e}_N = (1 + \tau_3)/2$  and  $\hat{\kappa}_B = \kappa_B^s + \tau_3 \kappa_B^v$  is the bare anomalous magnetic moment of nucleon, adjusted to provide the normalization Eq. (4.30) of the dressed vertex.

The method of solution of Eqs. (4.13) parallels that of Eqs. (2.30), described in Chapter 2. For convenience, we shall recapitulate the procedure briefly. The solution is obtained by iteration. Every iteration step proceeds

<sup>1</sup>As will be shown in Section 4.4.3, formula Eq. (4.13) implicitly represents 16 simultaneous equations for 16 unknown functions.



as follows. The imaginary or pole contributions of the loop integrals for both the propagators and the vertices are obtained by applying the cutting rules Eq. (2.13). Since the outgoing nucleon and the photon are on-shell and since, as required by Eq. (4.3), we retain only the real parts of the form factors and nucleon self-energies from the previous iteration step, the only kinematically allowed cuts are those shown in Fig. 4.3. All integrals on the r.h.s. of Eq. (4.13), except the one over  $\Gamma_{\mu,I}[2]$ , are inhomogeneities of the equation because they do not depend on the  $\gamma NN$  vertex. Therefore, they need to be calculated only once. The dressed  $\pi NN$  vertices and the nucleon propagator are taken from Chapter 2, where they have been constructed using a compatible procedure. The real parts of the form factors are calculated at every iteration step by applying dispersion relations [14] to the imaginary parts just calculated. The dispersion integrals are convergent due to a sufficiently fast falloff of the form factors in the  $\pi NN$  vertices, and therefore no form factors are required in the bare  $\gamma NN$  vertex Eq. (4.14). These steps are repeated to obtain a converged solution. The convergence criterion is imposed for a normalized root-mean-square difference  $d_n$  for the form factors between two subsequent iteration steps  $n$  and  $n + 1$ ; the convergence criterion is that  $d_n < 10^{-8}$  for a large number of iterations.

One of the advantages of the use of the cutting rules and dispersion integrals is that throughout the dressing procedure we deal solely with *half*-off-shell vertices (see Fig. 4.3), which are exactly the vertices required for the construction of the K matrix (see Figs. 4.2 and 2.1). In addition, the fact that we can forgo dealing with *full*-off-shell vertices makes the solution tractable mathematically.

Since in the dressing of the  $\pi NN$  vertex a bare form factor is necessary for regularization, the described procedure allows us to obtain form factors which obey analyticity only with certain qualifications (see remark “*Analyticity*” in Section 2.4.2).

#### 4.4.2 The loop integrals

The pole contribution  $\Gamma_{\mu,I}[1]$  of the first loop integral on the r.h.s. of Eq. (4.13) comes from cutting the nucleon propagator  $S(p - k)$  and the pion propagator  $D(k^2)$ , i.e. from putting the corresponding particles on their mass shell, as shown in Fig. 4.3. According to the cutting rules Eq. (2.13), we replace the nucleon propagator  $S(p - k)$  with  $-2i\pi(\not{p} - \not{k} + m)\delta((p - k)^2 - m^2)\theta(p_0 - k_0)$  and the pion propagator  $D(k^2)$  with  $-2i\pi\delta(k^2 - m_\pi^2)\theta(k_0)$ . The half-off-shell  $\pi NN$  vertex  $\Gamma_{5,\alpha}(p) = \tau_\alpha\Gamma_5(p)$  for an incoming off-shell nucleon with momentum  $p$  entering in the expressions is written as in Eq. (2.9), where

the form factors  $G_{1,2}(p^2)$  have been calculated in Chapter 2. The dressing procedure for the  $\pi NN$  vertex can be straightforwardly extended to calculate vertices in which both the pion and one of the nucleons are off-shell (for the pion momenta squared less than or equal to  $m_\pi^2$ ). As a result of such an extension, we find that the dependence of the form factor on the pion momentum is negligibly small. Therefore, this dependence is ignored, and the right-hand  $\pi NN$  vertex entering in  $\Gamma_{\mu,I}[1]$  is thus simply proportional to the pion-nucleon coupling constant,  $\gamma_5 G_1(m^2) = \gamma_5 g$ . Denoting  $g_i \equiv \text{Re}G_i$ , we write the pole contribution

$$\begin{aligned} \Gamma_{\mu,I}[1] &= \frac{2\tau_3}{8\pi^2} \int d^4k \gamma_5 g_1(m^2) (\not{p} - \not{k} + m) \gamma_5 \left[ g_1(p^2) + \frac{\not{p} - m}{m} g_2(p^2) \right] \\ &\times \frac{2k_\mu + q_\mu}{(k+q)^2 - m_\pi^2} \delta((p-k)^2 - m^2) \Theta(p_0 - k_0) \\ &\times \delta(k^2 - m_\pi^2) \theta(k_0), \end{aligned} \quad (4.15)$$

with the  $\gamma\pi\pi$  vertex

$$\Gamma_{\mu,\alpha\beta}(k', k) = (\hat{e}_\pi)_{\alpha\beta}(k_\mu + k'_\mu) \quad (4.16)$$

chosen so as to satisfy the Ward-Takahashi identity [67] with the free pion propagator,

$$(k' - k)^\mu \Gamma_{\mu,\alpha\beta}(k', k) = (\hat{e}_\pi)_{\alpha\beta} [D^{-1}(k'^2) - D^{-1}(k^2)], \quad (4.17)$$

where  $(\hat{e}_\pi)_{\alpha\beta} = -i\epsilon_{\alpha\beta 3}$  is the pion charge operator. Using the notation introduced in Eqs. (D.1,D.5), one can write

$$\Gamma_{\mu,I}[1] = \sum_{i=1}^4 c^i[1] (e_i)_\mu. \quad (4.18)$$

Here it has implicitly been taken into account that the final nucleon is on the mass shell and

$$\begin{aligned} c^i[1] &= \frac{r(p^2)}{16\pi p^2} \theta(p^2 - (m + m_\pi)^2) \int_{-1}^1 dx V^i(x) \frac{g_1(m^2)}{(k+q)^2 - m_\pi^2}, \quad (4.19) \\ V^i(x) &= \tau_3 \sum_{j=1}^6 (E^{-1})_j^i \left\langle (\theta^j)^\mu, \Lambda_+(p') (-\not{p} + \not{k} + m) [g_1(p^2) \right. \\ &\quad \left. + \frac{\not{p} - m}{m} g_2(p^2)] (2k_\mu + q_\mu) \right\rangle, \end{aligned} \quad (4.20)$$

where the brackets  $\langle \cdot, \cdot \rangle$  are defined in Eq. (D.2), the  $(\theta^j)^\mu$  is the basis in the dual space (see Appendix D),  $q = p' - p$  and the kinematic function  $r(p^2)$  has been introduced in Appendix A. The integral in Eq. (4.19) is a Lorentz scalar and therefore can be evaluated in any frame of reference. We choose the rest frame of the incoming nucleon, i.e. we put  $p_\mu = W \delta_{\mu 0}$ , where  $W = \sqrt{p^2}$  is the invariant mass of the off-shell nucleon. Furthermore, we introduced  $x$ , the cosine of the polar angle between the three-vectors  $(-\vec{q})$  and  $\vec{k}$ . The integral in Eq. (4.19) is done numerically.

The term  $\Gamma_{\mu,I}[2]$  depends on the unknown half-off-shell  $\gamma NN$  vertex and therefore has to be considered in the context of the iteration procedure. As explained above, when calculating  $\Gamma_{\mu,I}^{n+1}[2]$ , the pole contribution to the  $n+1$ st iteration for  $\Gamma_\mu[2]$ , we retain only the real parts of  $F_i^{\pm,n}(p^2)$  from the previous iteration and also only the real parts of the  $\pi NN$  form factors  $G_{1,2}$ . We do not have to impose this condition for the nucleon self-energy since the self-energy functions  $A(p^2)$  and  $B(p^2)$  (see Eq. (2.24)) are anyway real at the required kinematics. The functions  $\alpha(p^2)$ ,  $\xi(p^2)$ , given by Eq. (A.6), and the form factors  $G_{1,2}(p^2)$  were calculated in Chapter 2. Using the same approach as for  $\Gamma_{\mu,I}[1]$  we write

$$\Gamma_{\mu,I}^{n+1}[2] = \sum_{i=1}^4 c^{i,n+1}[2] (e_i)_\mu, \quad (4.21)$$

where

$$\begin{aligned} c^{i,n+1}[2] &= \frac{r(p^2)}{32\pi p^2} \theta(p^2 - (m + m_\pi)^2) \\ &\times \int_{-1}^1 dx \frac{U^i(x)}{\alpha((p' - k)^2)[(p' - k)^2 - \xi^2((p' - k)^2)]}, \quad (4.22) \\ U^i(x) &= \sum_{j=1}^6 (E^{-1})_j^i \left\langle (\theta^j)^\mu, \Lambda_+(p') \left\{ \tau_\alpha \gamma_5 [g_1((p' - k)^2) \right. \right. \\ &\quad \left. \left. + \frac{\not{p}' - \not{k} - m}{m} g_2((p' - k)^2)] (\not{p}' - \not{k} + \xi((p' - k)^2)) \right\} \right. \\ &\quad \times \left\{ \Lambda_+(p' - k) \left[ \gamma_\mu f_1^+((p' - k)^2) + i \frac{\sigma_{\mu\nu} q^\nu}{2m} f_2^+((p' - k)^2) \right] \right. \\ &\quad \left. \left. + \Lambda_-(p' - k) \left[ \gamma_\mu f_1^-((p' - k)^2) + i \frac{\sigma_{\mu\nu} q^\nu}{2m} f_2^-((p' - k)^2) \right] \right\} \right\rangle \end{aligned}$$

$$\times (\not{p} - \not{k} + m) \tau_\alpha \gamma_5 \left[ g_1(p^2) + \frac{\not{p} - m}{m} g_2(p^2) \right] \Bigg\} \Bigg\rangle, \quad (4.23)$$

with  $f_i^\pm(p^2) \equiv \text{Re}(F^\pm)_i(p^2)$ . Note that the  $f$ s contain isospin operators.

The term  $\Gamma_{\mu,I}[3]$  contains a ‘‘contact’’  $\gamma\pi NN$  vertex. We build such a vertex applying the procedure of minimal substitution to the dressed half-off-shell  $\pi NN$  vertex (see Appendix E.1 for details), resulting in

$$\begin{aligned} & \left( \Gamma_{\gamma\pi NN} \right)_\alpha^\mu(p', p, q) = \\ & -\tau_\alpha \hat{e} \left\{ \frac{2p^\mu + q^\mu}{(p+q)^2 - p^2} [\Gamma^5(p+q) - \Gamma^5(p)] \right. \\ & \left. + \gamma^5 \frac{g_2((p+q)^2)}{m} [\gamma^\mu - \not{q}] \frac{2p^\mu + q^\mu}{(p+q)^2 - p^2} \right\} \\ & -\hat{e} \tau_\alpha \left\{ \frac{2p'^\mu - q^\mu}{(p'-q)^2 - p'^2} [-\overline{\Gamma^5}(p'-q) + \overline{\Gamma^5}(p')] \right. \\ & \left. + [\gamma^\mu + \frac{2p'^\mu - q^\mu}{(p'-q)^2 - p'^2} \not{q}] \frac{g_2((p'-q)^2)}{m} \gamma^5 \right\}, \end{aligned} \quad (4.24)$$

where Eqs. (E.26,E.28),  $p' = p + q$  and Eq. (2.9) for the  $\pi NN$  vertex  $\Gamma^5(p)$  have been used. Using the same notation as before we obtain

$$\Gamma_{\mu,I}[3] = \sum_{i=1}^4 c^i[3] (e_i)_\mu, \quad (4.25)$$

with

$$\begin{aligned} c^i[3] &= -\frac{r(p^2)}{64\pi p^2} \theta(p^2 - (m + m_\pi)^2) \\ & \times \left[ (3 - \tau_3) \int_{-1}^1 dx W_1^i(x) + 3(1 + \tau_3) \int_{-1}^1 dx W_2^i(x) \right], \quad (4.26) \\ W_1^i(x) &= \sum_{j=1}^6 (E^{-1})_j^i \left\langle (\theta^j)^\mu, \Lambda_+(p') \left\{ (2p_\mu - 2k_\mu + q_\mu) \right. \right. \\ & \times \left[ \frac{g_{12}((p'-k)^2) - g_{12}(m^2)}{(p'-k)^2 - m^2} - \frac{\not{p} - \not{k}}{m} \frac{g_2((p'-k)^2) - g_2(m^2)}{(p'-k)^2 - m^2} \right] \\ & \left. \left. - \frac{\gamma^\mu}{m} g_2((p'-k)^2) \right\} (m - \not{p} + \not{k}) \left\{ g_{12}(p^2) + \frac{\not{p}}{m} g_2(p^2) \right\} \right\rangle, \end{aligned} \quad (4.27)$$

$$\begin{aligned}
W_2^i(x) &= \sum_{j=1}^6 (E^{-1})_j^i \left\langle (\theta^j)^\mu, \Lambda_+(p') \left\{ (2p'_\mu - q_\mu) \right. \right. \\
&\quad \times \left[ \frac{g_{12}(p^2) - g_{12}(m^2)}{p^2 - m^2} + \frac{g_2(p^2) - g_2(m^2)}{p^2 - m^2} \frac{\not{p}'}{m} \right] + \frac{\gamma_\mu}{m} g_2(p^2) \left. \right\} \\
&\quad \times (m - \not{p} + \not{k}) \left. \left\{ g_{12}(p^2) + \frac{\not{p}}{m} g_2(p^2) \right\} \right\rangle, \tag{4.28}
\end{aligned}$$

where  $g_{12} \equiv g_1 - g_2$ . An alternative expression for  $\Gamma_{\mu,I}[3]$  is obtained if, instead of Eq. (E.28), one uses the contact term Eq. (E.32). The choice of the contact term has an influence on the calculated  $\gamma NN$  form factors, as will be discussed below.

Since the half-off-shell form factors are analytic in the complex  $p^2$ -plane with the cut from the pion threshold  $(m + m_\pi)^2$  to infinity [14], dispersion relations can be used to construct the real parts from the imaginary parts. In our model the imaginary parts of the form factors  $F_2^\pm$  vanish at infinity. At every iteration step we thus write

$$\text{Re}F_2(p^2) = \hat{\kappa}_B + \frac{\mathcal{P}}{\pi} \int_{(m+m_\pi)^2}^{\infty} dp'^2 \frac{\text{Im}F_2(p'^2)}{p'^2 - p^2}, \tag{4.29}$$

where the superscripts  $\pm$  of the form factors have been dropped to keep the expression transparent. The constant  $\hat{\kappa}_B$  originates from the bare  $\gamma NN$  vertex Eq. (4.14) on the r.h.s. of Eq. (4.13). Note that, according to Eq. (4.14),  $\kappa_B^{s,v}$  are chosen the same for the form factors  $F_2^+(p^2)$  and  $F_2^-(p^2)$ . These bare constants are fixed by the requirement that the vertex reproduces the physical anomalous isoscalar and isovector magnetic moment when both nucleons are on the mass shell,

$$F_2^{+,s}(m^2) = -0.06 \quad \text{and} \quad F_2^{+,v}(m^2) = 1.85. \tag{4.30}$$

In terms of the nucleon propagator, Eq. (A.5), the Ward-Takahashi identity Eq. (F.1) gives

$$(F_1^-)^{s,v}(p^2) = \frac{\alpha(p^2)}{2} \tag{4.31}$$

and

$$(F_1^+)^{s,v}(p^2) = \frac{\alpha(p^2)m}{p^2 - m^2} \left[ \frac{p^2 + m^2}{2m} - \xi(p^2) \right]. \tag{4.32}$$

where  $\lim_{p^2 \rightarrow m^2} (F_1^+)^{s,v}(p^2)$  is finite because  $\lim_{p^2 \rightarrow m^2} \xi(p^2) = m$  due to the correct location of the pole of the renormalized propagator, see Eqs. (2.27).

As can be seen from Fig. 2.10, the loop contribution to the self-energy vanishes in the limit  $p^2 \rightarrow \infty$  and therefore it follows from Eqs. (A.6,4.31,4.32) that  $\lim_{p^2 \rightarrow \infty} (F_1^\pm)^{s,v}(p^2) - Z_2/2 = 0$ ,  $Z_2$  being the nucleon-field renormalization constant. The form factors  $(F_1^\pm)^{s,v}(p^2)$  thus obey the dispersion relations (omitting the superscripts)

$$\text{Re}F_1(p^2) = \frac{Z_2}{2} + \frac{\mathcal{P}}{\pi} \int_{(m+m_\pi)^2}^{\infty} dp'^2 \frac{\text{Im}F_1(p'^2)}{p'^2 - p^2}, \quad (4.33)$$

which are applied at every iteration step.

### 4.4.3 The electromagnetic dressing equations

The described dressing procedure amounts to finding a solution of a system of coupled integral equations for the dressed  $\gamma NN$  form factors, whose schematic form is given by Eqs. (4.13). Explicitly these equation can be written as

$$\left\{ \begin{array}{l} \Gamma_I^\mu(p) = \Gamma_I^\mu[1](p) + \Gamma_I^\mu[3](p) + \frac{1}{8\pi^2} \int d^4k \Gamma_{\alpha,R}^5(p' - k) S(p' - k) \\ \quad \times \overline{\Gamma_R^{\prime\mu}}(p' - k) (\not{p}' - \not{k} + m) \Gamma_{\alpha,R}^5(p) \\ \quad \times \delta((p - k)^2 - m^2) \theta(p_0 - k_0) \delta(k^2 - m_\pi^2) \theta(k_0), \\ \text{Re}(F_1^\pm)^{s,v}(p^2) = \frac{Z_2}{2} + \frac{\mathcal{P}}{\pi} \int_{(m+m_\pi)^2}^{\infty} dp'^2 \frac{\text{Im}(F_1^\pm)^{s,v}(p'^2)}{p'^2 - p^2}, \\ \text{Re}(F_2^\pm)^{s,v}(p^2) = \kappa_B^{s,v} + \frac{\mathcal{P}}{\pi} \int_{(m+m_\pi)^2}^{\infty} dp'^2 \frac{\text{Im}(F_2^\pm)^{s,v}(p'^2)}{p'^2 - p^2}, \end{array} \right. \quad (4.34)$$

where the notation is as follows. The terms  $\Gamma_I^\mu[1](p)$  and  $\Gamma_I^\mu[3](p)$  do not depend on the  $\gamma NN$  form factors and are given by Eqs. (4.18) and (4.25). The pole and regular parts of the dressed half-off-shell  $\gamma NN$  vertex are denoted as  $\Gamma_I^\mu(p)$  and  $\Gamma_R^\mu(p)$ , respectively. The expression for  $\Gamma_I^\mu(p)$  or  $\Gamma_R^\mu(p)$  is given by the r.h.s. of Eq. (4.12) (dropping the factor  $e$ ) in which only the imaginary or only the real parts or of the form factors  $(F_{1,2}^\pm)^{s,v}$  are retained, respectively. The primed operator  $\Gamma_R^{\prime\mu}(p)$  is given by the expression for  $\Gamma_R^\mu(p)$  in which one has to change the sign of the magnetic term  $\sim \sigma^{\mu\nu}$ . (This is because in the middle vertex of the second loop diagram in Fig. 4.3 the *incoming* nucleon is on-shell.) The regular part of the dressed half-off-shell  $\pi NN$  vertex  $\Gamma_{\alpha,R}^5(p)$  and the dressed nucleon propagator  $S(p)$  are the solution of the hadronic dressing equations Eqs. (2.30).

Taking into account that the  $\gamma NN$  vertex contains four independent Lorentz vectors and two independent isospin scalars (see Section 4.3), the first explicitly written equation above can be split into 8 scalar equations. Thus, Eqs. (4.34) is a system of 16 coupled integral equations for 16 scalar functions:  $\text{Im}(F_{1,2}^\pm)^{s,v}(p^2)$  and  $\text{Re}(F_{1,2}^\pm)^{s,v}(p^2)$ .

Note that the hadronic dressing equations Eqs. (2.30) and the electromagnetic equations Eqs. (4.34) constitute a closed system of 24 coupled integral equations for the dressed nucleon propagator and dressed half-off-shell  $\pi NN$  and  $\gamma NN$  vertices. In practice, due to the smallness of the electromagnetic coupling constant, the hadronic equations can be separated from the electromagnetic ones. For this reason, in solving Eqs. (4.34), we use the dressed nucleon propagator and dressed  $\pi NN$  vertex obtained as a solution of Eqs. (2.30).

## 4.5 Nucleon-photon form factors (nucleons, pions and photons only)

The results presented in this section are obtained using the  $\pi NN$  vertex calculated in Chapter 2. As shown there, the solution for the dressed  $\pi NN$  vertex depends on the choice of the bare form factor introduced in Eq. (2.21). However, the half-width of this form factor should not exceed a rather well defined maximum for the procedure to converge. For the present calculation of the  $\gamma NN$  form factors, we chose that solution of Eqs. (2.30) in which the bare pseudovector form factor is given by Eq. (2.31), a dipole with half-width  $\Lambda_N^2 = 1.28 \text{ GeV}^2$  (calculation (I) in Section 2.6). We also did the calculation using the other choice of the bare  $\pi NN$  vertex, given by Eq. (2.32), with the half-width  $\Lambda_N^2 = 1.33 \text{ GeV}^2$  (not shown), and found that the results for the  $\gamma NN$  form factors do not depend significantly on the choice of the  $\pi NN$  vertex.

Since the  $\gamma NN$  vertex obeys the Ward-Takahashi identity, the form factors  $F_1^\pm(p^2)$  are uniquely determined by the nucleon self-energy functions according to Eqs. (4.31,4.32). Due to the presence of the term  $\Gamma_I^\mu[3]$  in Eqs. (4.34), these constraints are satisfied by the converged vertex, which was checked numerically and also proved analytically (see Appendix F). One of the consequences of the Ward-Takahashi identity is that  $(F_1^\pm)^s = (F_1^\pm)^v$  and therefore  $F_1^\pm = 0$  for the neutron-photon vertex. The form factors  $F_1^\pm(p^2)$  in the proton-photon vertex are displayed in Fig. 4.4. They do not depend on the transverse part of the contact  $\gamma\pi NN$  vertex.

The dominant contribution to the form factors  $F_2$  is due to  $\Gamma_\mu[1]$ , repre-

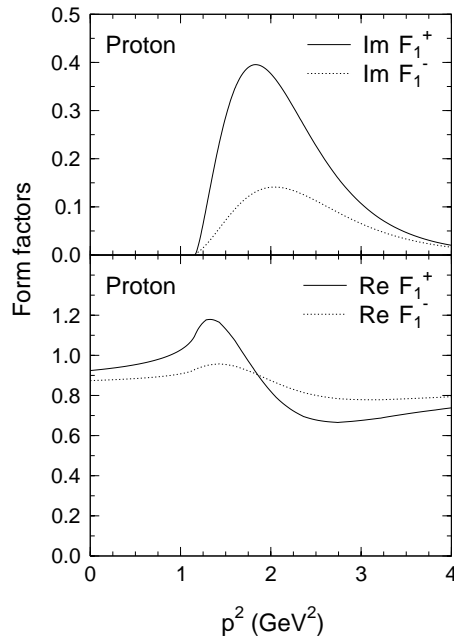


Figure 4.4: The imaginary (the upper panel) and real (the lower panel) parts of the form factors  $F_1^+$  (the solid curves) and  $F_1^-$  (the dotted curves) as functions of the momentum squared of the off-shell proton, obtained in the calculation with the nucleon, pion and photon degrees of freedom only.

sented by the first loop diagram on the r.h.s. of Fig. 4.3. Since this term is an inhomogeneity of the Eqs. (4.34), the bulk of the magnitude of the form factors is already generated in the first iteration. This however does not mean that the other integrals on the right-hand side of Eqs. (4.34) are of minor importance. In particular, they are crucial for satisfying the Ward-Takahashi identity. Thus, the Ward-Takahashi identity is not obeyed in the course of first few iteration steps and is only satisfied by the *converged* form factors.

In Fig. 4.5 the imaginary and real parts of the form factors  $F_2^\pm(p^2)$  are shown for the proton. The slope of  $\text{Im } F_2^-(p^2)$  at the pion threshold is much steeper as compared to that of  $\text{Im } F_2^+(p^2)$ . As a consequence of this, we obtain a pronounced cusp-like behaviour of  $\text{Re } F_2^-(p^2)$  at the threshold. The reason is that in pion photoproduction the  $E_{0+}$  multipole has a finite value at the threshold while other multipoles tend to zero. Since this multipole corresponds to spin and parity  $J^\pi = 1/2^-$  of the coupled nucleon-photon state, it contributes to the imaginary part of  $F_2^-$  which now obtains a term proportional to the 3-momentum of the cut intermediate pion,  $|\vec{k}| = r(p^2)/(2\sqrt{p^2})$ .



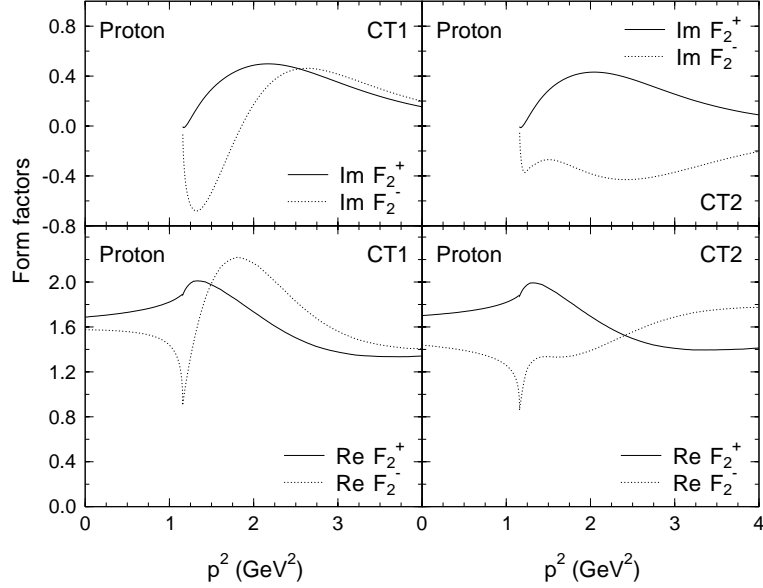


Figure 4.5: *The same as Fig. 4.4, but for the form factors  $F_2^\pm$ , for two different  $\gamma\pi NN$  contact terms, using Eq. (E.28) (left panel) and Eq. (E.32) (right panel).*

The real part of  $F_2^-$  calculated from a dispersion integral thus exhibits a pronounced cusp structure (see Appendix G). The magnitude of the cusp in  $F_2^-$  depends on the magnitude of the  $E_{0+}$  multipole multiplied by a weighted difference of the pseudoscalar and pseudovector form factors in the  $\pi NN$  vertex. By contrast, the real part of  $F_2^+$  does not have a cusp, because  $F_2^+$  is associated with the positive energy component of the off-shell nucleon carrying  $J^\pi = 1/2^+$  and thus is related to the multipoles vanishing at the threshold.

The form factors in Fig. 4.5, left panels, are calculated using the  $\gamma\pi NN$  contact term of Eq. (4.24) when evaluating  $\Gamma_{\mu,I}[3]$  in Eqs. (4.34). An alternative form of the  $\gamma\pi NN$  vertex is obtained by using Eq. (E.32) instead of Eq. (E.28). The difference between these two contact terms, Eq. (E.33), is transverse to the photon momentum. To illustrate the influence of the different choices of the contact terms on the  $\gamma NN$  vertex, in Fig. 4.5, right panels, we show the form factors  $F_2^\pm(p^2)$  calculated using the alternative contact term. From a comparison of left and right panels in Fig. 4.5, it follows that the different choices of the contact term affect mainly  $F_2^-(p^2)$ . The form factor  $F_2^+(p^2)$  is normalized at  $p^2 = m^2$  to the physical anomalous magnetic moment of the nucleon and is only slightly sensitive to the choice of the contact term. The difference between the two choices for the contact terms shows

most strongly in the  $E_{0+}$  multipole in pion photoproduction, which explains why mainly  $F_2^-(p^2)$  is affected. In a full calculation, discussed in the next chapter, including heavier meson and baryon degrees of freedom, we will fix the ambiguity in the contact  $\gamma\pi NN$  term from a comparison of the calculated  $E_{0+}$  multipole with data.

The results for the form factors  $F_2^\pm(p^2)$  in the neutron-photon vertex are shown in Fig. 4.6 for the two choices of the  $\gamma\pi NN$  term. The conclusions drawn above for the proton apply qualitatively to this case as well.

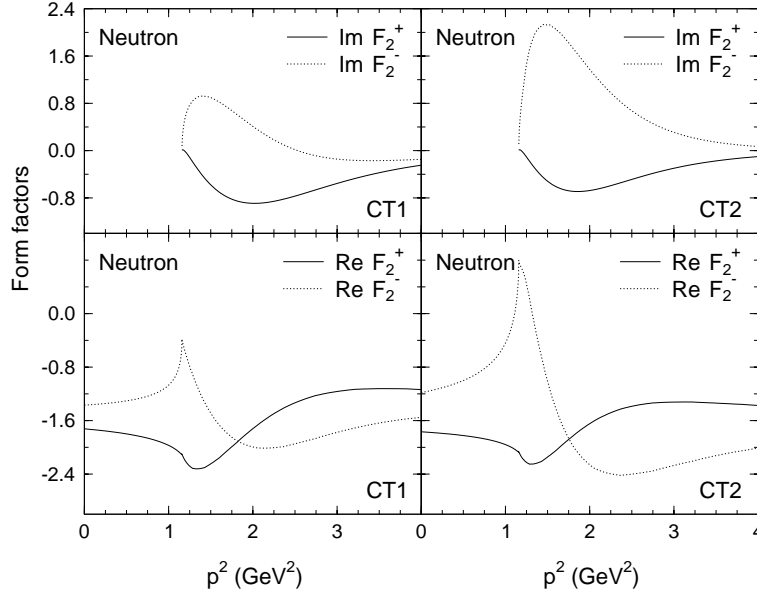


Figure 4.6: *The same as in Fig. 4.5, but for the neutron-photon vertex.*

The renormalization conditions Eq. (4.30) are fulfilled by adjusting the bare renormalization constants  $\kappa_B^{s,v}$  defined in Eq. (4.14). We obtain  $\kappa_B^s = 0.03$  and  $\kappa_B^v = 1.51$  for the calculation with the contact vertex containing Eq. (E.28) and  $\kappa_B^s = 0$  and  $\kappa_B^v = 1.6$  if the alternative term Eq. (E.32) is used.

As already stressed in connection with off-shell  $\pi NN$  vertices, the form factors in the present approach are constructed consistently with the nucleon self-energy and the K matrix, using the same representation to treat all these quantities. In particular, the self-energy functions and form factors generated through the dressing have an asymptotic behaviour which allows for the use of unsubtracted dispersion integrals. A certain circumspection should however be exercised in applying these form factors in other calculations.

## 4.6 Application in Compton scattering

As an example of the application of the formalism, Compton scattering off the nucleon is calculated in this section. Since a very restricted model space is considered in the present chapter, including only nucleons, pions and photons, for the time being we do not make a direct comparison with experimental data. For a quantitative comparison with experiment, other important degrees of freedom, such as the  $\Delta$  resonance, would have to be included. This will be the subject of the next chapter, where the full development of the model will be presented.

The amplitude for the Compton scattering process is obtained from the coupled-channel version of Eq. (2.6) in a partial wave basis [19]. The K matrix is constructed as a sum of Feynman diagrams depicted in Fig. 4.2, where the dressed vertices and propagators are used. The K matrix for Compton scattering can be written as

$$K_{\mu\nu}(q, k) = K_{\mu\nu}^s(q, k) + K_{\mu\nu}^u(q, k) + K_{\mu\nu}^c(q, k), \quad (4.35)$$

where the incoming and outgoing nucleon momenta are  $p$  and  $p'$ , respectively, the momenta of the incoming and outgoing photons are  $k^\nu$  and  $-q^\mu$  so that energy and momentum conservation reads  $p' = p + k + q$ . The nucleon-exchange contributions to Compton scattering are given by the uncrossed and crossed (s- and u-channel) diagrams,  $K_{\mu\nu}^s(q, k)$  and  $K_{\mu\nu}^u(q, k)$ , respectively.  $K_{\mu\nu}^c(q, k)$  denotes the matrix element of the crossing symmetric contact term given by Eq. (E.55). This term is added to obtain gauge invariant matrix elements and is constructed using the minimal substitution procedure (see Appendices E.2 and E.3 for details). The amplitude is crossing symmetric,  $K_{\mu\nu}(q, k) = K_{\nu\mu}(k, q)$ . Obeying gauge invariance and crossing as well as CPT symmetries is necessary to satisfy low-energy theorems [1] for the matrix elements.

The contact term Eq. (E.55) is, however, not unique and a purely transverse (with respect to the momenta of both photons) contribution may be added,

$$K_{\mu\nu}^{cI}(q, k) = \bar{u}(p') 4i \hat{e}^2 \left\{ F_c((p+k)^2) (e_4)_\mu(q, p' - q) \overline{(e_4)}_\nu(k, p+k) + \left[ \begin{array}{c} \mu \longleftrightarrow \nu \\ q \longleftrightarrow k \end{array} \right] \right\} u(p), \quad (4.36)$$

where the operator  $(e_4)_\mu(q, p' - q)$  is given by Eq. (D.1) (with photon momentum  $q$  and off-shell nucleon momentum  $p' - q$ ). The function  $F_c$  is given

by

$$F_c(p^2) = \frac{\mathcal{P}}{\pi} \int_{(m+m_\pi)^2}^{\infty} \frac{dp'^2}{p'^2 - p^2} \frac{\left(\text{Im}\tilde{F}_2^-(p'^2)\right)^2}{\text{Tr}\left(\Lambda_-(p')\tilde{\Sigma}_I(p'^2)\right)}, \quad (4.37)$$

where  $\tilde{\Sigma}_I$  and  $\text{Im}\tilde{F}_2^-$  are calculated from expressions similar to those for the imaginary parts of the nucleon self-energy and of the negative-energy form factor  $F_2^-$ , except that only the first loop diagram on the r.h.s. of Fig. 4.3 has been included and we have put  $G_2 = 0$  in the  $\pi NN$  vertex Eq. (2.9). The reason for adding this term is to take into account a principal-value contribution arising from the “handbag” 4-point one-particle irreducible loop diagram. The pole contribution from this diagram, generated in the unitarization procedure (i.e. by iterating the K matrix) and shown in Fig. 4.7, gives rise to a sharply increasing imaginary part of the Compton amplitude and thus to a pronounced cusp structure in the corresponding real part (diagram  $tt$  in Fig. 4.1). This real part was, however, not included in the model as developed up to now.

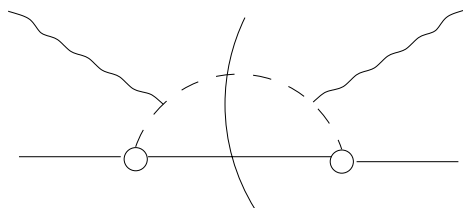


Figure 4.7: *The pole contribution to the “handbag” diagram, which contributes to the Compton amplitude through the iteration of the K matrix for pion photoproduction.*

To describe the structure of the additional “cusp” contact term  $K_{\mu\nu}^{cI}$ , it is helpful to resort to the following argument. The cut  $\pi N$  propagator can, in principle, be replaced with the sum over a complete set of partial wave states having total angular momentum and parity  $J^\pi$ . The dominant contribution to the dispersion integral will be generated by the partial wave with  $J^\pi = 1/2^-$  whose pole contribution corresponds to the pion photoproduction multipole  $E_{0+}$ , which is large at the pion threshold. To perform this projection in the most efficient manner in the present framework, two extra  $\pi NN$  vertices are inserted at the cut, allowing us to rewrite the diagram as a loop correction to the  $\gamma NN$  vertex multiplied by its conjugate (the coefficient 4 in Eq. (4.36) results from the corresponding isospin factors:  $(2\tau_3)^2 = 4$ ). However, the most

important contribution at low energies comes from the  $J^\pi = 1/2^-$  channel, i.e. the one related to  $F_2^-$ . (Please note that, due to current conservation, the bulk of the contribution arising from  $F_1^-$  is already included in Eq. (4.35) via the contact term  $K_{\mu\nu}^c$ .) To correct for the inserted  $\pi NN$  vertices, their contribution is divided out by the denominator in Eq. (4.37). Further, taking a purely pseudoscalar  $\pi NN$  vertex (by putting  $G_2 = 0$ ) reduces the coupling of positive energy states of the off-shell nucleon. The positive energy states should be suppressed because they are dominated by the channel with  $J^\pi = 1/2^+$ . The cusp behaviour of  $K_{\mu\nu}^{c'}(q, k)$  is provided by the application of the dispersion integral in Eq. (4.37). The matrix structure of  $K_{\mu\nu}^{c'}(q, k)$  ensures that it is transverse, crossing symmetric and that only negative-energy states of the intermediate nucleon are retained.

We checked numerically that the calculated amplitudes obey current conservation which was also proved analytically. In addition, the calculations obey constraints imposed by low-energy theorems [1].

Postponing a complete comparison with experiment until the next chapter, here we limit ourselves to a discussion of the  $f_{EE}^{1-}$  amplitude<sup>2</sup>. The  $f_{EE}^{1-}$  amplitude acts in the same total angular momentum and parity channel as the pion photoproduction multipole  $E_{0+}$  and therefore exhibits a highly nontrivial behaviour at the pion production threshold [4, 5, 7]. This cusp behaviour is a consequence of the unitarity and analyticity of the coupled-channel scattering matrix [69, 47]. The total angular momentum and parity of  $f_{EE}^{1-}$ ,  $J^\pi = 1/2^-$ , are the same as those of the pion photoproduction multipole  $E_{0+}^{1/2}$  which is large at the threshold, corresponding to the pion and nucleon emerging in the s-wave orbital state. Therefore, in the vicinity of pion threshold, the  $f_{EE}^{1-}$  amplitude receives a large contribution from the  $E_{0+}^{1/2}$  multipole through rescattering transitions such as  $\gamma p \rightarrow \pi^+ n \rightarrow \gamma p$ , leading to the observed cusp. (All other pion photoproduction multipoles, except  $E_{0+}$ , are small at the threshold, yielding a smooth behaviour of the real parts of the Compton partial amplitudes, except  $f_{EE}^{1-}$ .)

If the energy of the initial  $\gamma N$  pair is above threshold, the intermediate pion-nucleon state can be on the mass shell. An illustration of this situation is given by the cut handbag diagram in Fig. 4.7, which has a large imaginary part. To reproduce this feature, it suffices to have an S matrix which is unitary but not necessarily analytic. On the other hand, if the energy of the  $\gamma N$  pair is approaching the pion threshold from below, the intermediate  $\pi N$  pair can only

<sup>2</sup>This amplitude describes the  $\gamma N$  scattering in which the photons are in the electric mode, with the angular momentum  $L = 1$  of the initial photon, the total angular momentum being  $J = L - 1/2 = 1/2$ .

be off the mass shell. Although below the threshold the Compton amplitude has only a real part, this real part should be related to the imaginary part through dispersion relations. Thus, the analyticity constraints are crucial to obtain the cusp at the threshold. These constraints are incorporated (at least near the pion threshold) in the present model because dispersion integrals are used to construct the real parts of the 2- and 3-point functions as well as the additional ‘‘cusp’’  $\gamma\gamma NN$  term  $K_{\mu\nu}^{c'}$ . As a result, the calculated real part of the  $f_{EE}^{1-}$  amplitude, the solid line in Fig. 4.8, shows a distinct cusp structure at the pion production threshold. By contrast, the principal-value parts of the loop integrals contributing to the T matrix are neglected in the amplitude calculated using the K matrix with the bare vertices and the free nucleon propagator (see Eqs. (4.3,4.4)), and therefore this amplitude does not show the cusp (the dashed line in Fig. 4.8). The effect of unitarization on the real part of this amplitude is small, indistinguishable in the figure. We also show results of other calculations, where the Compton amplitude was obtained based on pion photoproduction data through the application of analyticity considerations [5, 7].

Assuming that Compton scattering is dominated by dipole process, the electric polarizability  $\bar{\alpha}$  of the proton can be calculated from  $f_{EE}^{1-}$  at small photon energies  $E_\gamma$  [5],

$$f_{EE}^{1-} = f_{EE,B}^{1-} + \frac{\bar{\alpha}}{3} E_\gamma^2, \quad (4.38)$$

where the subscript  $B$  denotes the Born amplitude. Using this relation we extract  $\bar{\alpha} = 11.6 \cdot 10^{-4} fm^3$ , which is close to the value obtained from chiral perturbation theory [70]. We will show in the next chapter that extending the model with other degrees of freedom will add a smooth function to the amplitudes, which will not affect the cusp structure of  $f_{EE}^{1-}$  but will change the value of the amplitudes at higher energies.

## 4.7 Summary

We have generalized the K-matrix formalism of Chapter 2 to obtain a coupled-channel approach to Compton scattering, pion photoproduction and pion-nucleon scattering. Accordingly, we have extended the nucleon dressing procedure to include interactions with photons. In this approach, special attention is paid to observing analyticity of the propagators and vertices in addition to unitarity, crossing symmetry and gauge invariance of the amplitude.

We have found that the dependence of the  $\gamma NN$  form factors on the

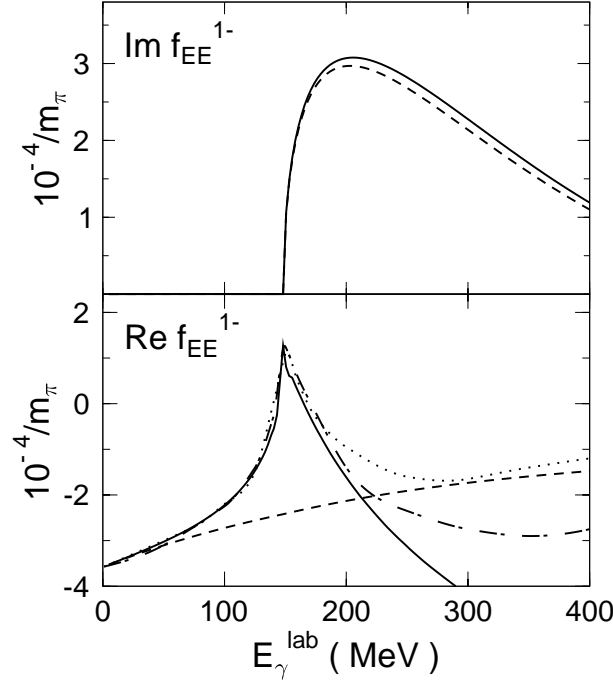


Figure 4.8: The  $f_{EE}^{1-}$  partial wave amplitude as a function of the photon energy, obtained in the calculation with the nucleon, pion and photon degrees of freedom only. The solid line represents the calculation where the dressed nucleon-photon, nucleon-pion vertices and the dressed nucleon propagator, as well as the  $\gamma\gamma NN$  contact term, are included in the  $K$  matrix. The dashed line is the calculation where the bare vertices and the free nucleon propagator are used. Results based on analyses of pion photoproduction data are shown by the dash-dotted (Ref. [5]) and dotted (Ref. [7]) lines.

momentum squared of the off-shell nucleon deviates from a monopole- (or dipole-) like shape adopted often in phenomenological applications. In particular, a characteristic feature of our results is a cusp structure of the form factors in the vicinity of the one-pion threshold, showing most clearly in the magnetic form factors corresponding to negative-energy states of the off-shell nucleon.

For the  $\gamma NN$  vertex to obey the Ward-Takahashi identity, a 4-point  $\gamma\pi NN$  term has been included in the dressing procedure. Applying the prescription of minimal substitution and using the fact that it yields a unique result only for the longitudinal part of the contact term, we have built two contact terms with different transverse components. We have found that the negative-energy magnetic form factors are influenced noticeably by the choice

of the contact term, while the effect on the positive-energy form factors is rather small.

With the present simplified model, including only nucleons, pions and photons, the discussion of effects of the dressing on observables has been limited to the  $f_{EE}^{1-}$  multipole for Compton scattering on the proton. Due to the inclusion of the contact  $\gamma\gamma NN$  vertex, built by minimal substitution, we obtain a current conserving amplitude satisfying the low-energy theorem. The additional gauge invariant contact term is crucial for obtaining the cusp of the  $f_{EE}^{1-}$  amplitude at the pion production threshold.

## Appendix D: Projection method

The calculation of the imaginary parts of the form factors (obtained from the pole contributions in Eq. (4.13)) is formulated in terms of the following projection method. The half-off-shell vertex Eq. (4.12) can be regarded as a vector in a formal four-dimensional linear space. For the sake of generality we present here the procedure for a virtual photon where the vertex is a vector in a six-dimensional space  $\mathcal{V}_6$  with the basis

$$\begin{aligned} (e_1)_\mu &= \Lambda_+(p')\gamma_\mu\Lambda_+(p), & (e_2)_\mu &= \Lambda_+(p')\gamma_\mu\Lambda_-(p), \\ (e_3)_\mu &= \Lambda_+(p')i\frac{\sigma_{\mu\nu}q^\nu}{2m}\Lambda_+(p), & (e_4)_\mu &= \Lambda_+(p')i\frac{\sigma_{\mu\nu}q^\nu}{2m}\Lambda_-(p), \\ (e_5)_\mu &= \Lambda_+(p')\frac{q_\mu}{m}\Lambda_+(p), & (e_6)_\mu &= \Lambda_+(p')\frac{q_\mu}{m}\Lambda_-(p), \end{aligned} \quad (\text{D.1})$$

defined over a ring of complex-valued functions (form factors). For the case of a real photon, as discussed in the present thesis, basis vectors  $e_5$  and  $e_6$  can be truncated from the space. Thus, to find contributions to the imaginary parts of the form factors  $F_i^\pm$  from the integrals  $\Gamma_{\mu,I}[k]$ ,  $k = 1, 2, 3$ , in Eq. (4.13), amounts to finding the coefficients of the expansion of  $\Gamma_{\mu,I}[k]$  in the basis Eq. (D.1).

The dual space  $\mathcal{V}_6^*$  can be defined as spanned over the basis  $(\theta^i)^\mu = g^{\mu\lambda}\overline{(e_i)_\lambda}$ , where the over-lining denotes the Dirac conjugate of an operator,  $\overline{A} \equiv \gamma_0 A^\dagger \gamma_0$ . We define the action of a covector  $\omega^\mu \in \mathcal{V}_6^*$  on a vector  $v_\mu \in \mathcal{V}_6$  as

$$\langle \omega^\mu, v_\mu \rangle = \text{Tr}(\omega^\mu v_\mu), \quad (\text{D.2})$$

with a tacit summation over  $\mu$  and the trace taken in spinor space. For the evaluation of the traces we used the algebraic programming system REDUCE [71]. Now if

$$v_\mu = \sum_{i=1}^6 c^i (e_i)_\mu, \quad (\text{D.3})$$



then the coefficients are obtained from the formula

$$c^k = \sum_{l=1}^6 (E^{-1})_l^k \langle (\theta^l)^\mu, v_\mu \rangle, \quad (\text{D.4})$$

where the matrix  $E_j^i = \langle (\theta^i)^\mu, (e_j)_\mu \rangle$ . The coefficients  $c^k$  are the form factors (or, more precisely, contributions to the imaginary parts of the form factors). Thus, we identify

$$\begin{aligned} c^1 &= \text{Im}F_1^+, & c^2 &= \text{Im}F_1^-, & c^3 &= \text{Im}F_2^+, \\ c^4 &= \text{Im}F_2^-, & c^5 &= \text{Im}F_3^+, & c^6 &= \text{Im}F_3^-. \end{aligned} \quad (\text{D.5})$$

We remark that this projection method could be utilized in Chapter 2 for the calculation of the pole contributions to the loop integrals for the  $\pi NN$  vertex. The only difference from the case of  $\gamma NN$  vertex is that a half-off-shell  $\pi NN$  vertex in Eq. (2.9) is a vector in the two-dimensional linear space

$$\mathcal{V}_2 = \text{Span} \left\{ \Lambda_+(p') \gamma_5, \Lambda_+(p') \gamma_5 \frac{\not{p}' - m}{m} \right\}. \quad (\text{D.6})$$

Although the calculational technique applied in Chapter 2 was different (see Appendix B), we checked that the projection method yields the same results.

## Appendix E.1: Minimal substitution in configuration space. $\gamma\pi NN$ vertex

To explain the technique of minimal substitution, we shall use examples of  $\pi NN$  vertices with off-shell nucleons and an on-shell pion. A generalization to any n-point function is straightforward.

Minimal substitution in the  $\pi NN$  vertex is discussed separately for the pseudoscalar vertex,

$$\left( \Gamma_{\pi NN}^{ps} \right)_\alpha = \tau_\alpha \gamma^5 f(p^2) + f(p'^2) \gamma^5 \tau_\alpha, \quad (\text{E.1})$$

and the pseudovector vertex,

$$\left( \Gamma_{\pi NN}^{pv1} \right)_\alpha = \tau_\alpha \gamma^5 g(p^2) \not{p}' + \not{p}' g(p'^2) \gamma^5 \tau_\alpha, \quad (\text{E.2})$$

where  $p$  and  $p'$  are the momenta of the incoming and outgoing nucleons, respectively. The sum of these reduces to the half-off-shell vertex Eq. (2.9) for  $f(p^2) = G_1(p^2) - G_2(p^2) - G_1(m^2)/2$  and  $g(p^2) = G_2(p^2)/m$ .

Let us first consider the pseudoscalar vertex Eq. (E.1). In configuration space it corresponds to the hermitian action functional of the form

$$I = -i \int d^4x \bar{\psi} \gamma^5 \tau_\alpha \phi^\alpha [f(-\square)\psi] - i \int d^4x \overline{[f(-\square)\psi]} \phi^\alpha \tau_\alpha \gamma^5 \psi, \quad (\text{E.3})$$

where the d'Alembertian  $\square \equiv \partial^2 = \partial_\mu \partial^\mu$ ,  $\psi(x)$  and  $\phi^\alpha(x)$  denote the nucleon spinor field and the pion pseudoscalar field, with the latter explicitly bearing the isospin index.  $f(-\square)$  is to be understood as a formal series expansion in powers of  $(-\square)$ , corresponding to an expansion of  $f(p^2)$  in powers of  $p^2$ . Note that, in general,  $I$  contains higher (i.e. not only first order) derivatives of the fields, thus it corresponds to a nonlocal action functional [72].

Let us switch on an external photon field  $A_\mu(x)$ . A standard way to make a theory invariant under the local  $U(1)$  gauge transformations

$$\begin{aligned} \psi(x) &\longrightarrow \exp(-i\hat{e}\alpha(x)) \psi(x), \\ A_\mu(x) &\longrightarrow A_\mu(x) + \partial_\mu \alpha(x), \end{aligned} \quad (\text{E.4})$$

is the minimal substitution procedure which consists in replacing all derivatives in the Lagrangian with their covariant counterparts,

$$\tilde{\partial}_\mu = \partial_\mu + i\hat{e}A_\mu, \quad (\text{E.5})$$

where  $\hat{e} = e\hat{e}_N = e(1 + \tau_3)/2$  is the nucleon charge operator. We are going to apply this prescription to the integrand of the functional Eq. (E.3). The d'Alembertian gets replaced with

$$\square + 2i\hat{e}A_\mu \partial^\mu + i\hat{e}(\partial^\mu A_\mu) - \hat{e}^2 A_\mu A^\mu. \quad (\text{E.6})$$

Correspondingly, due to the presence of the electromagnetic field, the functional  $I$  undergoes the transformation

$$I \longrightarrow \tilde{I} = I + \delta I, \quad (\text{E.7})$$

with the variation

$$\delta I = \int d^4x \left( \frac{\delta \tilde{I}}{\delta A_\mu} A_\mu + \mathcal{O}(A^2) \right), \quad (\text{E.8})$$

where it is tacitly understood that the variational derivative  $\delta \tilde{I} / \delta A_\mu$  is taken at the ‘‘point’’  $A_\mu = 0$ . In Eq. (E.8),  $\mathcal{O}(A^2)$  denotes all terms involving two or more photon fields. In addition to the original  $\pi NN$  vertex Eq. (E.1), the transformed action  $\tilde{I}$  contains the vertex corresponding to the first term in

the integrand of Eq. (E.8). It comprises two nucleon fields, one pion field and one photon field, i.e. it is the 4-point vertex we are after. Thus, the problem of deriving a contact  $\gamma\pi NN$  vertex has been re-expressed in terms of finding the variational derivative of  $\tilde{I}$  with respect to  $A_\mu$ . Incidentally, we note that the last term can be neglected in the covariant d'Alembertian Eq. (E.6), because the part of the variational derivative coming from this term will vanish for  $A_\mu = 0$ . So we will use only the relevant part of the covariant d'Alembertian, which reads

$$\tilde{\square} = \square + 2i\hat{e}A_\mu\partial^\mu + i\hat{e}(\partial^\mu A_\mu). \quad (\text{E.9})$$

The transformed action has the form of Eq. (E.3) with  $\square$  replaced by  $\tilde{\square}$ . It can be written as

$$\tilde{I} = \int d^4x F(A_\mu, \partial_\nu A_\mu, \partial_\nu \partial_\lambda A_\mu, \dots), \quad (\text{E.10})$$

where we have explicitly indicated only the dependence of the integrand  $F$  on the photon field and its derivatives. If  $F$  depends on  $A_\mu$  and its derivatives of the order up to and including  $N$ , then, by the Euler-Lagrange formula, the variational derivative of  $\tilde{I}$  equals

$$\frac{\delta \tilde{I}}{\delta A_\mu} = \frac{\partial F}{\partial A_\mu} + \sum_{n=1}^N (-)^n \partial_{\alpha_1} \dots \partial_{\alpha_n} \frac{\partial F}{\partial (\partial_{\alpha_1} \dots \partial_{\alpha_n} A_\mu)}. \quad (\text{E.11})$$

To give examples of the procedure outlined, we are going to build contact terms for the functionals  $I_1$  and  $I_2$  which are defined according to Eq. (E.3) with  $f(-\square) = -\square$  and  $f(-\square) = \square^2$ , respectively. Then we will generalize these results for the case of  $f(-\square) = (-\square)^k$ , for any natural  $k$ , which will allow us to formulate the contact vertex for the general form of the function  $f(-\square)$ .

First, let  $f(-\square) = -\square = -\partial^2$ . Then the corresponding  $\pi NN$  vertex Eq. (E.1) has the form

$$\tau_\alpha \gamma^5 p^2 + p'^2 \gamma^5 \tau_\alpha \quad (\text{E.12})$$

In this case, the action in the presence of electromagnetic field reads

$$\tilde{I}_1 = \int d^4x F_1(A_\mu, \partial_\nu A_\mu), \quad (\text{E.13})$$

where

$$\begin{aligned} F_1 = & i\bar{\psi} \gamma^5 \tau_\alpha \phi^\alpha [\partial^2 + 2i\hat{e}A_\mu\partial^\mu + i\hat{e}(\partial^\mu A_\mu)] \psi \\ & + i\bar{\psi} [\hat{\partial}^2 - 2i\hat{e}\hat{\partial}^\mu A_\mu - i\hat{e}(\partial^\mu A_\mu)] \tau_\alpha \phi^\alpha \gamma^5 \psi. \end{aligned} \quad (\text{E.14})$$

By Eq. (E.11),

$$\begin{aligned} \frac{\delta \tilde{I}_1}{\delta A_\mu} A_\mu &= i \left\{ 2i\tau_\alpha \hat{e} \bar{\psi} \gamma^5 \phi^\alpha (\partial^\mu \psi) - 2i\hat{e} \tau_\alpha (\bar{\psi} \overleftarrow{\partial}^\mu) \phi^\alpha \gamma^5 \psi \right. \\ &\quad \left. - i\tau_\alpha \hat{e} (\partial^\mu [\bar{\psi} \gamma^5 \phi^\alpha \psi]) + i\hat{e} \tau_\alpha ([\bar{\psi} \phi^\alpha \gamma^5 \psi] \overleftarrow{\partial}^\mu) \right\} A_\mu. \end{aligned} \quad (\text{E.15})$$

Substituting this into Eq. (E.8) and integrating the last two terms by parts (with an assumption that the interactions vanish at infinity), we obtain for the variation of  $I_1$ ,

$$\begin{aligned} \delta I_1 &= i \int d^4 x \left\{ 2i\tau_\alpha \hat{e} \bar{\psi} \gamma^5 \phi^\alpha (\partial^\mu \psi) A_\mu - 2i\hat{e} \tau_\alpha (\bar{\psi} \overleftarrow{\partial}^\mu) \phi^\alpha \gamma^5 \psi A_\mu \right. \\ &\quad \left. + i\tau_\alpha \hat{e} \bar{\psi} \gamma^5 \phi^\alpha \psi (\partial^\mu A_\mu) - i\hat{e} \tau_\alpha \bar{\psi} \phi^\alpha \gamma^5 \psi (\partial^\mu A_\mu) \right\}. \end{aligned} \quad (\text{E.16})$$

The 4-point vertex corresponding to this functional is

$$-\gamma^5 \{ \tau_\alpha \hat{e} (2p^\mu + q^\mu) + \hat{e} \tau_\alpha (2p'^\mu - q^\mu) \}, \quad (\text{E.17})$$

where  $q^\mu$  is the momentum of the incoming photon.

Now let  $f(-\partial^2) = \square^2 = \partial^4$ . Then the initial  $\pi NN$  vertex Eq. (E.1) is

$$\tau_\alpha \gamma^5 p^4 + p'^4 \gamma^5 \tau_\alpha \quad (\text{E.18})$$

and we have to take the variational derivative of the action

$$\tilde{I}_2 = \int d^4 x F_2(A_\mu, \partial_\nu A_\mu, \partial_\nu \partial_\lambda \partial_\rho A_\mu), \quad (\text{E.19})$$

where

$$\begin{aligned} F_2 &= -i\bar{\psi} \gamma^5 \tau_\alpha \phi^\alpha [\partial^4 + 4i\hat{e} A_\mu \partial^\mu \partial^2 + 2i\hat{e} (\partial^\mu A_\mu) \partial^2 + 2i\hat{e} (\partial^2 A_\mu) \partial^\mu \\ &\quad + i\hat{e} (\partial^2 \partial^\mu A_\mu) + 2i\hat{e} (\partial^\lambda \partial^\mu A_\mu) \partial_\lambda + 4i\hat{e} (\partial^\lambda A_\mu) \partial^\mu \partial_\lambda] \psi \\ &\quad - i\bar{\psi} [\overleftarrow{\partial}^4 - 4i\hat{e} \overleftarrow{\partial}^2 \overleftarrow{\partial}^\mu A_\mu - 2i\hat{e} \overleftarrow{\partial}^2 (\partial^\mu A_\mu) - 2i\hat{e} \overleftarrow{\partial}^\mu (\partial^2 A_\mu) \\ &\quad - i\hat{e} (\partial^2 \partial^\mu A_\mu) - 2i\hat{e} \overleftarrow{\partial}_\lambda (\partial^\lambda \partial^\mu A_\mu) - 4i\hat{e} \overleftarrow{\partial}_\lambda \overleftarrow{\partial}^\mu (\partial^\lambda A_\mu)] \tau_\alpha \phi^\alpha \gamma^5 \psi. \end{aligned} \quad (\text{E.20})$$

Again, applying Eq. (E.11), we find

$$\begin{aligned} \frac{\delta \tilde{I}_2}{\delta A_\mu} A_\mu &= -i \left\{ 4i\tau_\alpha \hat{e} \bar{\psi} \gamma^5 \phi^\alpha (\partial^\mu \partial^2 \psi) - 4i\hat{e} \tau_\alpha (\bar{\psi} \overleftarrow{\partial}^2 \overleftarrow{\partial}^\mu) \phi^\alpha \gamma^5 \psi \right. \\ &\quad \left. - 2i\tau_\alpha \hat{e} (\partial^\mu \bar{\psi} \gamma^5 \phi^\alpha (\partial^2 \psi)) - 4i\tau_\alpha \hat{e} (\partial_\lambda \bar{\psi} \gamma^5 \phi^\alpha (\partial^\lambda \partial^\mu \psi)) \right\} \end{aligned}$$

$$\begin{aligned}
& +2i\hat{e}\tau_\alpha(\partial^\mu(\overline{\psi}\overleftarrow{\partial}^2)\phi^\alpha\gamma^5\psi) + 4i\hat{e}\tau_\alpha(\partial_\lambda(\overline{\psi}\overleftarrow{\partial}^\lambda\overleftarrow{\partial}^\mu)\phi^\alpha\gamma^5\psi) \\
& +2i\tau_\alpha\hat{e}(\partial^2\overline{\psi}\gamma^5\phi^\alpha(\partial^\mu\psi)) + 2i\tau_\alpha\hat{e}(\partial^\lambda\partial^\mu\overline{\psi}\gamma^5\phi^\alpha(\partial_\lambda\psi)) \\
& -2i\hat{e}\tau_\alpha(\partial^2(\overline{\psi}\overleftarrow{\partial}^\mu)\phi^\alpha\gamma^5\psi) - 2i\hat{e}\tau_\alpha(\partial^\lambda\partial^\mu(\overline{\psi}\overleftarrow{\partial}_\lambda)\phi^\alpha\gamma^5\psi) \\
& -i\tau_\alpha\hat{e}(\partial^2\partial^\mu\overline{\psi}\gamma^5\phi^\alpha\psi) + i\hat{e}\tau_\alpha(\partial^2\partial^\mu\overline{\psi}\gamma^5\phi^\alpha\psi)\}A_\mu. \quad (\text{E.21})
\end{aligned}$$

Upon substituting this derivative in Eq. (E.8) and integrating the second to the sixth terms by parts once, the seventh to the tenth ones twice, and the last two terms thrice, we obtain the following 4-point vertex:

$$-\gamma^5\{\tau_\alpha\hat{e}(2p^\mu+q^\mu)[(p+q)^2+p^2]+\hat{e}\tau_\alpha(2p'^\mu-q^\mu)[(p'-q)^2+p'^2]\}. \quad (\text{E.22})$$

Next, let the  $\pi NN$  form factor in Eq. (E.1) be a monomial  $f(p^2) = p^{2k}$ ,  $k$  being a natural number. It corresponds to  $f(-\square) = (-\square)^k$  in Eq. (E.3). Following the same steps as for the two above considered cases, we obtain for the 4-point vertex:

$$-\gamma^5\{\tau_\alpha\hat{e}(2p^\mu+q^\mu)\sum_{l=0}^{k-1}p^{2l}(p+q)^{2(k-l-1)}+\hat{e}\tau_\alpha(2p'^\mu-q^\mu)\sum_{l=0}^{k-1}p'^{2l}(p'-q)^{2(k-l-1)}\}. \quad (\text{E.23})$$

A generic function  $f(p^2)$  in Eq. (E.1) can be formally expanded in powers of  $p^2$ ,

$$f(p^2) = \sum_k a_k p^{2k}. \quad (\text{E.24})$$

Using Eq. (E.23) and the identity

$$\sum_{l=0}^{k-1} x^{2l} y^{2(k-l-1)} = \frac{y^{2k} - x^{2k}}{y^2 - x^2}, \quad (\text{E.25})$$

the corresponding  $\gamma\pi NN$  vertex can be written

$$\begin{aligned}
\left(\Gamma_{\gamma\pi NN}^{ps}\right)_\alpha^\mu &= -\gamma^5\left\{\tau_\alpha\hat{e}(2p^\mu+q^\mu)\frac{f((p+q)^2)-f(p^2)}{(p+q)^2-p^2}\right. \\
& \left. +\hat{e}\tau_\alpha(2p'^\mu-q^\mu)\frac{f((p'-q)^2)-f(p'^2)}{(p'-q)^2-p'^2}\right\}, \quad (\text{E.26})
\end{aligned}$$

where  $p' = p + q$ .

As a following application, consider a pseudovector  $\pi NN$  vertex Eq. (E.2). The corresponding action functional can be written as

$$J = \int d^4x \overline{\psi}\gamma^5\tau_\alpha\phi^\alpha[g(-\square)\not{\partial}\psi] - \int d^4x \overline{g(-\square)}\not{\partial}\psi\phi^\alpha\tau_\alpha\gamma^5\psi, \quad (\text{E.27})$$

Following the procedure described above, we can write down the expression for the contact term resulting from the minimal substitution in the functional  $J$  of Eq. (E.27):

$$\begin{aligned} \left(\Gamma_{\gamma\pi NN}^{pv1}\right)_\alpha^\mu &= -\tau_\alpha \hat{e} \gamma^5 \left\{ (2p^\mu + q^\mu) \not{p} \frac{g((p+q)^2) - g(p^2)}{(p+q)^2 - p^2} + \gamma^\mu g((p+q)^2) \right\} \\ &\quad - \hat{e} \tau_\alpha \left\{ (2p'^\mu - q^\mu) \frac{g((p'-q)^2) - g(p'^2)}{(p'-q)^2 - p'^2} \not{p}' \right. \\ &\quad \left. + \gamma^\mu g((p'-q)^2) \right\} \gamma^5. \end{aligned} \quad (\text{E.28})$$

An important remark is in order here. Along with  $J$  in Eq. (E.27), an equivalent form of the action functional could be written, corresponding to the vertex

$$\left(\Gamma_{\pi NN}^{pv2}\right)_\alpha = \tau_\alpha \gamma^5 \not{p} g(p^2) + g(p'^2) \not{p}' \gamma^5 \tau_\alpha, \quad (\text{E.29})$$

which is equal to the vertex in Eq. (E.2). This alternative functional reads

$$K = \int d^4x \bar{\psi} \gamma^5 \tau_\alpha \phi^\alpha [\not{\partial} g(-\square) \psi] - \int d^4x \overline{[\not{\partial} g(-\square) \psi]} \phi^\alpha \tau_\alpha \gamma^5 \psi. \quad (\text{E.30})$$

Since the operators  $\square$  and  $\not{\partial}$  commute,  $K = J$ . Switching on the electromagnetic field amounts to the replacements  $\not{\partial} \rightarrow \tilde{\not{\partial}}$  and  $\square \rightarrow \tilde{\square}$ , see Eqs. (E.5, E.9), and correspondingly  $J \rightarrow \tilde{J}$  and  $K \rightarrow \tilde{K}$ . Now we note that  $\tilde{K} \neq \tilde{J}$ , owing to the fact that  $\tilde{\square}$  and  $\tilde{\not{\partial}}$  do not commute,

$$[\tilde{\square}, \tilde{\not{\partial}}] = i\hat{e}(\partial^2 A) + 2i\hat{e}(\partial_\mu A) \partial^\mu - 2i\hat{e}(\not{\partial} A_\mu) \partial^\mu - i\hat{e}(\not{\partial} \partial^\mu A_\mu) + \mathcal{O}(A^2). \quad (\text{E.31})$$

One can build the contact term corresponding to the functional  $K$  in Eq. (E.30),

$$\begin{aligned} \left(\Gamma_{\gamma\pi NN}^{pv2}\right)_\alpha^\mu &= -\tau_\alpha \hat{e} \gamma^5 \left\{ (2p^\mu + q^\mu) (\not{p} + \not{q}) \frac{g((p+q)^2) - g(p^2)}{(p+q)^2 - p^2} + \gamma^\mu g(p^2) \right\} \\ &\quad - \hat{e} \tau_\alpha \left\{ (2p'^\mu - q^\mu) \frac{g((p'-q)^2) - g(p'^2)}{(p'-q)^2 - p'^2} (\not{p}' - \not{q}) \right. \\ &\quad \left. + \gamma^\mu g(p'^2) \right\} \gamma^5. \end{aligned} \quad (\text{E.32})$$

The difference between the vertices in Eq. (E.28) and Eq. (E.32) equals

$$\begin{aligned} \Delta^\mu &= -\tau_\alpha \hat{e} \gamma^5 \left\{ (2p^\mu + q^\mu) \not{q} \frac{g((p+q)^2) - g(p^2)}{(p+q)^2 - p^2} + \gamma^\mu [g(p^2) - g((p+q)^2)] \right\} \\ &\quad - \hat{e} \tau_\alpha \left\{ (2p'^\mu - q^\mu) \frac{g((p'-q)^2) - g(p'^2)}{(p'-q)^2 - p'^2} (-\not{q}) \right. \\ &\quad \left. + \gamma^\mu [g(p'^2) - g((p'-q)^2)] \right\} \gamma^5, \end{aligned} \quad (\text{E.33})$$

which is transverse to the photon momentum,  $q \cdot \Delta = 0$ . This presents one example of the known ambiguity in constructing such contact vertices: terms transverse to the photon momentum are not uniquely determined by the minimal substitution prescription.

## Appendix E.2: Minimal substitution in momentum space

The technique applied here is essentially equivalent to that used in Appendix E.1, except all manipulations now will be done directly in momentum space, without resorting explicitly to variational derivatives of an action functional with higher derivatives.

The minimal substitution in momentum space amounts to the following replacement of the nucleon momentum,  $P_\mu \longrightarrow \tilde{P}_\mu = P_\mu - \hat{e}A_\mu$ , where  $P_\mu$  has to be considered as an operator acting on the right. If in a given term  $P_\mu$  is the rightmost operator and thus acts on the field of the incoming nucleon, it gives  $p_\mu$  which has c-number components. Our procedure is similar to that of Ref. [73] (other constructions of contact terms can be found in Refs. [74]). Throughout this appendix we assume that the electromagnetic field  $A_\mu$  carries the momentum  $q_\mu$  directed inwards the vertex,  $[P_\nu, A_\mu] = q_\nu A_\mu$ . We thus obtain

$$P^2 A_\mu = A_\mu (P + q)^2 = A_\mu (p + q)^2 = (p + q)^2 A_\mu, \quad (\text{E.34})$$

where for ease of writing the nucleon spinor fields have been omitted. More generally, for any smooth function  $f(p^2)$  one obtains

$$f(P^2) A_\mu = A_\mu f((p + q)^2). \quad (\text{E.35})$$

Under the minimal substitution, the nucleon momentum squared changes as

$$P^2 \longrightarrow \tilde{P}^2 = p^2 - 2\hat{e}A \cdot p - \hat{e}A \cdot q + \mathcal{O}(A^2) = p^2 - \hat{e}A^\mu (2p_\mu + q_\mu) + \mathcal{O}(A^2). \quad (\text{E.36})$$

Collecting the coefficients of the terms linear in  $A^\mu$  results in the photon vertex. This procedure is indicated by the symbol  $\mapsto$  (not to be confused with  $\longrightarrow$  which is used to denote the replacement of operators due to the minimal substitution), i.e.

$$p^2 \mapsto -\hat{e}(2p_\mu + q_\mu), \quad (\text{E.37})$$

which reads that upon minimal substitution a  $p^2$  term in an n-point Green's function generates an (n-point+photon) function corresponding to the vertex  $\Gamma_\mu = -\hat{e}(2p_\mu + q_\mu)$ .

To generalize this for an arbitrary function  $f(p^2)$ , we first consider the following combination:

$$\begin{aligned} P^2 \tilde{P}^2 &= p^4 - 2\hat{e}q^2 A \cdot p - 2\hat{e}A \cdot p p^2 - 4\hat{e}q \cdot p A \cdot p - \hat{e}q^2 A \cdot q - \hat{e}A \cdot q p^2 \\ &\quad - 2\hat{e}A \cdot q q \cdot p + \mathcal{O}(A^2) = p^4 - \hat{e} A^\mu (2p_\mu + q_\mu) (p+q)^2 + \mathcal{O}(A^2), \end{aligned} \quad (\text{E.38})$$

where Eq. (E.36) has been used. The next step is to find the result of the minimal substitution in the monomials  $p^{2n}$ ,  $n = 1, 2, 3 \dots$ . Using Eqs. (E.34, E.36) and Eq. (E.38), we have

$$\begin{aligned} P^{2n} \longrightarrow \tilde{P}^{2n} &= p^{2n} - [2\hat{e}A \cdot p + \hat{e}A \cdot q] \overbrace{P^2 \dots P^2}^{n-1} \\ &\quad - P^2 [2\hat{e}A \cdot p + \hat{e}A \cdot q] \overbrace{P^2 \dots P^2}^{n-2} \\ &\quad - \dots - \overbrace{P^2 \dots P^2}^{n-1} [2\hat{e}A \cdot p + \hat{e}A \cdot q] + \mathcal{O}(A^2) \\ &= p^{2n} - \hat{e} A^\mu (2p_\mu + q_\mu) \sum_{m=0}^{n-1} (p+q)^{2m} p^{2(n-1-m)} + \mathcal{O}(A^2). \end{aligned} \quad (\text{E.39})$$

The corresponding vertex is thus given by

$$p^{2n} \longmapsto -\hat{e} (2p_\mu + q_\mu) \frac{(p+q)^{2n} - p^{2n}}{(p+q)^2 - p^2}, \quad (\text{E.40})$$

where the identity Eq. (E.25) has been used. Since a generic function  $f(p^2)$  can be formally expanded in powers of  $p^2$  as in Eq. (E.24), we obtain

$$f(p^2) \longmapsto -\hat{e} (2p_\mu + q_\mu) \frac{f((p+q)^2) - f(p^2)}{(p+q)^2 - p^2}. \quad (\text{E.41})$$

Minimal substitution in  $\not{p}$  results in

$$\not{p} \longmapsto -\hat{e}\gamma_\mu. \quad (\text{E.42})$$

Under minimal substitution the product  $f(p^2)\not{p}$  changes as

$$\begin{aligned} f(P^2)\not{P} &\longrightarrow f(\tilde{P}^2)\tilde{\not{P}} = f(\tilde{P}^2)\not{p} - f((p+q)^2)\hat{e}A^\mu\gamma_\mu + \mathcal{O}(A^2) \\ &= f(p^2)\not{p} - \hat{e}A^\mu(2p_\mu + q_\mu) \frac{f(p+q)^2 - f(p^2)}{(p+q)^2 - p^2} \not{p} \\ &\quad - \hat{e}A^\mu\gamma_\mu f((p+q)^2) + \mathcal{O}(A^2), \end{aligned} \quad (\text{E.43})$$



and hence

$$f(p^2)\not{p} \mapsto -\hat{e}(2p_\mu + q_\mu) \frac{f(p+q)^2 - f(p^2)}{(p+q)^2 - p^2} \not{p} - \hat{e} \gamma_\mu f((p+q)^2). \quad (\text{E.44})$$

Using the above formulae, one can obtain the  $\gamma\pi NN$  contact terms Eqs. (E.26,E.28,E.32) directly in momentum space by doing the minimal substitution in Eqs. (E.1,E.2,E.29), respectively.

Some other useful formulae are stated without proof,

$$g(p \cdot k) \mapsto -\hat{e} k_\mu \frac{g((p+q) \cdot k) - g(p \cdot k)}{q \cdot k}, \quad (\text{E.45})$$

$$\frac{1}{(p+k)^2 - p^2} \mapsto -\hat{e} \frac{2k_\mu}{[(p+k+q)^2 - (p+q)^2][(p+k)^2 - p^2]}, \quad (\text{E.46})$$

$$f(p^2)g(p \cdot k) \mapsto -\hat{e} \left\{ (2p_\mu + q_\mu) \frac{f((p+q)^2) - f(p^2)}{(p+q)^2 - p^2} g(p \cdot k) + k_\mu f((p+q)^2) \frac{g((p+q) \cdot k) - g(p \cdot k)}{q \cdot k} \right\}, \quad (\text{E.47})$$

$$p_\mu \mapsto -\hat{e} g_{\mu\nu}, \quad (\text{E.48})$$

where  $k$  is the incoming momentum of an uncharged third particle and  $g(p \cdot k)$  is a generic function.

The formulae for minimal substitution in  $P'$ , the momentum associated with the outgoing nucleon, are analogous to the above, except that everywhere  $q$  should be replaced by  $-q$ .

Please note that the terms generated by this minimal substitution procedure are free from poles in the limit of  $q \rightarrow 0$ .

### Appendix E.3: $\gamma\gamma NN$ vertex from minimal substitution

As a first step, the  $\gamma NN$  vertex needs to be constructed which reduces to the appropriate half-off-shell vertex and in addition obeys the Ward-Takahashi identity. It is constructed through minimal substitution in the inverse dressed nucleon propagator,

$$S^{-1}(p) = \frac{1}{2}[\alpha(p^2)\not{p} + \not{p} \alpha(p^2)] + \beta(p^2), \quad (\text{E.49})$$

where  $\beta(p^2) = -\alpha(p^2)\xi(p^2)$  in terms of Eq. (A.5). We can use Eqs. (E.41,E.44) to write the nucleon-photon vertex obtained by the minimal substitution as

$$\Gamma_\mu^{min}(p', p) = \hat{e}_N \left\{ \frac{p'_\mu + p_\mu}{p'^2 - p^2} [S^{-1}(p') - S^{-1}(p)] \right.$$

$$+ \frac{\alpha(p'^2) + \alpha(p^2)}{2} [\gamma_\mu - \not{q} \frac{2p_\mu + q_\mu}{p'^2 - p^2}], \quad (\text{E.50})$$

where  $p' = p + q$ . This vertex clearly satisfies the Ward-Takahashi identity Eq. (F.1). In principle, both nucleons can be off the mass shell in this vertex.

A general form for the vertex can now be written as

$$\begin{aligned} \Gamma_\mu(p', p) &= \Gamma_\mu^{min}(p', p) + [\not{q}, \gamma_\mu] \{F(p^2)(\not{p} - m) + H(p^2)\} \\ &+ \{(\not{p}' - m)F(p'^2) + H(p'^2)\}[\not{q}, \gamma_\mu]. \end{aligned} \quad (\text{E.51})$$

To obtain the half-off-shell vertex with the outgoing on-shell nucleon, we apply Eq. (E.51) to a positive-energy spinor  $\bar{u}(p')$  on the left,  $\bar{u}(p')\not{p}' = \bar{u}(p')m$ . Equating the resulting half-off-shell vertex to Eq. (4.12) the functions  $F(p^2)$  and  $H(p^2)$  can be determined,

$$\begin{aligned} (F)^{s,v}(p^2) &= \frac{(F_2^+)^{s,v}(p^2) - (F_2^-)^{s,v}(p^2)}{8m^2} + \frac{\alpha(p^2) - \alpha(m^2)}{8(p^2 - m^2)} \quad (\text{E.52}) \\ (H)^{s,v}(p^2) &= \frac{2(F_2^+)^{s,v}(p^2) - (F_2^+)^{s,v}(m^2)}{8m} + \frac{\alpha(p^2)m + \beta(p^2)}{4(p^2 - m^2)} + \frac{\alpha(m^2) - 1}{16m}, \end{aligned} \quad (\text{E.53})$$

where an analogue of the Gordon identity has been used in the form

$$\bar{u}(p') (p_\mu + p'_\mu) = \bar{u}(p') (\gamma_\mu \not{p} + \gamma_\mu m - i\sigma_{\mu\lambda} q^\lambda). \quad (\text{E.54})$$

To obtain the contact  $\gamma\gamma NN$  vertex we perform a minimal substitution in Eq. (E.51), with a second photon field carrying an incoming momentum  $k$  and polarization index  $\nu$ . Since both incoming ( $p$ ) and outgoing ( $p'$ ) nucleons are on the mass shell in Compton scattering, we need only the matrix element of the contact  $\gamma\gamma NN$  vertex between the positive-energy spinors of the incoming and outgoing nucleons,

$$\begin{aligned} K_{\mu\nu}^{ct}(q, k) &= \bar{u}(p') \Gamma_{\mu\nu}^{ct}(q, k) u(p) = \bar{u}(p') i\hat{e}^2 \left\{ \frac{\alpha((p+q)^2)m + \beta((p+q)^2)}{2[(p+q)^2 - m^2]} \right. \\ &\times \left[ \frac{(p_\mu + p'_\mu - k_\mu)(p_\nu + p'_\nu + q_\nu)}{(p+q)^2 - m^2} \right. \\ &\left. - \frac{(p_\mu + p'_\mu + k_\mu)(p_\nu + p'_\nu - q_\nu)}{(p+k)^2 - m^2} + 2g_{\mu\nu} \right] \\ &\left. + \frac{\alpha((p+q)^2) - \alpha(m^2)}{2[(p+q)^2 - m^2]} \left[ (p_\nu + p'_\nu + q_\nu)\gamma_\mu + (p_\mu + p'_\mu - k_\mu)\gamma_\nu \right] \right\} \end{aligned}$$

$$\begin{aligned}
& + \frac{H((p+q)^2) - H(m^2)}{(p+q)^2 - m^2} \left[ [\not{k}, \gamma_\nu](p_\mu + p'_\mu - k_\mu) \right. \\
& + (p_\nu + p'_\nu + q_\nu)[\not{q}, \gamma_\mu] \\
& \left. + F((p+q)^2) \left[ [\not{k}, \gamma_\nu]\gamma_\mu + \gamma_\nu[\not{q}, \gamma_\mu] \right] + \left[ \begin{array}{c} \mu \longleftrightarrow \nu \\ q \longleftrightarrow k \end{array} \right] \right\} u(p),
\end{aligned} \tag{E.55}$$

where  $p' = p + k + q$  and the notation introduced in Eqs. (E.49,E.52,E.53) has been used. In Eq. (E.55)  $H = H^s + H^v$  (and analogously for  $F$ ) since the contact term vanishes for the neutron. The contact term is explicitly crossing symmetric due to the last term in Eq. (E.55).

## Appendix F: Gauge invariance of the model

The Ward-Takahashi identity, a consequence of gauge invariance, imposes an important constraint on the nucleon-photon vertex [67],

$$q \cdot \Gamma(p', p) = \hat{e}_N [S^{-1}(p') - S^{-1}(p)], \tag{F.1}$$

with the photon momentum  $q^\mu = p'^\mu - p^\mu$ . In the following we prove that the photon vertex obtained in our procedure fulfills the Ward-Takahashi identity.

Initially we assume that the  $\gamma NN$  vertex on the r.h.s. of Eq. (4.13) obeys the Ward-Takahashi identity. As a first step, we prove that the pion photo-production  $K$  matrix is gauge invariant. This  $K$  matrix is written as a sum of the s-, u-, and t-channel contributions and a contact term, as shown in Fig. 4.2,

$$K_\alpha^\mu = \sum_{i=s,u,t,c} K_{i,\alpha}^\mu. \tag{F.2}$$

The incoming pion carries momentum  $k$ , the outgoing photon  $-q$  while  $p$  and  $p'$  are the momenta of the incoming and outgoing nucleons, respectively ( $p' = p + k + q$ ). Contracting each term in Eq. (F.2) with the photon momentum yields

$$q_\mu K_{s,\alpha}^\mu = \tau_\alpha \hat{e}_N \bar{u}(p') \Gamma^5(p' - k) u(p), \tag{F.3}$$

$$q_\mu K_{u,\alpha}^\mu = \hat{e}_N \tau_\alpha \bar{u}(p') \bar{\Gamma}^5(p' - q) u(p), \tag{F.4}$$

$$q_\mu K_{t,\alpha}^\mu = \tau_\beta (\hat{e}_\pi)_{\beta\alpha} \bar{u}(p') \gamma^5 g u(p), \tag{F.5}$$

$$\begin{aligned}
q_\mu K_{c,\alpha}^\mu &= -\tau_\alpha \hat{e}_N \bar{u}(p') [\Gamma^5(p' - k) - \gamma^5 g] u(p) \\
&\quad - \hat{e}_N \tau_\alpha \bar{u}(p') [\bar{\Gamma}^5(p' - q) + \gamma^5 g] u(p),
\end{aligned} \tag{F.6}$$

where we have used Eq. (F.1) and the fact that for an on-shell nucleon with momentum  $p$ ,  $\bar{u}(p)S^{-1}(p) = 0 = S^{-1}(p)u(p)$ . We also used the normalization condition for the  $\pi NN$  vertex with both nucleons on the mass shell, Eq. (2.27). Adding Eqs. (F.3–F.6) and using  $[\hat{e}_N, \tau_\alpha] = \tau_\beta(\hat{e}_\pi)_{\beta\alpha}$ , we obtain the desired result,  $q_\mu K_\alpha^\mu = 0$ .

Next we use the gauge invariance of the pion photoproduction amplitude to show that the dressed  $\gamma NN$  vertex obtained as a solution of Eq. (4.13) (whose analytic form is given by Eqs. (4.34) and the diagrammatic form by Fig. 4.3) obeys the Ward-Takahashi identity Eq. (F.1). This can be done in a transparent way with the help of diagrammatic expressions. The pole

Figure 4.9: *The diagrammatic equation for the pole contribution to the  $\gamma NN$  vertex as used in the proof of the consistency of the method with the Ward-Takahashi identity. The notation is as in Fig. 4.2. The asterisk denotes an integration over the phase space of the cut nucleon and pion lines.*

contribution to the vertex is given by the sum of cut loop diagrams entering in the dispersion integral in Eq. (4.13), see Fig. 4.3. (We assume here that the convergence of the procedure has been reached.) This sum can be rewritten by adding and subtracting a diagram containing the pole contribution to the self-energy in the incoming nucleon leg, as shown in Fig. 4.9, top. Index

$I$  on the l.h.s. of this equation indicates that only the pole contribution to the vertex is considered. To evaluate the scalar product of the r.h.s. with the photon momentum  $q_\mu$ , it is convenient to rewrite the equation as shown in Fig. 4.9, bottom. Here, a common sub-diagram, which is a nucleon-pion vertex, has been extracted from the r.h.s., and the asterisk indicates that an integration is tacitly understood over the phase space of the cut (on-shell) nucleon and pion lines. Such separation of a sub-diagram is consistent with the interpretation of Cutkosky rules as a unitarity condition [53, 54]. Note also that the Dirac spinor  $\bar{u}(p')$  is identified with the outgoing nucleon line. The sum of diagrams in the parentheses is the considered above scattering amplitude  $K_\alpha^\mu$  for pion photoproduction, which is gauge invariant. Therefore, only the last diagram on the r.h.s. contributes to

$$q_\mu \bar{u}(p') \Gamma_I^\mu(p) = -q_\mu \bar{u}(p') \Gamma^\mu(p) S(p) \Sigma_I(p) = \hat{e}_N \bar{u}(p') \Sigma_I(p), \quad (\text{F.7})$$

where  $\Sigma_I(p)$  stands for the pole contribution to the nucleon self-energy and we have used Eq. (F.1) for the vertex on the r.h.s. Eq. (F.7) corresponds precisely to the Ward-Takahashi identity for the pole contribution of the vertex since  $S^{-1}(p) = S_0^{-1}(p) - \Sigma(p)$  and the pole contribution to  $S_0^{-1}(p) = (\not{p} - m)$  is zero.

## Appendix G: Cusp from the dispersion integral

Here we show that the real part of an analytic function  $f(x)$  has a cusp provided its imaginary part rises sharply at the threshold  $x_0$ . Such a behaviour is characteristic for the imaginary parts of the form factors  $F_2^-(p^2)$ , as can be seen from the calculations presented in Figs. 4.5 and 4.6, with  $x = p^2$ ,  $x_0 = (m + m_\pi)^2$ .

Since we are interested in the threshold region only, for the purpose of illustration we assume that  $\text{Im}f(x) = \beta\sqrt{x - x_0}$  for all  $x$ , and regularize the dispersion integral by a cut-off  $L$ ,

$$\text{Re}f(x) = \beta \mathcal{P} \int_{x_0}^L dx' \frac{\sqrt{x' - x_0}}{x' - x}, \quad (\text{G.1})$$

where we have dropped the coefficient  $1/\pi$  for brevity. By varying the coefficient  $\beta$  we have a simple way to model the steepness of the imaginary part at the threshold. In particular, if  $\beta$  is very small, we can regard  $\text{Im}f(x)$  as rising smoothly at the threshold. To exhibit the cusp structure of  $\text{Re}f(x)$ , we are going to calculate the left-hand and right-hand limits of  $\text{Re}f(x)$  and

$d(\text{Ref}(x))/dx$  as  $x \rightarrow x_0 \pm 0$  (actually, the proper derivative does not exist at the threshold, as will be seen below).

Let  $x > x_0$ . In this case the pole of the integrand lies in the integration region and therefore it is not permissible to interchange the order of taking the limit  $x \rightarrow x_0 + 0$  and doing the principal-value integral in Eq. (G.1). On changing the variable of integration,  $x' = y + x$ , the principal-value integral can be written by definition,

$$\text{Ref}(x) = \beta \lim_{\epsilon \rightarrow +0} \left( \int_{x_0-x}^{-\epsilon} dy \frac{\sqrt{y+(x-x_0)}}{y} + \int_{\epsilon}^{L-x} dy \frac{\sqrt{y+(x-x_0)}}{y} \right). \quad (\text{G.2})$$

Having done the two integrals and taken more straightforward limits, we arrive at

$$\text{Ref}(x) = 2\beta\sqrt{L-x_0} + \beta\sqrt{x-x_0} \ln \frac{\sqrt{L-x_0} - \sqrt{x-x_0}}{\sqrt{L-x_0} + \sqrt{x-x_0}} + \beta\sqrt{x-x_0} \ln U, \quad (\text{G.3})$$

$$U = \lim_{\epsilon \rightarrow +0} \left[ \frac{x-x_0 - \sqrt{(x-x_0)^2 - \epsilon^2} + \sqrt{(x-x_0)(x-x_0+\epsilon)} - \sqrt{(x-x_0)(x-x_0-\epsilon)}}{x-x_0 - \sqrt{(x-x_0)^2 - \epsilon^2} + \sqrt{(x-x_0)(x-x_0+\epsilon)} - \sqrt{(x-x_0)(x-x_0-\epsilon)}} \right]^{-1}. \quad (\text{G.4})$$

The limit  $U$  is a 0/0 indeterminate form which can be treated using L'Hôpital's rule, resulting in  $U = 1$ . Thus, for  $x > x_0$ , the dispersion integral in Eq. (G.1) equals

$$\text{Ref}(x) = 2\beta\sqrt{L-x_0} + \beta\sqrt{x-x_0} \ln \frac{\sqrt{L-x_0} - \sqrt{x-x_0}}{\sqrt{L-x_0} + \sqrt{x-x_0}}, \quad x > x_0. \quad (\text{G.5})$$

Now we take the right-hand limit at the threshold,  $x \rightarrow x_0 + 0$ ,

$$\lim_{x \rightarrow x_0+0} \text{Ref}(x) = 2\beta\sqrt{L-x_0}. \quad (\text{G.6})$$

The case of  $x < x_0$  is simpler because the integrand in Eq. (G.1) does not have a pole and therefore the integral is proper, which allows one to interchange the order of the limit  $x \rightarrow x_0 - 0$  and the integration. Taking the left-hand limit under the integral sign and subsequently doing the integral, we obtain

$$\lim_{x \rightarrow x_0-0} \text{Ref}(x) = 2\beta\sqrt{L-x_0}. \quad (\text{G.7})$$

From the equality of the left-hand and right-hand limits, Eqs. (G.6,G.7), it follows that  $\lim_{x \rightarrow x_0} \text{Ref}(x)$  exists and  $\text{Ref}(x)$  is finite at the threshold  $x_0$ .

However, the same cannot be said of the derivative  $d(\text{Re}f(x))/dx$ . Indeed, from Eq. (G.5) we get the right-hand limit of the derivative

$$\lim_{x \rightarrow x_0+0} \frac{\text{Re}f(x)}{dx} = -\frac{2\beta}{\sqrt{L-x_0}}. \quad (\text{G.8})$$

The left-hand limit can be calculated directly from Eq. (G.1) (since for  $x < x_0$  the dispersion integral is proper and the differentiation  $d/dx$  can be done prior to doing the integral),

$$\lim_{x \rightarrow x_0-0} \frac{\text{Re}f(x)}{dx} = -\frac{2\beta}{\sqrt{L-x_0}} + \lim_{x \rightarrow x_0-0} \frac{2\beta}{\sqrt{x_0-x}}. \quad (\text{G.9})$$

It is seen that the left-hand limit  $x \rightarrow x_0 - 0$  of the derivative tends to infinity, which indicates that  $\text{Re}f(x)$  has a cusp at the threshold  $x_0$ . We also note that the proper derivative of  $\text{Re}f(x)$  does not exist at the threshold  $x_0$ , since the left-hand and right-hand limits, Eqs. (G.8,G.9), are not equal to each other. This is a manifestation of the fact that the function  $f(x)$  is not analytic at the threshold since the latter is a branch point. The strength (sharpness) of the cusp can be defined as the difference between the left-hand and right-hand limits,

$$\left( \lim_{x \rightarrow x_0-0} - \lim_{x \rightarrow x_0+0} \right) \frac{\text{Re}f(x)}{dx} = \lim_{x \rightarrow x_0-0} \frac{2\beta}{\sqrt{x_0-x}}. \quad (\text{G.10})$$

We see that if the slope of the imaginary part  $\text{Im}f(x)$  is gentle at the threshold, i.e. if  $\beta$  is very small, the r.h.s. of Eq. (G.10) could be finite and the cusp could be blunted.

## Chapter 5

# Pion photoproduction and Compton scattering

### 5.1 Introduction

In this chapter the full development of the model is presented. The  $\Delta$  resonance and the  $\rho$ ,  $\omega$  and  $\sigma$  mesons are included in the coupled-channel K-matrix approach to pion-nucleon scattering, pion photoproduction and Compton scattering. These degrees of freedom are important not only at intermediate but also at low photon energies. The effects due to the  $\Delta$ ,  $\rho$  and  $\sigma$  are incorporated in the dressing of the  $\gamma NN$  vertex through the use of the  $\pi NN$  vertices and nucleon self-energy obtained in Chapter 3. In addition, to obtain a quantitative description of pion photoproduction, the  $\omega$  meson is included in the K matrix and, correspondingly, in the dressing procedure.

We apply the full model to calculate multipoles for pion photoproduction as well as differential cross sections and polarization observables for Compton scattering on the proton, achieving a good quantitative description of these processes up to photon energies of 500 MeV. We also compute the two scalar and six spin polarizabilities of the proton and neutron and compare them with the predictions of other approaches and with the values extracted from recent measurements. To study effects of the dressing on the observables, the full calculation in which the K matrix is built with the dressed vertices and propagators is compared with the calculation in which bare vertices and free propagators are used.



## 5.2 Full K matrix and dressing procedure

In this section the structure of the K matrix for the calculation of pion photoproduction and Compton scattering is described. The coupled-channel K-matrix formalism was outlined in Section 4.2. The pion-nucleon scattering entry  $K_{\pi\pi}$  of the K matrix Eq. (4.5) is given in Fig. 3.1, and the pion photoproduction and Compton scattering entries,  $K_{\pi\gamma}$  and  $K_{\gamma\gamma}$ , are shown in Figs. 5.1 and 5.2, respectively.

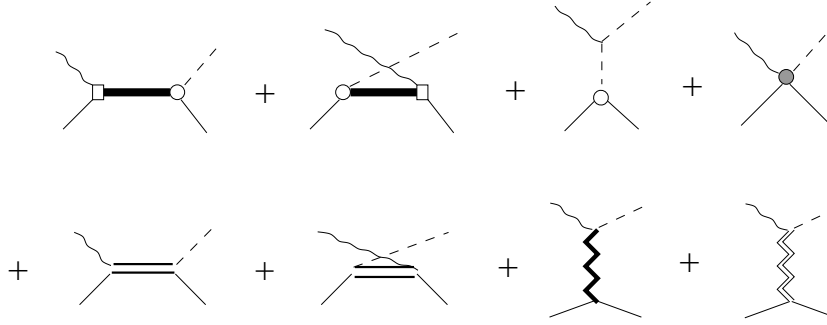


Figure 5.1: *The sum of diagrams included in the K matrix for pion photoproduction. The solid lines are nucleons, the dashed lines pions, the wavy lines photons; the straight double-lines are  $\Delta$  resonances, the zigzag line is a  $\rho$  meson and the zigzag double-line an  $\omega$  meson. The white circle and square are dressed  $\pi NN$  and  $\gamma NN$  vertices, respectively. The shaded circle is the contact  $\gamma\pi NN$  vertex. The propagators of all particles are dressed, except for the pion and the  $\omega$ .*

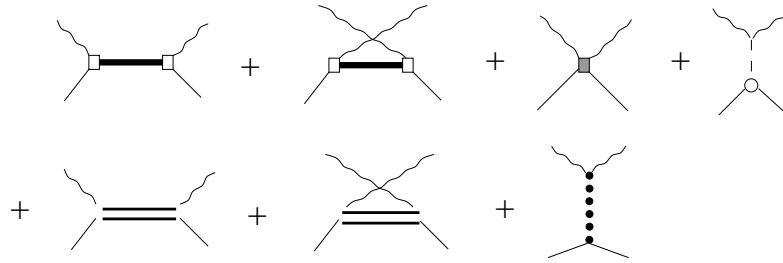


Figure 5.2: *The sum of diagrams included in the K matrix for Compton scattering. The notation is as in Fig. 5.1. In addition, the dotted line denotes the  $\sigma$  meson and the shaded square is the contact  $\gamma\gamma NN$  vertex.*

The dressed nucleon propagator and dressed  $\pi NN$  vertices used in the full K matrix have been calculated in Chapter 3. The full dressing procedure for the  $\gamma NN$  vertex is shown in Fig. 5.3. This equation is solved using the same

method as the one described in Chapter 4. The resulting dressed half-off-shell

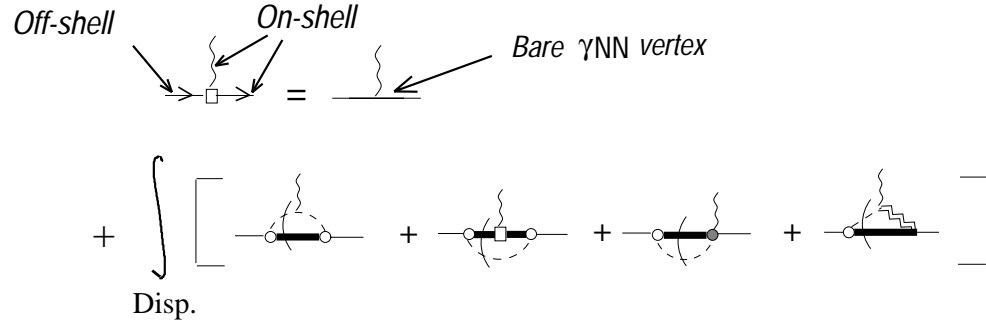


Figure 5.3: Equation for the irreducible  $\gamma NN$  vertex used in the full model. See Fig. 5.1 for explanation of the notation.

$\gamma NN$  vertex has the form given in Eq. (4.12).

The  $\Delta$ ,  $\rho$  and  $\sigma$  degrees of freedom are incorporated in the equation for the  $\gamma NN$  vertex through the dressed  $\pi NN$  vertices obtained from the equation in Fig. 3.2. The  $\omega$  meson is included in addition since it is known to be important for the description of pion photoproduction. The mass of the  $\omega$  meson is taken according to [63],  $m_\omega = 781$  MeV (the masses of the other included particles are given in Table 3.1).

The contact  $\gamma\pi NN$  and  $\gamma\gamma NN$  vertices, which are necessary for gauge invariance of the model, are constructed by minimal substitution in the dressed  $\pi NN$  vertex and nucleon propagator, as was explained in the previous chapter. The  $\gamma\gamma NN$  vertex also contains the “cusp” contact term, given by Eqs.(4.36,4.37), where the functions  $\text{Im}\tilde{F}_2^-$  and  $\tilde{\Sigma}_I$  are now obtained from the full dressing procedure.

The analytic form of the K matrix can be written by applying Feynman rules, with the 3-point vertices and propagators given in Appendix H. Below we describe only those building blocks of the K matrix which were not addressed in the purely hadronic sector of the model in Chapter 3. No additional form factors are introduced in the vertices below.

### 5.2.1 Vertices

The  $\omega\pi\gamma$  and  $\rho\pi\gamma$  vertices are taken as

$$-ie \frac{g_{V\pi\gamma}}{m_\pi} \epsilon^{\mu\nu\rho\sigma} q_\rho q'_\sigma, \quad (5.1)$$

apart from the isospin factor  $\delta_{\alpha 3}$  or  $\delta_{\alpha\beta}$  for the case of  $V = \omega$  or  $V = \rho$ , respectively. Here the incoming photon momentum is  $q$ , the incoming

pion momentum is  $q'$ , and the outgoing vector particle has momentum  $q + q'$ . Further, the polarization indices of the photon and meson are  $\mu$  and  $\nu$ , respectively. The coupling constants are fixed from the corresponding decay widths, according to the Particle Data Group values [63]:  $g_{\rho^0\pi\gamma} = 0.131$ ,  $g_{\rho^\pm\pi\gamma} = 0.103$  and  $g_{\omega\pi\gamma} = 0.313$ .

The  $\omega NN$  vertex is taken in the form ( $q$  is the  $\omega$  momentum)

$$-i g_{\omega NN} \left[ \gamma^\mu + i \kappa_\omega \frac{\sigma^{\mu\nu} q_\nu}{2m} \right], \quad (5.2)$$

where the coupling constants  $g_{\omega NN}$  and  $\kappa_\omega$  are found using the calculated pion photoproduction multipoles (all adjusted coupling constants are given in Table 5.1).

The vertex describing coupling of a neutral pion to two photons is given according to [75],

$$-i \frac{e^2 g_{\pi\gamma\gamma}}{m_\pi} \epsilon^{\mu\nu\rho\sigma} q_\rho q'_\sigma \delta_{\alpha 3}, \quad (5.3)$$

where the momenta of the photons (both pointing either inwards or outwards) are  $q$  and  $q'$ ,  $\alpha$  is the isospin index of the pion. The coupling constant  $g_{\pi\gamma\gamma}$  is fixed so that the width of the pion decay into two photons is 7.37(1.5) eV [63].

Using the same notation, the  $\sigma\gamma\gamma$  vertex is written

$$-i \frac{e^2 g_{\sigma\gamma\gamma}}{m_\sigma} [q'^\mu q^\nu - \delta^{\mu\nu} (q \cdot q')], \quad (5.4)$$

where the value of constant  $g_{\sigma\gamma\gamma}$  is found from a comparison of the calculated Compton cross section with experiment.

The  $\Delta N\gamma$  vertex is taken in the form

$$\begin{aligned} & \frac{ie}{2m_\Delta^2} \left\{ g_1 [g^{\nu\mu} \not{p} \not{q} - p^\nu \gamma^\mu \not{q} - \gamma^\nu \gamma^\mu (p \cdot q) + \gamma^\nu q^\mu \not{p}] \right. \\ & \left. + g_2 [q^\mu p^\nu - g^{\mu\nu} (p \cdot q)] \right\} \left( 1 - a \frac{\not{p}}{m_\Delta} \right) \gamma^5 T_3, \end{aligned} \quad (5.5)$$

where the incoming  $\Delta$  resonance has momentum  $p$  and Lorentz vector index  $\mu$ , the incoming photon has momentum  $q$  and Lorentz vector index  $\nu$ , and  $T_3$  is an isospin 3/2 to 1/2 transition operator. Similar to the  $\Delta N\pi$  vertex, Eq. (3.9), this vertex is chosen in such a way that  $p \cdot \Gamma = 0$ , thereby enabling us to retain only the spin-3/2 component of the Rarita-Schwinger propagator. The coupling constants in the vertex are found from a comparison of pion photoproduction multipoles and the Compton scattering cross section with data.

### 5.3 Discussion of the results

Very similar descriptions of Compton scattering and pion photoproduction can be obtained at photon laboratory energies up to 500 MeV using the two different bare  $\pi NN$  form factors from Section 3.6 – with the half-width  $\Lambda_N^2 = 2 \text{ GeV}^2$  (calculation N) and with the half-width  $\Lambda_N^2 = 3 \text{ GeV}^2$  (calculation W). Because of this small sensitivity to the bare form factor, we will present only the results obtained using  $\Lambda_N^2 = 3 \text{ GeV}^2$ . The five parameters of the purely hadronic sector of the model have been fixed in Chapter 3, providing a reasonable description of pion-nucleon phase shifts (see Table 3.3 and Fig. 3.4). The six new parameters, associated with the  $\Delta N\gamma$ ,  $\omega NN$ ,  $\sigma\gamma\gamma$  vertices in Eqs. (5.2,5.4,5.5), were determined from a comparison of the calculations with multipoles for pion photoproduction and differential cross sections as well as polarization observables for Compton scattering. The values of these parameters are summarized in Table 5.1. The values of the other coupling constants,  $g_{\rho\pi\gamma}$ ,  $g_{\omega\pi\gamma}$  and  $g_{\pi\gamma\gamma}$ , were fixed from the corresponding decay widths, as given in Section 5.2.1.

Table 5.1: *Values of the parameters which were varied in the calculations of pion photoproduction and Compton scattering on the proton, see Eqs. (5.2,5.4,5.5).*

$g_{\omega NN}$	$\kappa_\omega$	$g_{\sigma\gamma\gamma}$	$g_1$	$g_2$	$a$
10	-1.5	-1.3	-2.36	-1.5	-4

#### 5.3.1 Half-off-shell $\gamma NN$ form factors

The  $\gamma NN$  vertex Eq. (4.12) is obtained as a result of the dressing shown in Fig. 5.3. The form factors  $F_{1,2}^\pm$  are calculated using the dressed  $\pi NN$  form factors and nucleon self-energy functions shown in Figs. 3.6 and 3.8, respectively.

Since the model is gauge invariant – and thus the  $\gamma NN$  vertex obeys the Ward-Takahashi identity – there is a one-to-one correspondence between the electric form factors  $F_1^\pm$  and the nucleon self-energy, which is given by Eqs. (4.31) and (4.32). In particular, the neutron-photon electric form factors are zero. The proton form factors  $F_1^\pm(p^2)$  are shown in Fig. 5.4 as functions of the momentum squared of the proton. The magnetic form factors  $F_2^\pm$  are shown in Fig. 5.5 for the proton and in Fig. 5.6 for the neutron. If the

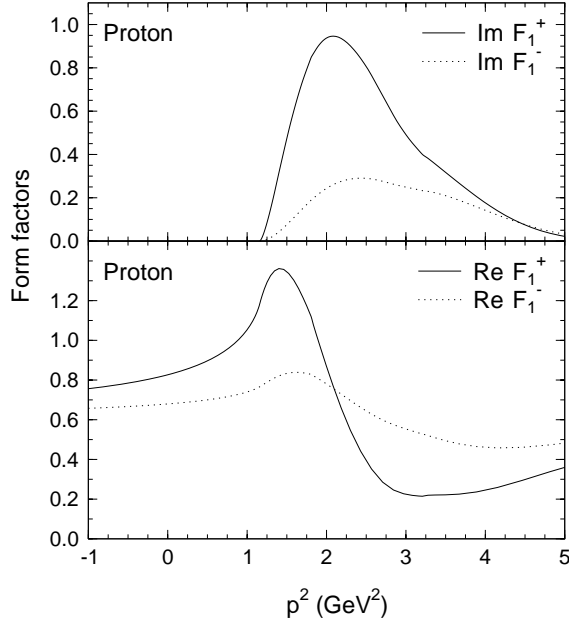


Figure 5.4: *Dependence of the electric form factors  $F_1^\pm(p^2)$  on the momentum squared of the off-shell proton.*

derivative of the imaginary part tends to infinity as  $p^2$  approaches the pion threshold from above, the real part has a sharp cusp. The cusp is blunted in the present calculation because the imaginary part rises relatively smoothly at the threshold. Both these situations are illustrated in Appendix G.

The dressed vertex is renormalized by adjusting  $\hat{\kappa}_B$  in the bare  $\gamma NN$  vertex Eq. (4.14) to fulfill the normalization conditions Eqs. (4.30). In the present calculation we find  $\kappa_B^s = 0.08$  and  $\kappa_B^v = 1.59$ .

Using minimal substitution, two  $\gamma\pi NN$  vertices were derived in the previous chapter, which differ by a purely gauge invariant (transverse) term Eq. (E.33). We showed that the form factor  $F_2^-$  is more sensitive than  $F_2^+$  to the choice of a contact  $\gamma\pi NN$  vertex, see Figs. 4.5 and 4.6. Since the electric form factors  $F_1^\pm$  are uniquely related to the nucleon self-energy through the Ward-Takahashi identity, they are completely unaffected by the ambiguity in the  $\gamma\pi NN$  vertex. In the present calculation, the contact term was chosen as the average of the two  $\gamma\pi NN$  vertices constructed in Appendix E.1,

$$\left(\Gamma_{\gamma\pi NN}^{ps}\right)_\alpha^\mu + \frac{1}{2} \left[ \left(\Gamma_{\gamma\pi NN}^{pv1}\right)_\alpha^\mu + \left(\Gamma_{\gamma\pi NN}^{pv2}\right)_\alpha^\mu \right], \quad (5.6)$$

in terms of Eqs. (E.26,E.28,E.32). The reason for this choice will be discussed

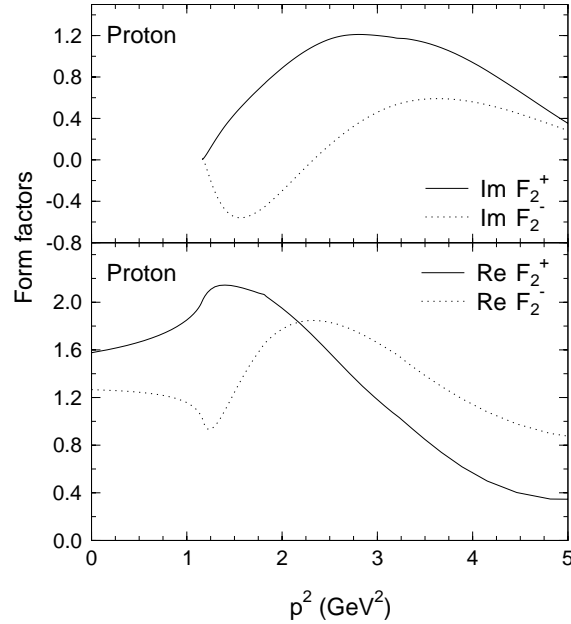


Figure 5.5: *Magnetic half-off-shell form factors  $F_2^\pm(p^2)$  for the proton.*

later, when discussing results for pion photoproduction.

In the following we shall be discussing effects of the dressing of vertices and propagators on observables by comparing two calculations (referred to as calculations B and D) based on two different K matrices. Although both these K matrices have the topological structure depicted in Figs. 5.1 and 5.2, their contents are quite different:

- *Calculation B.* The “bare” K matrix,  $K_B$ , consists of the free propagators and the bare vertices for all particles. No form factors are included, except in the bare  $\pi NN$  and  $\pi N\Delta$  vertices, Eqs. (3.2,3.9), which is necessary for the convergence of the dressing procedure. For current conservation,  $K_B$  includes the  $\gamma\pi NN$  contact term constructed by minimal substitution in the bare  $\pi NN$  vertex. Since the bare  $\gamma NN$  vertex does not have form factors, no  $\gamma\gamma NN$  term is required in  $K_B$ . The corresponding T matrix contains only the pole parts of the loop diagrams.
- *Calculation D.* The “dressed” K matrix,  $K_D$ , is composed of the dressed propagators for the nucleon,  $\Delta$ ,  $\rho$  and  $\sigma$  (the propagators of the pion and  $\omega$  are taken free) and the dressed  $\pi NN$  and  $\gamma NN$  vertices. The

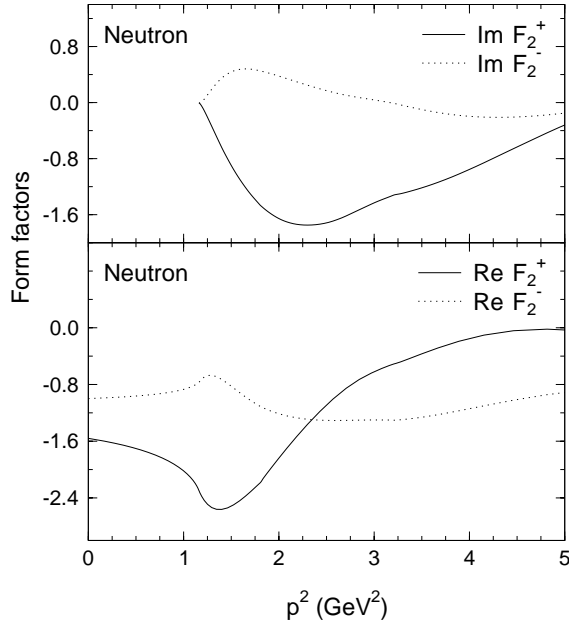


Figure 5.6: *Same as in Fig. 5.5 but for the neutron.*

other vertices are kept the same as in the “bare”  $K$  matrix. The contact  $\gamma\pi NN$  vertex is calculated by minimal substitution in the dressed  $\pi NN$  vertex. Since the dressed  $\gamma NN$  vertex contains form factors, a  $\gamma\gamma NN$  is included in  $K_D$  to provide gauge invariance of the Compton scattering amplitude. This  $\gamma\gamma NN$  vertex includes the additional “cusp” term (see Section 4.6 for details). Now both pole and principal-value parts are taken into account of a wide class of loop diagrams which contribute to the  $T$  matrix.

In both calculations B and D, the  $\pi NN$  and  $\gamma NN$  vertices are normalized on the mass shell to reproduce the physical pion-nucleon coupling constant and the nucleon anomalous magnetic moment, respectively. In addition, the Roper resonance P11 is included in the calculation of the  $K$  matrix in both calculations B and D, although not present in the dressing. This was also done in the description of pion-nucleon scattering in Chapter 3, where the contribution of the Roper resonance improved the P11 phase shift at energies above  $\approx 300$  MeV and did not affect the other phase shifts. Similarly, the inclusion of the Roper resonance is important only for the  $M_{1-}^{1/2}$  pion photoproduction multipole (which is characterized by the same isospin, orbital and

total angular momenta as the P11 phase shift) and has a marginal influence on the other multipoles.

### 5.3.2 Pion photoproduction

The calculated multipoles for pion photoproduction on the proton are shown in Fig. 5.7, where the results of both calculations D and B are given. The usual nomenclature for the multipoles is used [76]. Thus, the multipole  $M_{1-}^{3/2}$ , for example, corresponds to the transition in which the final state has total isospin  $I = 3/2$ , orbital momentum  $L = 1$  and total angular momentum  $J = L - 1/2 = 1/2$ , with the photon being in the magnetic mode.

While a satisfactory overall description of the data is achieved, it is clear that additional resonance degrees of freedom would be needed for a better agreement at higher energies. For example, the  $M_{2-}^{1/2}$  and  $E_{2-}^{1/2}$  multipoles are strongly affected by the D13 resonance, which has not been included at present. However, since we are more interested in effects of the dressing rather than in extracting parameters of resonances, we chose not to supplement the model with more degrees of freedom. Comparing the solid and dashed lines in Fig. 5.7, it is seen that effects of the dressing are most prominent in the electric and magnetic dipole multipoles  $E_{0+}^{1/2}$  and  $M_{1-}^{1/2}$ .

As pointed out earlier, gauge invariance alone does not provide sufficient restrictions on the  $\gamma\pi NN$  contact term constructed by minimal substitution: its transverse part cannot be determined unambiguously. We found that the choice of the transverse part has an influence on the multipole  $E_{0+}^{1/2}$ . By choosing different transverse parts we obtain threshold values of the  $E_{0+}^{1/2}$  multipole which differ by about 15% from the value given by the data (the other multipoles are hardly affected). The particular choice of the contact term in Eq. (5.6) allows us to fix the transverse part so that the threshold value of the  $E_{0+}^{1/2}$  multipole is in agreement with experiment. This could be interpreted in the following way. While the pole parts of one-particle irreducible diagrams are included in the pion photoproduction T matrix by iterating the K matrix, the corresponding principal-value parts are not calculated explicitly in the model. The appropriate choice of the transverse part of the contact term allows us to take these contributions into account indirectly, thus partly restoring analyticity of the T matrix. It has been shown in the context of chiral perturbation theory [78] that one-particle irreducible diagrams are important for the low-energy limit of the  $E_{0+}$  multipole.

While the correct threshold value of  $E_{0+}^{1/2}$  can be obtained in the full calculation D, it is seen that calculation B is in disagreement with the data.



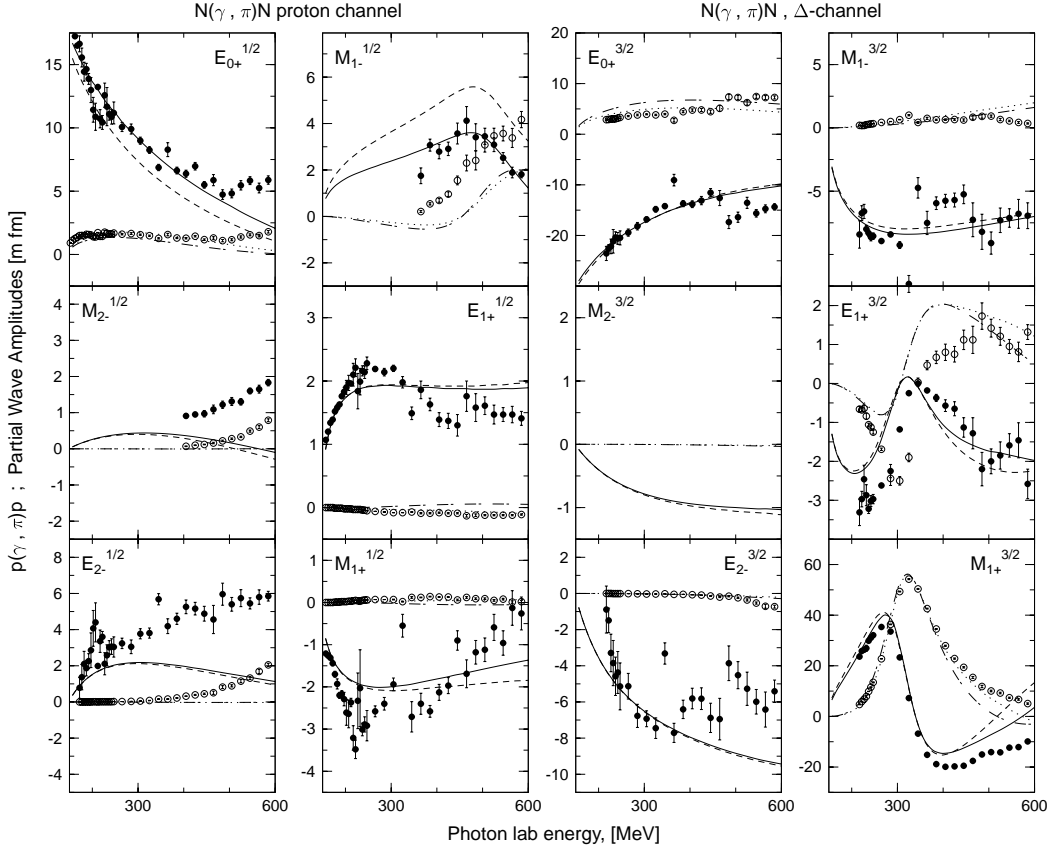


Figure 5.7: *The pion photoproduction multipoles. The solid and dotted lines are the real and imaginary parts, respectively, of the multipoles from calculation D. The dashed and dash-dotted lines are the corresponding quantities obtained without the dressing, i.e. from calculation B. The data are from Ref. [77].*

To investigate whether this feature is a genuine effect of the dressing, we attempted to obtain the correct threshold limit in calculation B by a refitting of parameters (not shown), but could not obtain a comparable overall fit. We conclude that with the “bare” K matrix  $K_B$ , it is impossible to obtain a satisfactory description of the  $E_{0+}^{1/2}$  multipole, including the low-energy limit.

As regards the non-nucleon contributions to the amplitude, it is well known that the behaviour of the  $M_{1+}^{3/2}$  and  $E_{1+}^{3/2}$  multipoles is governed by the s-channel  $\Delta$ -exchange. We also found that the  $\omega$ -exchange in the t-channel diagram (see Fig. 5.1) is important to get a good description of the  $E_{0+}^{3/2}$  and

$M_{1-}^{3/2}$  multipoles. The diagram with the  $\rho$  meson affects mainly  $M_{1+}^{1/2}$ , with a marginal influence on the other multipoles (it should be noted, however, that, in contrast to  $g_{\omega NN}$  and  $\kappa_{\omega}$ , the coupling constants in the  $\rho NN$  vertex have been fixed from  $\pi N$  scattering and thus not varied in the present calculation).

### 5.3.3 Compton scattering

The model is capable of a good description of Compton scattering on the proton up to photon energies of 500 MeV (at higher energies, degrees of freedom become important which have not been explicitly taken into account, the D13 resonance most notably). In the upper panel of Fig. 5.8 the Compton cross section is shown as a function of the photon laboratory energy, at a scattering angle of  $90^\circ$ . Also shown are the photon (beam) asymmetry at  $90^\circ$  and the proton (target) polarization at  $100^\circ$ . The latter are accessible in experiments with polarized photons or nucleons, respectively. For example, the photon asymmetry reflects the difference between the scattering of the photons with polarizations orthogonal and parallel to the scattering plane<sup>1</sup>. The observables exhibit a cusp structure at the pion threshold, especially pronounced for the photon asymmetry. As discussed in Section 4.6, this cusp is a consequence of the unitarity and analyticity properties of the coupled-channel scattering matrix, affecting primarily the  $f_{EE}^{1-}$  partial wave amplitude.

The effect of the dressing on the  $f_{EE}^{1-}$  amplitude can be seen in Fig. 5.9, where also the results of three dispersion analyses are quoted for comparison. Note that the imaginary parts of  $f_{EE}^{1-}$  from calculations B and D are rather similar in the vicinity of threshold. The cusp is generated by the analyticity considerations invoked in constructing the ‘‘cusp’’ contact  $\gamma\gamma NN$  term  $K_{\mu\nu}^{c'}$ , as described in Section 4.6. In Born approximation, the T matrix equals the sum of the first two graphs in Fig. 5.2 with the bare (but properly normalized to the physical anomalous moment)  $\gamma NN$  vertices and the free nucleon propagator. Such a calculation is not unitary, thus resulting in a purely real amplitude. By contrast, both calculations B and D are unitary, and the full calculation D in addition includes the dressing. Since gauge invariance, crossing and CPT symmetries are fulfilled in the model, all these calculations obey the low-energy theorem [1], having therefore the same limit for vanishing photon energy.

As can be seen from Fig. 5.8, effects of the dressing become very conspicuous in the region of the  $\Delta$  resonance. However, even at lower energies there are appreciable differences between calculations B and D. These are best seen

---

<sup>1</sup>For the precise definition of the observables, see Refs. [6, 8].

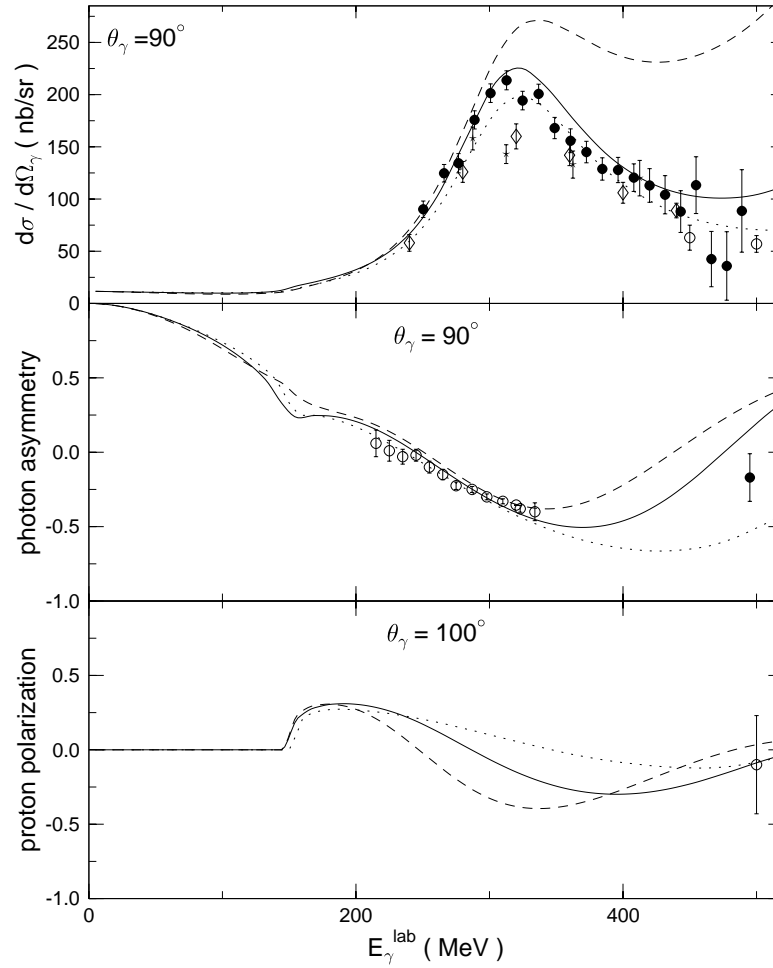


Figure 5.8: The differential cross section (top), photon asymmetry (middle) and proton polarization (bottom) as functions the photon laboratory energy, for proton Compton scattering. The solid and dashed lines are from the calculations D and B, respectively. The results of the dispersion calculation from Ref. [6] are shown by the dotted lines. The data points are taken from the following experiments. For the cross section:  $\bullet$  [7],  $\diamond$  [79],  $\star$  [80],  $\circ$  [81]; for the photon asymmetry:  $\circ$  [82],  $\bullet$  [83]; for the proton polarization:  $\circ$  [84].

if one extracts the scalar and vector polarizabilities of the nucleon, discussed in the next subsection.

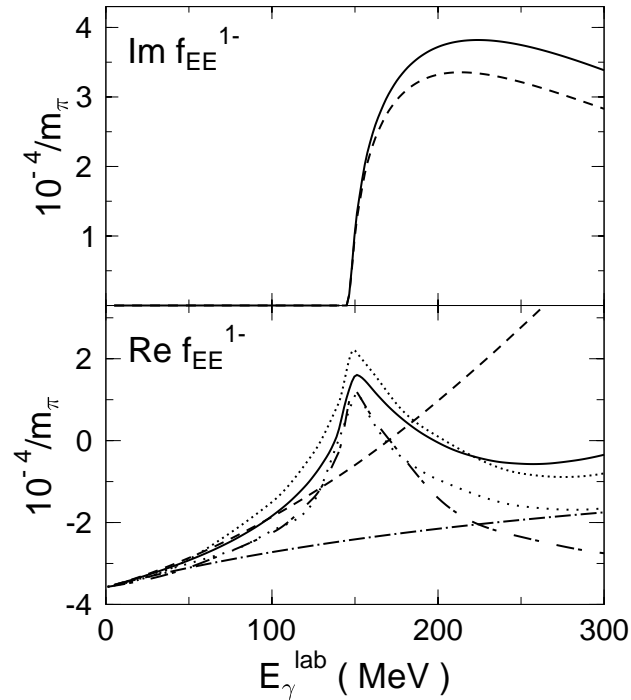


Figure 5.9:  $f_{EE}^{1-}$  partial amplitude of Compton scattering on the proton. Solid line: full calculation D; dashed line: calculation B; dense dash-dots: Born approximation. Also shown are the results of three calculation in which analyticity and unitarity constraints were incorporated: sparse dots: Ref. [7]; dense dots: Ref. [4]; sparse dash-dots: Ref. [5].

### 5.3.4 Nucleon polarizabilities

The polarizabilities characterize response of the nucleon to an externally applied electromagnetic field [85, 86]. They can be defined as coefficients in a low-energy expansion of the cross section or partial amplitudes of Compton scattering. We adhere to the standard notation for the partial amplitudes [4, 5]. Thus, the amplitude  $f_{EM}^{1+}$ , for example, describes the transition of a photon in the electric mode to one in the magnetic mode, with the angular momentum of the initial photon  $L = 1$  and the total angular momentum  $J = L + 1/2 = 3/2$ . We will attach the superscript  $NB$  (non-Born) to the difference between the full amplitude obtained in the full calculation D and the amplitude in the Born approximation. According to the low-energy theorem [1], the zeroth and first orders in an expansion of the amplitude in the small photon energy  $\omega$  are model-independent and are reproduced by the Born contribution alone. The polarizabilities enter starting at second order

and are model-dependent. Therefore, it is important to test whether the developed model yields realistic values of the nucleon polarizabilities. We are in particular interested in the role of the dressing procedure in this connection.

To calculate the polarizabilities, we use formulae given in Ref. [8]. The electric and magnetic (scalar) polarizabilities are determined using the equations

$$\alpha_E \simeq \frac{(f_{EE}^{1-} + 2f_{EE}^{1+})^{NB}}{\omega^2}, \quad \beta_M \simeq \frac{(f_{MM}^{1-} + 2f_{MM}^{1+})^{NB}}{\omega^2}. \quad (5.7)$$

The spin (vector) polarizabilities are related to third order coefficients in the low-energy expansion,

$$\gamma_{E1} \simeq \frac{(f_{EE}^{1+} - f_{EE}^{1-})^{NB}}{\omega^3}, \quad \gamma_{M1} \simeq \frac{(f_{MM}^{1+} - f_{MM}^{1-})^{NB}}{\omega^3}, \quad (5.8)$$

$$\gamma_{E2} \simeq \frac{6(f_{ME}^{1+})^{NB}}{\omega^3}, \quad \gamma_{M2} \simeq \frac{6(f_{EM}^{1+})^{NB}}{\omega^3}. \quad (5.9)$$

We calculate also the forward- and backward-angle spin polarizabilities, given by

$$\gamma_0 = -\gamma_{E1} - \gamma_{M1} - \gamma_{E2} - \gamma_{M2}, \quad \gamma_\pi = -\gamma_{E1} + \gamma_{M1} + \gamma_{E2} - \gamma_{M2}, \quad (5.10)$$

respectively. We obtained similar values for the polarizabilities extracted at the energies in the range between  $\omega = 20$  MeV and  $\omega = 100$  MeV, whereas at lower energies the numerical extraction was unreliable due to the closeness of the amplitude to the nucleon pole. For this reason, we applied a linear extrapolation to  $\omega = 0$  through the values of polarizabilities calculated at  $\omega = 80$  MeV and  $\omega = 40$  MeV (the points used for the extrapolation are immaterial within the indicated range of moderately low energies).

Our results for the electric, magnetic and spin polarizabilities of the nucleon are given in Tables 5.2 and 5.3, where also results of other calculations are summarized together with the values extracted from recent experiments. It is known [8] that the t-channel  $\pi^0$ -exchange diagram (see Fig. 5.2) gives a large contribution to the spin polarizabilities  $\gamma$ , while not affecting the scalar polarizabilities  $\alpha_E$  and  $\beta_M$ . For this reason, this contribution is often subtracted from the  $\gamma$ s, as is also done in Tables 5.2 and 5.3. We find that the  $\pi^0$ -exchange diagram gives a contribution of +10.62 to  $\gamma_{E1}^p$ ,  $\gamma_{M2}^p$ ,  $\gamma_{M1}^n$ ,  $\gamma_{E2}^n$  and -10.62 to  $\gamma_{E1}^n$ ,  $\gamma_{M2}^n$ ,  $\gamma_{M1}^p$ ,  $\gamma_{E2}^p$  (earlier works quote similar numbers:  $\pm 11.3$  [70]  $\pm 11.2$  [6],  $\pm 10.9$  [86],  $\pm 10.7$  [91]). The effect of the dressing on the polarizabilities can be seen by comparing the values given in columns D and B. In particular, the dressing tends to decrease  $\alpha_E$  while increasing  $\beta_M$ . Among the spin polarizabilities,  $\gamma_{M2}$  is affected much less than the other  $\gamma$ s.

Table 5.2: *Polarizabilities of the proton. The units are  $10^{-4}fm^3$  for  $\alpha_E$  and  $\beta_M$  and  $10^{-4}fm^4$  for the  $\gamma$ s. The  $\gamma$ s are given without the anomalous  $\pi^0$  contribution. The first two columns contain polarizabilities obtained in the full calculation D and in calculation B, respectively. Results of other approaches are quoted with the corresponding reference number. The three columns named  $\chi_{PT}$  contain the polarizabilities calculated in the chiral perturbation theory: leading order, next-to-leading order and  $\mathcal{O}(\epsilon^3)$ , from left to right. Results of dispersion analyses are collected in columns DA. The experimental values are taken from Ref. [87] for  $\alpha_E^p$  and  $\beta_E^p$ , and from Ref. [88] for  $\gamma_\pi^p$ .*

			$\chi_{PT}$			DA			Exper.
	D	B	[70]	[89, 90] ( [91] )	[86]	[6]	[66]	[9]	
$\alpha_E^p$	13.59	20.73	12.2	10.5±2.0	16.4	11.9			12.1±1.3
$\beta_M^p$	4.94	0.91	1.2	3.5±3.6	9.1	1.9			2.1∓1.3
$\gamma_{E1}^p$	-4.92	-1.54	-5.7	-1.9 ( -1.3 )	-5.4	-3.4	-4.5	-4.3	
$\gamma_{M1}^p$	2.30	3.23	-1.1	0.4 ( 3.3 )	1.4	2.7	3.4	2.9	
$\gamma_{E2}^p$	-0.55	-1.27	1.1	1.9 ( 1.8 )	1.0	1.9	2.3	2.2	
$\gamma_{M2}^p$	2.38	2.50	1.1	0.7 ( 0.2 )	1.0	0.3	-0.6	0.0	
$\gamma_0^p$	0.79	-2.91	4.6	-1.1 ( -4.0 )	2.0	-1.5	-0.6	-0.8	
$\gamma_\pi^p$	4.29	1.00	4.6	3.5 ( 6.2 )	6.8	7.7	10.8	9.4	17.3±3.4

Various contributions to the full calculation D of the polarizabilities are summarized in Tables 5.4 and 5.5 for the proton and neutron, respectively. The different rows contain the results obtained with the K matrix  $K_D$  in which only certain graphs are included (see Fig. 5.2). Thus, the polarizabilities in the first row are obtained keeping in  $K_D$  only the nucleon diagrams plus the  $\gamma\gamma NN$  contact vertex (including the “cusp” term) and the Roper resonance contribution; the second row is obtained if the  $\Delta$ -exchange dia-

Table 5.3: *Polarizabilities of the neutron. Explanation of the entries is as in Table 5.2, except that the experimental values for  $\alpha_E^n$  and  $\beta_M^n$  are taken from Ref. [92] and Ref. [93], respectively.*

			$\chi$ PT			DA			Exper.
	D	B	[70]	[89, 90] ( [91] )	[86]	[6]	[66]	[9]	
$\alpha_E^n$	14.04	20.79	12.2	13.4±1.5	16.4	13.3			12.0±2.5
$\beta_M^n$	4.35	0.65	1.2	7.8±3.6	9.1	1.8			0.0±5.0
$\gamma_{E1}^n$	-4.76	-1.57	-5.7	-4.3 ( 4.0 )	-5.4	-5.6	-5.5	-6.0	
$\gamma_{M1}^n$	2.95	3.32	-1.1	0.4 ( 2.3 )	1.4	3.8	3.4	3.9	
$\gamma_{E2}^n$	-0.60	-1.27	1.1	2.3 ( 2.2 )	1.0	2.9	2.6	3.2	
$\gamma_{M2}^n$	2.20	2.47	1.1	0.5 ( 0.4 )	1.0	-0.7	-0.6	-1.0	
$\gamma_0^n$	0.21	-2.95	4.6	1.1 ( -0.9 )	2.0	-0.4	0.1	-0.1	
$\gamma_\pi^n$	4.91	1.15	4.6	6.5 ( 8.1 )	6.8	13.0	12.1	14.1	

grams are included in addition, etc. The full result is shown in the last row. The  $\pi^0$  t-channel diagram is included in all calculations, except for the  $\gamma_s$ . As mentioned earlier, an additional degree of freedom which is included in the K matrix, but not incorporated in the dressing, is the Roper resonance P11. The second last row in Tables 5.4 and 5.5 indicates that the effect of the P11 on most polarizabilities is small (it is zero for the neutron because the isoscalar and isovector parts of the  $\gamma N(P11)$  vertex have been chosen equal to each other). The third last row shows the effect of the additional “cusp” contact term. In particular, it is seen that this term influences the electric polarizability  $\alpha_E$  much more than the magnetic polarizability  $\beta_M$ . The reason for this is that by construction, the “cusp” contact term affects primarily the electric partial amplitude  $f_{EE}^{1-}$  (corresponding to the the spin and parity of

Table 5.4: *Contributions to the full calculation of the proton polarizabilities. The notation is explained in the text.*

	$\alpha_E^p$	$\beta_M^p$	$\gamma_{E1}^p$	$\gamma_{M1}^p$	$\gamma_{E2}^p$	$\gamma_{M2}^p$
$N$	3.15	-0.96	-3.69	0.25	0.41	0.02
$N + \Delta$	-5.08	23.60	-4.91	2.29	-0.55	2.37
$N + \sigma$	21.82	-19.63	-3.69	0.25	0.40	0.03
$N(\text{no cusp}) + \Delta + \sigma$	10.45	4.88	-1.59	1.98	-0.73	2.23
$N + \Delta + \sigma(\text{no P11})$	13.65	4.68	-4.94	2.39	-0.41	2.22
$N + \Delta + \sigma$	13.59	4.94	-4.92	2.30	-0.55	2.38

Table 5.5: *Same as in Table 5.4, but for the neutron polarizabilities.*

	$\alpha_E^n$	$\beta_M^n$	$\gamma_{E1}^n$	$\gamma_{M1}^n$	$\gamma_{E2}^n$	$\gamma_{M2}^n$
$N$	3.54	-1.29	-3.50	0.81	0.36	-0.13
$N + \Delta$	-4.63	23.02	-4.75	2.95	-0.59	2.19
$N + \sigma$	22.20	-19.95	-3.51	0.81	0.35	-0.12
$N(\text{no cusp}) + \Delta + \sigma$	10.90	4.30	-1.43	2.62	-1.05	2.33
$N + \Delta + \sigma(\text{no P11})$	14.04	4.35	-4.76	2.95	-0.60	2.20
$N + \Delta + \sigma$	14.04	4.35	-4.76	2.95	-0.60	2.20

the exchanged nucleon  $J^\pi = 1/2^-$ ) rather than the magnetic amplitude  $f_{MM}^{1-}$  ( $J^\pi = 1/2^+$ ), and hence, by Eqs. (5.7), it is  $\alpha_E$  rather than  $\beta_M$  that receives the contribution of the cusp. Both the  $\Delta$  and the  $\sigma$  have a very significant effect on the polarizabilities, giving large contributions of opposite signs. It is noteworthy that only the nucleon and the  $\Delta$  (plus the Roper resonance) seem to suffice to obtain the full results for the spin polarizabilities. Also note that the  $\sigma$  meson does not affect the sum of the scalar polarizabilities,  $\alpha_E + \beta_M$ . To understand this feature, we recall that the second order term in the low-energy expansion of the differential cross section in the laboratory



frame of reference can be expressed in terms of the polarizabilities as [94]

$$-\frac{m}{2\alpha} \left[ (\alpha_E + \beta_M)(1 + \cos\theta)^2 + (\alpha_E - \beta_M)(1 - \cos\theta)^2 \right] \omega^2, \quad (5.11)$$

$\alpha$  being the fine structure constant,  $\alpha = 1/137$ . Taking into account that the t-channel  $\sigma$ -exchange diagram does not contribute at forward angles, because the  $\sigma\gamma\gamma$  vertex in Eq. (5.4) vanishes at  $\theta = 0^\circ$ , it is clear why  $\alpha_E + \beta_M$  is unaffected by the  $\sigma$ . We checked that an explicit inclusion of the D13 resonance does not affect the polarizabilities significantly.

## 5.4 Summary

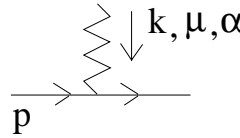
In this chapter the model for pion photoproduction and Compton scattering has been supplemented with contributions of the  $\Delta$  resonance and the  $\rho$ ,  $\omega$  and  $\sigma$  mesons. While a good overall agreement with experiment can be achieved at the photon energies up to about 500 MeV, an extension of the model to higher energies would require an inclusion of other degrees of freedom, most notably the D13 and S11 resonances.

We have shown that effects of the dressing on observables can be significant, even at relatively low energies. They are especially pronounced for the  $E_{0+}$  and  $M_{1-}$  multipoles in pion photoproduction and for the polarization observables in Compton scattering. We have found that, in our model, the low-energy behaviour of the  $E_{0+}$  multipole provides a constraint on the ambiguous transverse part of the  $\gamma\pi NN$  vertex built by minimal substitution. The contribution of the dressing is crucial for the calculated scalar and spin polarizabilities of the nucleon to be consistent with their experimental values, which lends additional support to the developed approach.

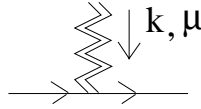
## Appendix H: Feynman rules

The vertices and propagators used in this work are summarized below.

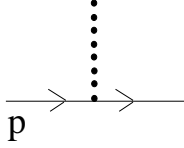
### VERTICES



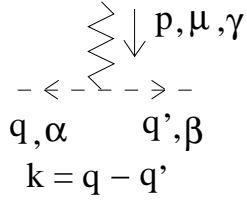
$$(\Gamma_{\rho NN})_{\alpha}^{\mu} = -i g_{\rho NN} F_N(p^2) \frac{\tau_{\alpha}}{2} \left[ \gamma^{\mu} + i \kappa_{\rho} \frac{\sigma^{\mu\nu} k_{\nu}}{2m} \right]$$



$$(\Gamma_{\omega NN})^\mu = -i g_{\omega NN} \left[ \gamma^\mu + i \kappa_\omega \frac{\sigma^{\mu\nu} k_\nu}{2m} \right]$$

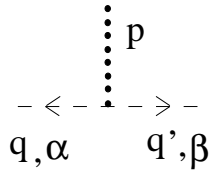


$$\Gamma_{\sigma NN} = -i g_{\sigma NN} F_N(p^2)$$

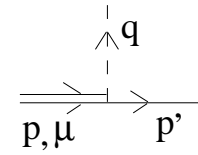


$$(\Gamma_{\rho\pi\pi})_{\alpha\beta\gamma}^\mu = (-i \epsilon_{\alpha\beta\gamma}) i g_{\rho\pi\pi} F_\rho(p^2) \left[ k^\mu - \frac{(p \cdot k)}{p^2} p^\mu \right]$$

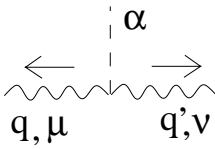
$k = q - q'$



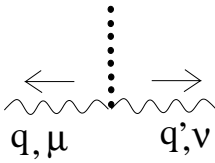
$$(\Gamma_{\sigma\pi\pi})_{\alpha\beta} = -i \frac{g_{\sigma\pi\pi}}{m_\pi} F_\sigma(p^2) \delta_{\alpha\beta} (q \cdot q')$$



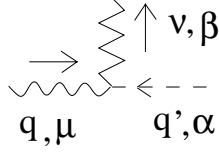
$$(\Gamma_{\pi N \Delta})_\alpha^\mu = i \frac{g_{\pi N \Delta}}{m_\pi^2} T_\alpha F_\Delta(p^2) F_N(p'^2) [\not{p} q^\mu - (p \cdot q) \gamma^\mu]$$



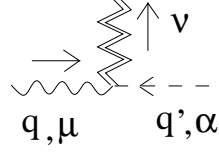
$$(\Gamma_{\pi\gamma\gamma})_{\alpha}^{\mu\nu} = -i \frac{e^2 g_{\pi\gamma\gamma}}{m_\pi} \epsilon^{\mu\nu\rho\sigma} q_\rho q'_\sigma \delta_{\alpha 3}$$



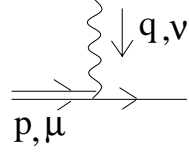
$$(\Gamma_{\sigma\gamma\gamma})^{\mu\nu} = -i \frac{e^2 g_{\sigma\gamma\gamma}}{m_\sigma} [q'^\mu q^\nu - \delta^{\mu\nu} (q \cdot q')]$$



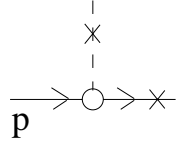
$$(\Gamma_{\rho\pi\gamma})_{\alpha\beta}^{\mu\nu} = -ie \frac{g_{\rho\pi\gamma}}{m_\pi} \epsilon^{\mu\nu\rho\sigma} q_\rho q'_\sigma \delta_{\alpha\beta}$$



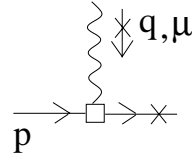
$$(\Gamma_{\omega\pi\gamma})_{\alpha}^{\mu\nu} = -ie \frac{g_{\omega\pi\gamma}}{m_\pi} \epsilon^{\mu\nu\rho\sigma} q_\rho q'_\sigma \delta_{\alpha 3}$$



$$(\Gamma_{\Delta N\gamma})^{\mu\nu} = \frac{ie}{2m_\Delta^2} \left\{ g_1 [g^{\nu\mu} \not{p} \not{q} - p^\nu \gamma^\mu \not{q} - \gamma^\nu \gamma^\mu (p \cdot q) + \gamma^\nu q^\mu \not{p}] + g_2 [q^\mu p^\nu - g^{\mu\nu} (p \cdot q)] \right\} \times \left( 1 - a \frac{\not{p}}{m_\Delta} \right) \gamma^5 T_3$$

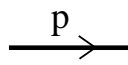


$$(\Gamma_{\pi NN})_\alpha = \tau_\alpha \gamma^5 \left[ G_S(p^2) + \frac{\not{p} + m}{2m} G_V(p^2) \right]$$



$$(\Gamma_{\gamma NN})^\mu = \sum_{l=\pm} \left[ \gamma^\mu F_1^l(p^2) + i \frac{\sigma^{\mu\nu} q_\nu}{2m} F_2^l(p^2) \right] \frac{\not{p} + m}{2m}$$

## PROPAGATORS



$$S_N = \frac{i}{\not{p} - m - \Sigma_N(p) + i0'}$$

$$\Sigma_N(p) = \overbrace{A_N(p^2) \not{p} + B_N(p^2) m}^{\Sigma_{N,L}(p)}$$

$$-(Z_2^N - 1)(\not{p} - m) - Z_2^N \delta m$$

$$\text{---} \left( \begin{array}{c} \mathbf{P} \\ \text{---} \end{array} \right) \text{---} \quad 2\pi(\not{p} + m) \delta(p^2 - m^2) \theta(p_0)$$

$$\begin{aligned} \mathbf{v} \text{---} \left( \begin{array}{c} \mathbf{P} \\ \text{---} \\ \text{---} \end{array} \right) \text{---} \boldsymbol{\mu} \quad (S_\Delta)^{\mu\nu} &= \frac{-i}{\not{p} - m_\Delta - \Sigma_\Delta(p)} \mathcal{P}_{3/2}^{\mu\nu}(p), \\ &\quad \underbrace{\Sigma_\Delta(p)}_{\Sigma_{\Delta,L}(p)} \\ \Sigma_\Delta(p) &= A_\Delta(p^2) \not{p} + B_\Delta(p^2) m_\Delta \\ &\quad - (Z_2^\Delta - 1)(\not{p} - m_\Delta) - Z_2^\Delta \delta m_\Delta, \\ \mathcal{P}_{3/2}^{\mu\nu}(p) &= g^{\mu\nu} - \frac{1}{3} \gamma^\mu \gamma^\nu - \frac{1}{3p^2} (\not{p} \gamma^\mu p^\nu + p^\mu \gamma^\nu \not{p}) \end{aligned}$$

$$\begin{aligned} \mathbf{v} \text{---} \left( \begin{array}{c} \mathbf{P} \\ \text{---} \\ \text{---} \end{array} \right) \text{---} \boldsymbol{\mu} \quad 2 \left[ \not{p} \operatorname{Im} \frac{1}{\eta(p^2)(p^2 - \omega^2(p^2))} + \operatorname{Im} \frac{\omega(p^2)}{\eta(p^2)(p^2 - \omega^2(p^2))} \right] \mathcal{P}_{3/2}^{\mu\nu}(p) \theta(p_0), \\ \eta(p^2) = Z_2^\Delta - A_\Delta(p^2), \quad \omega(p^2) = \frac{(Z_2^\Delta + B_\Delta(p^2)) - Z_2^\Delta \delta m_\Delta}{\eta(p^2)} \end{aligned}$$

$$\text{---} \text{---} \text{---} \text{---} \text{---} \text{---} \quad \mathbf{k} \quad D_\pi^0 = \frac{i}{k^2 - m_\pi^2 + i0}$$

$$\text{---} \left( \begin{array}{c} \mathbf{k} \\ \text{---} \end{array} \right) \text{---} \quad 2\pi \delta(k^2 - m_\pi^2) \theta(k_0)$$

$$\begin{aligned} \dots \dots \dots \quad \mathbf{k} \quad D_\sigma &= \frac{i}{k^2 - m_\sigma^2 - \Pi_\sigma(k^2)}, \\ \Pi_\sigma(k^2) &= \Pi_{\sigma,L}(k^2) - (Z_\sigma - 1)(k^2 - m_\sigma^2) - Z_\sigma \delta m_\sigma^2 \end{aligned}$$

$$\dots \left( \begin{array}{c} \mathbf{k} \\ \dots \end{array} \right) \dots - 2 \left[ \text{Im} \frac{1}{k^2 - m_\sigma^2 - \Pi_\sigma(k^2)} \right] \theta(k_0)$$

$$\nu \begin{array}{c} \mathbf{k} \\ \text{zigzag} \end{array} \mu \quad (D_\rho)^{\mu\nu} = \frac{-i \mathcal{P}_1^{\mu\nu}(k)}{k^2 - m_\rho^2 - \Pi_\rho(k^2)}, \quad \mathcal{P}_1^{\mu\nu}(k) = g^{\mu\nu} - \frac{k^\mu k^\nu}{k^2},$$

$$\Pi_\rho(k^2) = \Pi_{\rho,L}(k^2) - (Z_\rho - 1)(k^2 - m_\rho^2) - Z_\rho \delta m_\rho^2$$

$$\nu \begin{array}{c} \mathbf{k} \\ \text{zigzag} \end{array} \mu \quad 2 \left[ \text{Im} \frac{\mathcal{P}_1^{\mu\nu}(k)}{k^2 - m_\rho^2 - \Pi_\rho(k^2)} \right] \theta(k_0)$$

$$\nu \begin{array}{c} \mathbf{k} \\ \text{zigzag} \end{array} \mu \quad (D_\omega^0)^{\mu\nu} = \frac{-i \mathcal{P}_1^{\mu\nu}(k)}{k^2 - m_\omega^2 + i0}$$

# Concluding remarks

The main part of this thesis has been devoted to the development of the dressing procedure for the nucleon self-energy and for the  $\pi NN$  and  $\gamma NN$  vertices. As the framework for the dressing procedure, we have chosen a Lorentz invariant, unitary and crossing symmetric K-matrix approach. Furthermore, causality constraints are invoked in the model as we employ dispersion relations to construct the form factors and self-energy functions with appropriate analyticity properties. We would like to conclude with a reflection on the role of general principles underlying our model for the dressed 2- and 3-point Green's functions.

We have stressed that off-shell form factors and self-energy functions should be calculated together with the scattering amplitude in the same framework. However, due to the representation-dependence of the off-shell Green's functions on the one hand and the representation-independence of the observables on the other, experiment cannot provide an unequivocal guideline for setting up a model to calculate the Green's functions. In these circumstances, additional constraints on such a model should come from basic principles of quantum field theory. The Lorentz invariant model of this thesis exploits constraints from unitarity and causality inasmuch as it is based on the use of cutting rules and dispersion relations whose proof rests on those principles.

Unitarity implies conservation of quantum mechanical probability, irrespective of the reaction mechanism. It lies at the basis of the cutting rules which we utilize to calculate the imaginary parts of the form factors and self-energy functions from the pole contributions to the loop integrals. Causality states that two events cannot affect each other if they happen outside each other's light cones, i.e. if an unphysical signal propagating faster than light is required to connect them. The tenet of causality is of a special significance for our approach. In particular, the analyticity properties of the half-off-shell form factors and self-energy functions, which are exploited in the dressing procedure through the use of dispersion relations, can be established only

provided the interacting fields are causal.

The above argumentation can be regarded as justified only if the scattering amplitude constructed out of the resulting dressed Green's functions is consistent with experiment. We have shown that the model is capable of a good quantitative description of pion-nucleon scattering, pion photoproduction and Compton scattering at low and intermediate energies, even though the range of parameters is constrained by the dressing procedure. Particularly noteworthy is that, due to the implementation of causality constraints, we reproduce the cusp structure of the observables for Compton scattering. Also, the calculated nucleon polarizabilities are close to their measured values. The last two features were not possible to achieve in the traditional K-matrix approaches, where no dressing was taken into account.

Perhaps the most promising extension of the present approach is to apply the developed dressing technique to one-particle irreducible 4-point functions. This means treating  $\pi\pi NN$ ,  $\gamma\pi NN$  and  $\gamma\gamma NN$  vertices dynamically, i.e. calculating the principal-value parts of the one-particle irreducible diagrams by applying dispersion relations to the corresponding pole parts generated through unitarization. Such a model would give a fuller account of the analyticity properties of the scattering amplitude. Another interesting line of development is an inclusion of nuclear medium effects in our model. This is important for studying the scattering of pions and photons from nuclei, where the constituent nucleons are bound and therefore can be far off the mass shell. We have done exploratory calculations which indicate that such an extension of the model is indeed possible.

# Bibliography

- [1] F.E. Low, Phys. Rev. **96**, 1428 (1954); M. Gell-Mann and M.L. Goldberger, Phys. Rev. **96**, 1433 (1954).
- [2] S. Weinberg, *The Quantum Theory of Fields*, vol. 1 and 2 (Cambridge University Press, 1996).
- [3] S. Weinberg, Physica A **96**, 327 (1979); J. Gasser and H. Leutwyler, Ann. Phys. (Leipzig) **158**, 142 (1984); J. Gasser, M.E. Sainio, and A. Švarc, Nucl. Phys. B **307**, 779 (1988); E. Jenkins and A.V. Manohar, Phys. Lett. B **255**, 558 (1991); H. Leutwyler, Ann. Phys. (N.Y.) **235**, 165 (1994); T. Becher and H. Leutwyler, Eur. Phys. J. **C9**, 643 (1999).
- [4] W. Pfeil, H. Rollnik, and S. Stankowski, Nucl. Phys. B **73**, 166 (1974).
- [5] J.C. Bergstrom and E.L. Hallin, Phys. Rev. C **48**, 1508 (1993).
- [6] A.I. L'vov, V.A. Petrun'kin, and M. Schumacher, Phys. Rev. C **55**, 359 (1997).
- [7] A. Hünger, J. Peise, A. Robbiano et al., Nucl. Phys. A **62**, 385 (1997).
- [8] D. Babusci, G. Giordano, A.I. L'vov, G. Matone, and A.M. Nathan, Phys. Rev. C **58**, 1013 (1998).
- [9] D. Drechsel, M. Gorchtein, B. Pasquini, and M. Vanderhaeghen, Phys. Rev. C **61**, 015204 (2000).
- [10] M. Gell-Mann, M.L. Goldberger, and W.E. Thirring, Phys. Rev. **95**, 1612 (1954); M.L. Goldberger, Phys. Rev. **97**, 508 (1955).
- [11] N.N. Bogoliubov and D.V. Shirkov, *Introduction to The Theory of Quantized Fields* (Interscience Publishers, Inc., New York, 1959).



- 
- [12] *Dispersion Relations and The Abstract Approach to Field Theory*, ed. L. Klein (Gordon and Breach, Publishers, Inc., New York, 1961).
- [13] N.N. Bogolubov, A.A. Logunov, and I.T. Todorov, *Introduction to Axiomatic Quantum Field Theory* (W.A. Benjamin, Inc., London 1975).
- [14] A. Bincer, Phys. Rev. **118**, 855 (1960).
- [15] G. Barton, *Dispersion Techniques in Field Theory* (W.A. Benjamin, New York, 1965).
- [16] P.F.A. Goudsmit, H.J. Leisi, E. Matsinos, B.L. Birbrair, and A.B. Gridnev, Nucl. Phys. **A575**, 673 (1994).
- [17] O. Scholten, A.Yu. Korchin, V. Pascalutsa, and D. Van Neck, Phys. Lett. B **384**, 13 (1996).
- [18] T. Feuster and U. Mosel, Phys. Rev. C **58**, 457 (1998).
- [19] A. Yu. Korchin, O. Scholten, and R.G.E. Timmermans, Phys. Lett. B **438**, 1 (1998).
- [20] T. Feuster and U. Mosel, Phys. Rev. C **59**, 460 (1999).
- [21] E.F. Salpeter and H.A. Bethe, Phys. Rev. **84**, 1232 (1951).
- [22] A.D. Lahiff and I.R. Afnan, Phys. Rev. C **60** (1999), 024608.
- [23] B.C. Pearce and B.K. Jennings, Nucl. Phys. **A528**, 655 (1991).
- [24] F. Gross and Y. Surya, Phys. Rev. C **47**, 703 (1993).
- [25] C. Schütz, J.W. Durso, K. Holinde, and J. Speth, Phys. Rev. C **49**, 2671 (1994); C. Schütz, J. Haidenbauer, J. Speth, and J.W. Durso, Phys. Rev. C **57**, 1464 (1998).
- [26] V. Pascalutsa and J.A. Tjon, Nucl. Phys. **A631**, 534c (1998); Phys. Lett. B **435**, 245 (1998); Phys. Rev. C **61**, 054003 (2000).
- [27] S. Nozawa, B. Blankleider, and T.-S.H. Lee, Nucl. Phys. A **513**, 459 (1990); T.-S.H. Lee and B.C. Pearce, Nucl. Phys. A **530**, 532 (1991).
- [28] Y. Surya and F. Gross, Phys. Rev. C **53**, 2422 (1996).
- [29] V. Pascalutsa, Ph.D.-thesis, University of Utrecht, 1998.

- [30] E.M. Nyman, Nucl. Phys. A **160**, 517 (1971); S. Kondratyuk, G. Martinus, and O. Scholten, Phys. Lett. B **418**, 20 (1998); Yi Li, M.K. Liou, and W.M. Schreiber, Phys. Rev. C **57**, 507 (1998).
- [31] T. Sato and T.-S.H. Lee, Phys. Rev. C **54**, 2660 (1996).
- [32] F. Gross, J.W. Van Orden, and K. Holinde, Phys. Rev. C **45**, 2094 (1992).
- [33] D. Drechsel, O. Hanstein, S.S. Kamalov, and L. Tiator, Nucl. Phys. A **645**, 145 (1999).
- [34] A.Yu. Korchin, O. Scholten, and F. de Jong, Phys. Lett. B **402**, 1 (1997).
- [35] K. Nakayama, A. Szczurek, C. Hanhart, J. Haidenbauer, and J. Speth, Phys. Rev. C **57**, 1580 (1998); J. Haidenbauer, C. Hanhart, J. Speth, K. Nakayama, and J.W. Durso, in Proceedings of the 8-th International Conference on the Structure of Baryons "Baryons'98", eds. D.W. Menze and B. Metsch (World Scientific, Singapore, 1999), p. 583.
- [36] M. Ida, Phys. Rev. **136**, B1767 (1964); G.N. Epstein, Phys. Lett. **79B**, 195 (1978).
- [37] S.D. Drell and H.R. Pagels, Phys. Rev. **140**, B397 (1965); E.M. Nyman, Nucl. Phys. A **154**, 97 (1970); M.G. Hare, Ann. Phys. **74**, 595 (1972).
- [38] W.T. Nutt and C.M. Shakin, Phys. Rev. C **16**, 1107 (1977); T. Mizutani, C. Fayard, G.H. Lamot, and S. Nahabetian, Phys. Rev. C **24**, 2633 (1981).
- [39] H.W. Naus and J.H. Koch, Phys. Rev. C **36**, 2459 (1987); P.C. Tiemeijer and J.A. Tjon, Phys. Rev. C **42**, 599 (1990); J.W. Bos, S. Scherer, and J.H. Koch, Nucl. Phys. A **547**, 488 (1992); X. Song, J.P. Chen, and J.S. McCarthy, Z. Phys. **A341**, 275 (1992); J.W. Bos and J.H. Koch, Nucl. Phys. A **563**, 539 (1993); H.C. Dönges, M.Schäfer, and U. Mosel, Phys. Rev. C **51**, 950 (1995).
- [40] E.C. Nelson, Phys. Rev. **60**, 830 (1941); F.J. Dyson, Phys. Rev. **73**, 929 (1949); K.M. Case, Phys. Rev. **76**, 14 (1949).
- [41] R. Haag, Dan. Mat. Fys. Medd. **29**, no. 12, 3 (1955); D. Hall and A.S. Wightman, Mat. Fys. Medd. Dan. Vid. Selsk. **31**, no. 5, 3 (1957); R. Haag, Phys. Rev. **112**, 669 (1958); O. Greenberg, Phys. Rev. **115**, 706 (1959); H. Ekstein, Phys. Rev. **117**, 1590 (1960).

- [42] R.F. Streater and A.S. Wightman, *PCT, Spin and Statistics, and all that* (W.A. Benjamin, Inc., London 1964).
- [43] J.S.R. Chisholm, Nucl. Phys. **26**, 469 (1961); S. Kamefuchi, L. O’Raifeartaigh, and A. Salam, Nucl. Phys. **28**, 529 (1961); S. Coleman, J. Wess, and B. Zumino, Phys. Rev. **177**, 2239 (1969).
- [44] G. Barton, *Introduction to Advanced Field Theory* (Interscience Publishers, 1963).
- [45] S. Scherer and H.W. Fearing, Phys. Rev. C **51**, 359 (1995); H.W. Fearing, Phys. Rev. Lett. **81**, 758 (1998); H.W. Fearing and S. Scherer, nucl-th/9909076; R.M. Davidson and G.I. Poulis, Phys. Rev. D **54**, 2228 (1996); J. Adam, Jr., F. Gross, and J.W. Van Orden, Few Body Syst. **25**, 73 (1998).
- [46] H. Lehmann, K. Symanzik, and W. Zimmermann, Nuovo Cimento **1**, 205 (1955); A.S. Wightman, Phys. Rev. **101**, 860 (1956).
- [47] R.G. Newton, *Scattering Theory of Waves and Particles* (Springer, New York, 1982).
- [48] F.J. Dyson, Phys. Rev. **75**, 1736 (1949).
- [49] J.D. Bjorken and S.D. Drell, *Relativistic Quantum Mechanics* (McGraw-Hill, 1964); C. Itzykson and J.-B. Zuber, *Quantum Field Theory* (McGraw-Hill, Inc., 1986).
- [50] E. Kazes, Nuovo Cimento **13**, 1226 (1959).
- [51] V.B. Berestetskii, E.M. Lifshitz, and L.P. Pitaevskii, *Quantum Electrodynamics* (Pergamon Press, 1982).
- [52] R.W. Haymaker and R. Blankenbeckler, Phys. Rev. **171**, 1581 (1968).
- [53] R.E. Cutkosky, J. Math. Phys. **1**, 429 (1960); S. Mandelstam, Phys. Rev. **115**, 1741 (1959); G. ’t Hooft and M. J.G. Veltman, *Diagrammar*, CERN Yellow Report 73-09; M. Veltman, *Diagrammatica. The Path to Feynman Rules* (Cambridge University Press 1994).
- [54] M. Veltman, Physica **29**, 186 (1963).
- [55] S. Bauberger and M. Böhm, Nucl. Phys. **B445**, 25 (1995); A. Frink, J.G. Körner, and J.B. Tausk, hep-ph/9709490; P. Post and J.B. Tausk, Mod. Phys. Lett. A **11**, 2115 (1996).

- [56] J. Flender and M.F. Gari, *Phys. Rev. C* **51**, R1619 (1995).
- [57] R.W. Haymaker, *Phys. Rev.* **181**, 2040 (1969).
- [58] S. Mandelstam, *Phys. Rev.* **112**, 1344 (1958); R.J. Yaes, *Phys. Rev. D* **2**, 2457 (1970).
- [59] Ulf-G. Meissner, *Czech. Jour. Phys.* **45**, 153 (1995).
- [60] W.D. Brown, R.D. Puff, and L. Wilets, *Phys. Rev. C* **2**, 331 (1970); G. Krein, M. Nielsen, R.D. Puff, and L. Wilets, *Phys. Rev. C* **47**, 2485 (1993); M.E. Bracco, A. Eiras, G. Krein, and L. Wilets, *Phys. Rev. C* **49**, 1299 (1994); C.A. da Rocha, G. Krein, and L. Wilets, *Nucl. Phys. A* **616**, 625 (1997).
- [61] V. Pascalutsa, *Phys. Rev. D* **58**, 096002 (1998).
- [62] Smio Tani, *Phys. Rev.* **115**, 711 (1959).
- [63] Particle Data Group, *Eur. Phys. J.* **C3**, 1 (1998).
- [64] R.A. Arndt, I.I. Strakovskii, and R.L. Workman, *Phys. Rev. C* **52**, 2120 (1995).
- [65] D. Schwela, H. Rollnik, R. Weizel, and W. Korth, *Z. Phys.* **202**, 452 (1967); D. Schwela and R. Weizel, *Z. Phys.* **221**, 71 (1969); I.G. Aznauryan, *Phys. Rev. D* **57**, 2727 (1998).
- [66] D. Drechsel, G. Krein, and O. Hanstein, *Phys. Lett. B* **420**, 248 (1998); O. Hanstein, D. Drechsel, and L. Tiator, *Phys. Lett. B* **385**, 45 (1996); *Phys. Lett. B* **399**, 13 (1996); *Nucl. Phys. A* **632**, 561 (1998).
- [67] Y. Takahashi, *Nuovo Cimento* **6**, 371 (1957).
- [68] N.M. Kroll and M.A. Ruderman, *Phys. Rev.* **93**, 233 (1954).
- [69] E.P. Wigner, *Phys. Rev.* **73**, 1002 (1948).
- [70] V. Bernard, N. Kaiser, and Ulf-G. Meissner, *Int. J. Mod. Phys.* **E4**, 193 (1995).
- [71] REDUCE user's manual, version 3.1, ed. A.C. Hearn, The Rand Corporation, Santa Monica, 1984.
- [72] A. Pais and G.E. Uhlenbeck, *Phys. Rev.* **79**, 145 (1950).

- [73] K. Ohta, Phys. Rev. C **40**, 1335 (1989).
- [74] F. Gross and D.O. Riska, Phys. Rev. C **36**, 1928 (1987); V.P. Barannik and Yu.V. Kulish, Ukrain. Fiz. Zh. **32**, 978 (1987) (in Russian); S.I. Nagorny and A.E.L. Dieperink, nucl-th/9803007; H. Haberzettl, Phys. Rev. C **56**, 2041 (1997).
- [75] J. Wess and B. Zumino, Phys. Lett **37B**, 95 (1971); E. Witten, Nucl. Phys. B **223**, 422 (1983).
- [76] H. Garcilazo and E. Moya de Guerra, Nucl. Phys. A **562**, 521 (1993).
- [77] R.A. Arndt, I.I. Strakovskii, and R.L. Workman, Phys. Rev. C **53**, 430 (1996).
- [78] V. Bernard, N. Kaiser, J. Gasser, and Ulf-G. Meissner, Phys. Lett. B **268**, 291 (1991); G. Ecker and Ulf-G. Meissner, Comm. Nucl. Part. Phys. A, Vol. 21, No. 6 (1995).
- [79] H. Genzel, M. Jung, R. Wedemeyer, and H.J. Weyer, Z. Phys. A **279**, 399 (1976).
- [80] J.W. DeWire, M. Feldman, V.L. Highland, and R. Littauer, Phys. Rev. **124**, 909 (1961).
- [81] K. Toshioka, M. Chiba, S. Kato *et al.*, Nucl. Phys. B **141**, 364 (1978).
- [82] G. Blanpeid, M. Blecher, A. Caracappa *et al.*, Phys. Rev. Lett. **76**, 1023 (1996).
- [83] F.V. Adamyan, A.Yu. Buniatian, G.S. Frangulian *et al.*, J. Phys. G: Nucl. Part. Phys. **19** (1993) L139.
- [84] Y. Wada, K. Egawa, A. Imanishi *et al.*, Nucl. Phys. B **247**, 313 (1984).
- [85] B.R. Holstein, hep-ph/9710548.
- [86] T.R. Hemmert, B.R. Holstein, and J. Kambor, Phys. Rev. D **57**, 5746 (1998).
- [87] B.E. MacGibbon *et al.*, Phys. Rev. C **52**, 2097 (1995).
- [88] J. Tonnison, A.M. Sandorfi, S. Hoblit, and A.M. Nathan, Phys. Rev. Lett. **80**, 4382 (1998).

- 
- [89] V. Bernard, N. Kaiser, A. Schmidt, and Ulf-G. Meissner, Phys. Lett. B **319**, 269 (1993).
- [90] G.C. Gellas, T.R. Hemmert, and Ulf-G. Meissner, nucl-th/0002027.
- [91] K.B. Vijaya Kumar, J.A. McGovern, and M.C. Birse, hep-ph/0002133.
- [92] J. Schmiedmayer, P. Rieths, J.A. Harvey, and N.W. Hill, Phys. Rev. Lett. **66**, 1015 (1991).
- [93] L. Koester *et al*, Phys. Rev. C **51**, 3363 (1995).
- [94] I. Guiasu, C. Pomponiu, and E.E. Radescu, Ann. Phys. **114**, 296 (1978).



# Samenvatting

Het nucleon, pion en andere hadronische deeltjes zijn opgebouwd uit de fundamentele deeltjes van de sterke wisselwerking, quarks en gluonen. Het is echter tot nu toe onmogelijk om alle eigenschappen van hadronische deeltjes direct te berekenen in termen van quarks en gluonen. Het is echter in veel gevallen mogelijk om de wisselwerking tussen hadronische deeltjes te beschrijven zonder de details van hun interne structuur te weten. Als de energie van de hadronen laag genoeg is of ze relatief ver van elkaar verwijderd zijn kan de wisselwerking tussen de hadronen beschreven worden door uit te gaan van hadronen als fundamentele deeltjes van de sterke wisselwerking. In dit geval wordt de kracht tussen twee nucleonen beschreven door middel van de uitwisseling van pionen (of in het algemeen mesonen) tussen de twee nucleonen. Het gedeelte van de sterke wisselwerking dat niet beschreven wordt door deze benadering, wordt dan geparаметriseerd door middel van functies, vormfactoren genaamd. Een andere functie die van belang is voor de beschrijving van de propagatie van nucleonen is de zelf-energie.

Dit proefschrift beschrijft een model, gebaseerd op deze benadering, voor de nucleon-pion en nucleon-foton koppelingen. Deze koppelingen zijn belangrijk om pion-nucleon verstrooiing, de fotoproductie van pionen en de verstrooiing van fotonen door nucleonen (Compton-verstrooiing) te kunnen beschrijven. Deze reacties behoren tot de meest eenvoudige processen waarbij een nucleon betrokken is. Zij zijn daarom van fundamenteel belang voor het begrip van de sterke en elektromagnetische interactie van hadronen. Door middel van Compton-verstrooiing kan men bijvoorbeeld de vervorming van het nucleon door een extern elektromagnetische veld bestuderen. Deze vervorming wordt uitgedrukt door middel van constanten, de nucleon-polarizatie coëfficiënten. De laatste jaren is er veel aandacht besteed aan deze nucleon-polarizatie coëfficiënten zowel in experimentele als theoretische studies.

De drie genoemde reacties zijn niet onafhankelijk van elkaar te beschrijven omdat ze ieder als een tussenstap van de andere reactie kunnen plaats vinden. Beschouw bijvoorbeeld, het geval van Compton verstrooiing  $\gamma N \rightarrow \gamma N$ . De



verstrooiing van het foton kan ook plaats vinden door middel van fotoproductie van een pion dat vervolgens weer een foton produceert  $\gamma N \rightarrow \pi N \rightarrow \gamma N$ . Op een soortgelijke manier beïnvloedt pion-nucleon verstrooiing de fotoproductie van pionen. Deze herverstrooiing bijdragen zijn belangrijk om aan de conditie te voldoen dat de som van de kansen, voor alle mogelijk transitie van een initiële toestand naar alle eind toestanden gelijk aan één is. Deze conditie wordt aangeduid als de unitariteits conditie. Een ander belangrijk aspect waar realistische modellen aan moeten voldoen is causaliteit. Met name het causaliteits principe speelt een bijzonder grote rol in het model dat hier beschreven is. Dit principe is zeer simpel en intuïtief te begrijpen. Het komt er op neer dat iets dat vandaag gebeurt geen invloed heeft op iets dat gisteren gebeurd is. Dit eenvoudige principe is de basis voor dispersie relaties. Deze dispersie relaties zijn een zeer krachtig mathematisch hulpmiddel is voor de hadronische fysica.

In het model dat hier beschreven is worden de dispersie relaties gebruikt om het reële deel van de nucleon vormfactoren uit te rekenen gebruik makend van het imaginaire deel. De imaginaire delen kunnen worden uitgerekend door een conditie gebaseerd op unitariteit toe te passen. Door middel van iteratie wordt de zelf-consistent oplossing van de gekoppelde integraal vergelijkingen voor de vormfactoren en zelf-energie verkregen. De natuurkundige interpretatie van deze wiskundige methode is dat men rekening houdt met de mogelijkheid dat er virtuele pionen en andere mesonen kunnen bestaan gedurende de reactie. Populair wordt deze procedure beschreven als het aankleden (“dressing”) van het nucleon, het nucleon krijgt een “jas” van virtuele deeltjes. Om een convergente oplossing te krijgen, introduceren we een “bare”  $\pi NN$  vormfactor, die de effecten voor kleine afstanden parametrizeerd, die niet in het model worden meegenomen. Voor de aankleed procedure nemen we zowel nucleonen en pionen, als ook andere hadronische vrijheidsgraden mee, waarvan bekend is dat ze belangrijk zijn voor lage en intermediaire energieën — de  $\Delta$  resonantie en de  $\rho$ ,  $\omega$  en  $\sigma$  mesonen.

De methode is zo ontworpen dat het consistent is met implementatie in het zogenaamde K-matrix formalisme. De termen die bijdragen aan de imaginaire gedeelte van de zelf-energie en vormfactoren corresponderen met die, die in het K-matrix formalisme in rekening worden gebracht. Een bijkomend voordeel is dat dit formalisme een goed raamwerk bied voor het model voor de  $\pi NN$  en  $\gamma NN$  vormfactoren. De vormfactoren in het hier gepresenteerde model beschrijven de wisselwerking waarbij een virtueel nucleon (“off-shell”) betrokken is. Virtuele nucleonen kunnen niet bestaan als vrije deeltjes en kunnen dus niet direct worden gedetecteerd. Echter gedurende tussenstappen in Compton-verstrooiing, fotoproductie van pionen en pion-nucleon verstrooiing

kunnen “off-shell” nucleonen wel bestaan. De nucleon vormfactoren die in dit model gebruikt worden beschrijven de wisselwerking tussen een pion en een nucleon en tussen een foton en een nucleon en worden “off-shell” nucleon vormfactoren genoemd.

Een belangrijk conditie waaraan model ook moet voldoen is dat de elektromagnetische stroom behouden moet zijn als er fotonen bij het proces betrokken zijn. Om aan stroombehoud te voldoen moet het foton aan elk geladen deeltje koppelen. Dit is de essentie van de minimale substitutie procedure die we gebruiken om de zogenoemde contact termen te construeren. Als gevolg van deze contact termen, krijgen we een behouden stroom beschrijving van pionfotoproductie en Compton-verstrooiing.

Normaliter wordt in K-matrix modellen, de bijdrage van processen waarbij virtuele deeltjes betrokken zijn verwaarloosd. In het huidige model worden deze bijdrages meegenomen, als we de berekende nucleon vormfactoren en zelf-energie gebruiken voor de constructie van de K matrix. Door het gebruik van dispersie relaties worden bepaalde causaliteits voorwaarden in het K-matrix formalisme geïmplementeerd. In dit proefschrift zijn de effecten van deze contributies op de observabelen in Compton-verstrooiing, fotoproductie van pionen en pion-nucleon verstrooiing nader onderzocht. Het resultaat geeft aan dat deze effecten significant kunnen zijn. Zij zijn met name belangrijk om de gemeten nucleon-polarisatie coëfficiënten te kunnen reproduceren. Het gebruik van de dispersie relaties is belangrijk om het cusp-effect in Compton-verstrooiing van fotonen met een energie dichtbij de drempelenergie voor pionproductie te kunnen beschrijven. Dit demonstreert het belang van de causaliteits voorwaarden en ondersteunt de ontwikkelde procedure voor het aankleden van een nucleon.



# Acknowledgments

First and foremost, I wish to express my deep gratitude to my supervisor, Olaf Scholten, for his constant encouragement, guidance and help. I have learned so much from his professionalism and never waning optimism, and I feel both privileged and fortunate to have had such a scientific advisor. Thank you, Olaf!

I would also like to thank my promoter, Rudi Malfliet, for his advice and criticism. I have benefited from his experience and broad knowledge of physics. Remarks and recommendations of the members of the reading committee, Justus Koch, Alex Lande and John Tjon, have contributed positively to the final version of the thesis.

My numerous discussions with Alex Korchin, Rob Timmermans and Vladimir Pascalutsa have always been very interesting and thought-provoking. I wish to thank them for their interest in my work and for their friendly advice.

Working at the KVI, I have enjoyed company of many fellow Ph.D.-students. Due to Marc-Jan van Goethem, Fabrice Fleurot, Vladimir Kravchuk, Teake Penninga, Marcel Volkerts, Volker Hannen, Karsten Ermisch, Dan Cozma, Gerard Martinus, Paul Vogt, Marieke Hoefman, Susana Schneider, Harry Huisman, Johan Messchendorp, the four years I spent in Groningen will always remain a very memorable period of my life. My special thanks go to Marc-Jan and Teake for their indispensable help in writing the Dutch “samenvatting”.

I thank my housemates Amol, Madhu, Ilya, Stefania and Yiannis, for sharing both sunny and rainy days with me, and for the many discussions, chats and laughs we have had over these years.

I greatly appreciate the assistance of the secretaries and administration of the institute, and in particular Hilde van der Meer and Grietje van der Tuin, who helped me on many occasions to deal with the intricacies of legal paperwork.

Finally, and most importantly, I thank my mother without whose support and understanding this thesis would have never been started, let alone finished.